Delft University of Technology

Department of Civil Engineering and Geosciences

Quality assessment of a graph-based approach for a multi-methods determination of geotechnical model parameters

Author:
M. Hauth

Committee:
Dr. ir. R.B.J. Brinkgreve, TU Delft
Prof. dr. K.G. Gavin, TU Delft
Ir. K. de Jong, Witteveen+Bos
Dr. Ir. R. C. Lanzafame, TU Delft
Ir. H.J. Lengkeek, TU Delft

to obtain the degree of Master of Science
at the Delft University of Technology,
to be defended publicly on Wednesday October 21, 2020 at 14:45.

Preface

When I started studying at the university in my hometown seven years ago, little did I know that I would find my way to Delft and the Netherlands. After taking a few unexpected turns that led me to study Geo-engineering at TU Delft, I finally reached the conclusion of the student life. The present thesis marks the end of this thrilling seven-year journey that has been paved with highs and lows, and wonderful people. I would like to

First of all, I would like to thank my graduation committee for their guidance and their constant enthusiasm in my graduation project. I thank Ronald Brinkgreve for introducing me to this topic, and for his commitment into the APD project. I highly acknowledged Arny Lengkeek's expertise both in geotechnical engineering and in statistics, who always give quite helpful feedback and inputs. I greatly appreciated Robert Lanzafame's enthusiasm, our conversations were always rich in ideas and his suggestions were very valuable. It was a genuine pleasure working with my daily supervisor Koen de Jong, I appreciated our niche discussions about programming and I learned a lot of Python tricks while working by his side. I am also grateful to the company Witteveen+Bos which allowed me to work among one of its department.

This journey would not have been the same without all the friends I met along the way. I have a particular thought towards my classmates from Mines Nancy with whom I spent two incredible and crazy years. I would like to express deep thanks to my TMP roommates in Delft who gave me the warmest welcome to the Netherlands. I feel incredibly lucky to have found such a nice house that I can proudly call home.

Finally, I would like to warmly thank my parents for their love and their unconditional support in my life choices.

Matthias Hauth
October 2020

Abstract

The determination of geotechnical parameters from in-situ tests heavily relies on the use of empirical correlations relating field measurements to soil properties. A large number of these correlations can be found across the literature, each of them yielding a different outcome for the parameter value. This results in a high variability of the potential results, which is not necessarily properly accounted for in the current geotechnical engineering practice. A new approach using graphs has recently been proposed by van Berkom [1] to automatically generate multiple parameter values based on a given set of correlations and equations.

The present thesis assesses the quality of the estimates obtained from this new graph system and investigates how multiples outcomes can be combined into a unique result. The quality of the parameter's estimates is appraised both in terms of accuracy or uncertainty, and in terms of validity. The combination of results from multiple methods showed that it is possible to either build confidence or distrust in the combined outcome depending of the consistency of the contributing results. As a result, this framework enabled a quantitative description of the inter-correlations variability.

The conceptual framework has been then applied to geotechnical parameters and CPT-based correlations for coarse-grained soils. The range of applicability of the correlations (e.g. soil type, state of consolidation) is a critical factor that actively influences the final outcome of the system. This automatic system demonstrated its ability to produce parameter values relatively close to the values obtained with the current practices. Further validation is required to assess the overall performance of the system on a broader scale.

Keywords: parameter determination, graphs, combination of forecasts, model averaging, uncertainty.

Contents

List of Figures

List of Tables

Chapter 1

Introduction

1.1 Context

Motivation

When it comes to choosing a computer software to perform geotechnical calculations, engineers tend to favor traditional geotechnical design methods over finite element numerical analysis. Yet, the latter generally offers a more refined description of the true behavior of the ground with a higher level of details. Numerical analysis relies on the need of a constitutive model that mathematically characterizes the stress-strain relationship of soil. Over the last few decades, researchers have developed a large number of these models integrating more features than the older and the less sophisticated ones. For instance, the Mohr-Coulomb model which is arguably the most well-known and accepted model in geomechanics can only provide a first order approximation. Recent models are now able to properly characterize several effects from unloading-reloading, hardening-softening, creep to name but a few of the soil features. It is good practice and sometimes necessary to make use of these complex models because they describe more accurately the reality and eventually lead to a better design.

As constitutive models are constantly evolving and becoming ever more complex, an increasing number of model parameters is required to capture the intricate behavior of soils. This makes the understanding of modern models and numerical analysis even more complicated. According to Brinkgreve [13], this lack of knowledge in the mechanics of the models and the limited availability of soil data are among the main reasons geotechnical consultants dismiss numerical analysis.

Once one realizes the relevance of selecting the right constitutive model, one should also be aware that determining the model parameters meticulously is of utmost importance. As the engineers themselves determine parameters, the outcome of the numerical analysis highly relies on the understanding of the user and his skill to select parameter values. Moreover, several methods, correlations and equations often lead to the same model parameter but not the same value. This results in practice to a large variety of outcomes for a same given input data from site investigation and the confidence in the numerical methods is subsequently altered. Ten different consultants are likely to provide ten different answers for a same given case study and soil profile. An automatic method to determine model parameters would serve as a valuable aid to the engineer to mitigate the human factor and to efficiently and reliably perform numerical simulations. By doing so, uncertainty in numerical analysis will hopefully decrease, as well as the reluctance in using these practices.

Towards an automated method for parameter determination

Against the backdrop of automatic selection of constitutive model parameter, van Berkom [1] has developed a framework to estimate parameters from in-situ input data. This framework based on graph theory collects and combines many correlations, either empirical or analytical, that are often used by geotechnical experts or encountered in the scientific literature. Together, the correlations form a network that links soil parameters, soils properties and model parameters. The idea is: starting from input source parameters (e.g. CPT profile), it is possible to find numerous ways to calculate a destination parameter via correlations and intermediate parameters as shown in figure

1.1. In this basic representation each arrow can be seen as a pairwise correlation function relating two parameters.

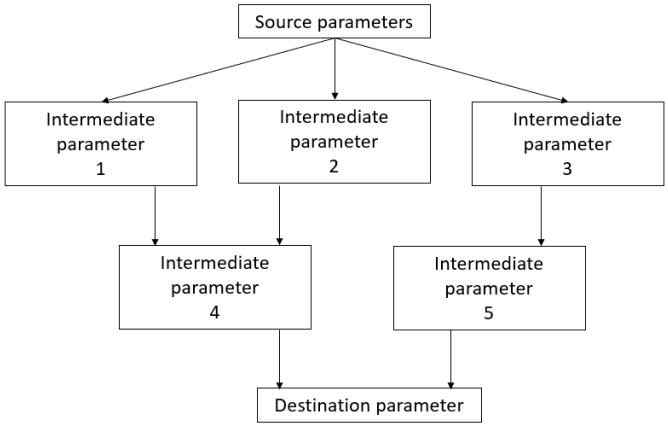

Figure 1.1: Schematic representation of the automatic parameter determination

The large number of existing formulas will inevitably lead to multiple answers. Therefore, we expect with this framework to obtain several paths of calculations to spawn the same geotechnical destination parameter starting from a common set of source parameters. The algorithm has proven so far to be able to exhaustively find all the paths of a given graph, and to calculate the values for all the parameters.

1.2 Aim, Scope and Objectives

Aim

The main purpose of this research is to provide reliable estimates of geotechnical constitutive parameters based on a general framework combining multiple models and expert elicitation. Such a framework based on graphs has already been partly elaborated and implemented in Python by van Berkom [1], but there is much work to be done to assess the overall quality of the derived parameters. Quantitative evaluation of the parameter's quality expressed in terms of accuracy and range of validity will be the core concerns of this work.

Moreover, providing trustworthy estimates from multi-model inference might hopefully mitigate human factor for parameter determination and build confidence in constitutive modelling for numerical analysis. Transparency in the network and in the performed calculations is vital so that the framework can be trusted and improved by the community. Flexibility of the framework would also allow experts to interfere and include their own belief on parameter values and accuracy.

The main research question is formulated as follows:

> *How to combine results from multiple correlations and chains of correlations to estimate geotechnical parameter values and how to assess the quality of these estimates ?*

Scope

This graduation thesis is part of a much bigger and exciting project to create a workable open-source tool for automatic parameter determination from in-situ tests. The goal of this thesis is to show that such system could potentially provide reliable results, therefore boundaries are set to focus on a few primary objectives.

- Only CPT-based correlations for coarse-grained soils will be used for this research. The set of correlations that has already been gathered and compiled in [1] will be directly reused and expanded.

- Particular attention is paid to the transparency of the calculations in the network. Therefore, black-box techniques like machine learning or neural network are discarded from this research.

- An external pre-processing step of CPT profiles will be assumed. This thesis will not deal with an automatic processing of the soil profiles into different layers. In concrete terms, the following parameters will be regarded as given input parameters, either for an averaged layer or a single CPT measurement: the cone resistance q_c, the sleeve resistance f_s, the penetration pore water pressure u_2, the cone area ratio a, the atmospheric pressure $p_a = 100$kPa, the depth at which measurements are taken z_{ref}, the phreatic level, the specific weight of water γ_w. This list might be subject to modifications if additional information is provided about the soil properties.

- The object-oriented programming language Python has been selected to implement the automated system.

Objectives

The several objectives of this thesis are outlined as follows:

- **Designing and implementing validation of parameters:** The first step that needs to be taken is the validation of the outcomes given by all the different paths. These outcomes must be meaningful from a physical and geotechnical point of view. Unrealistic outcomes should be discarded if they lie outside acceptable boundaries.

- **Dealing with circular connections:** The system cannot cope with loops in the graph because of the recursive architecture of the of the system when determining parameter values. The geotechnical meaning of these circular connections will be addressed in this research.

- **Characterizing and propagating uncertainty:** The concepts of uncertainty and accuracy need to be properly defined and quantified in order to assess the quality of a parameter's estimate. Each parameter carries an inherent variability which makes the true value of this parameter uncertain; this aspect is particularly relevant to geotechnical parameters. Correlations too are inaccurate for they are merely an approximation and can never fully describe the reality of the physical system. Once the uncertainties are defined and calculated, they need to be aggregated together and then propagated downstream into the network.

- **Comparing Methods selection and Method averaging:** Through a quality assessment of the methods (i.e. correlations), it is possible to directly compare the methods with each other and select the most accurate one. A different approach consists in using a weighted average of all the model responses based on their individual performance. These two perspectives are valuable and provide different information to the user. They should be both available to future users or at least be investigated and compared in this research.

- **Validity of correlations:** Pairwise correlations found in the literature are only valid for a certain type of soil: the one tested and used to generate the database of the experiment. As a result, these correlations should only be used to soil samples that are similar to the original database. It is essential to consider only the relevant correlations for the tested sample and to evaluate the inaccuracies accordingly.

- **Validation of the framework:** Once the estimate of the destination parameter and its accuracy have been produced by the framework, the final outcome must be confronted with actual experimental data and previous case studies. Such comparison will either legitimize or disprove the ability of the framework to reliably determine parameters.

- **Transparency of the framework** The user should always have a clear understanding of how calculations are conceptually performed in the network. The framework should remain transparent and adjustable, and should not be seen as a black-box by the user. It should also allow expert users to overwrite (intermediate) parameter values.

1.3 Thesis outline

This report shows a logical progression towards the construction of a framework that combines multiple correlations for the determination of model parameter values. As this thesis is part of the continuation of a previous master thesis [1], chapter 2 introduces the Automatic Parameter Determination system elaborated in this previous work and summarises its main features and shortcomings. It acts as a starting point from which the rest of this study expands. Chapter 3 covers a few preliminary considerations that need to be addressed before assessing the quality of the system: a pre-validation of the parameter values and circular connections will be tackled in this chapter. The fourth chapter introduces the statistical framework implemented to the system. It redefines the notion of accuracy and examines how it can be propagated throughout the network. Chapter 5 builds on the previous chapter and explores how multiple results can be interpreted and combined to one final value. This chapter explains how confidence or distrust can be built based on such a combination. Finally, the sixth chapter applies the whole APD system to an actual case study to determine the model parameters for the Hardening Soil small-strain model.

Chapter 2

A starting point: on the use of graphs for parameter determination

A new approach to parameter interpretation from in-situ tests has been proposed by van Berkom [1] who developed an automated system that determines geotechnical parameters based on concepts from graph theory. A proof of concept has been presented to show the feasibility of using graphs to determine constitutive model parameters. This chapter summarizes some of the basic aspects introduced and developed in [1] to facilitate the comprehension of the following chapters. It serves as a starting point from which this study is expanding and enhancing. Discussion points and recommendations mentioned in [1] are also highlighted here to link the objectives of this thesis with previous works.

2.1 A graph to visualize relationships

2.1.1 General aspects

A graph is a mathematical representation of a network that connects different entities based on their relationships. It is composed of two types of objects: the *nodes* that form the actual entities of the graph, and the *edges* that portray the relationships between two *nodes*. Graphs turn out to be very useful and efficient when modelling complex networks like a road network, but they are also applicable to describe relations that are much more simple: the equation $y = f(x)$ express the relation between two nodes x and y linked by a single edge which is the function f (figure 2.1). This concept is particularly suitable for geotechnical engineering as there are correlations and formulas galore in the literature to connect the many soil parameters. It also enables an easy and transparent visualisation of these connections.

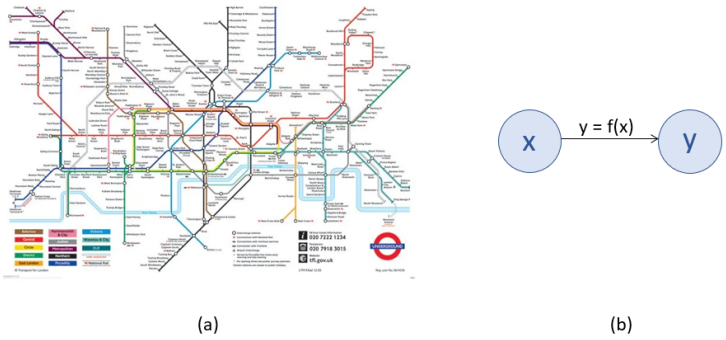

Figure 2.1: (a) A complex graph of the underground network in London. (b) A basic graph representing the relation $y = f(x)$

The focus is put here on a specific type of graph: the *directed* and *weighted* graph. These adjectives mean that the relationships or the edges between the nodes are uni-directional and are assigned with a weight that quantitatively characterizes the relation. The graph (a) from figure 2.1 is an example of undirected graph as commuters can travel in any direction, the weights could be for instance the travel time between two stations. The graph (b) is directed as indicated by the arrow, the variable y is determined from x via the function f but the variable x cannot be calculated from y if f is not bijective[1]. These two aspects of direction and weights will be defined and discussed in this thesis.

2.1.2 Framework for parameter determination

As mentioned in introduction, the network connects the input in-situ test measurements to the geotechnical parameters and the soil properties via a set of correlations. We use here the word *parameter* as a generic term to characterize the nodes of the network, and the term *method* for the correlations and formulas linking these parameters. A parameter can be split between one of these three categories: a *source parameter* if it is an input data to the system, a *destination parameter* if the parameter is the desired soil property to be estimated, and an *intermediate parameter*. The figure 2.2 from [1] portrays the description of the framework.

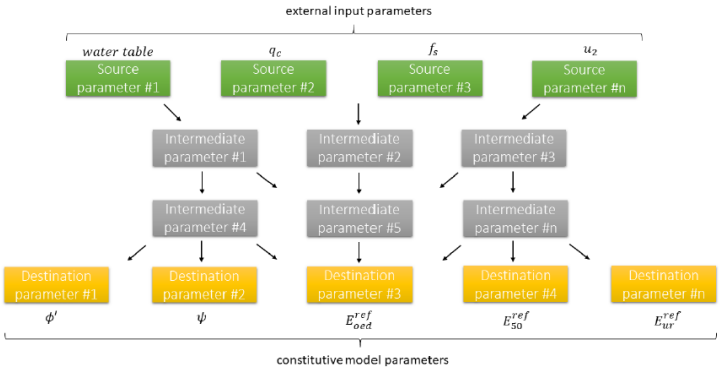

Figure 2.2: Graphical representation of the network of geotechnical parameters. Source: [1]

The conceptual representation of the network in figure 2.2 falls short when more than one method exist for an intermediate or a destination parameter. Such a situation makes the interpretation and the visualisation of the graph difficult, as be can seen on the graph b) in figure 2.3. It becomes then necessary to introduce two different types of nodes: the parameter node and the method node. With this description, the edges of the graph only account for the relationship between the input variables and the output variable of a method, and do not carry any additional information (graph a) from figure 2.3).

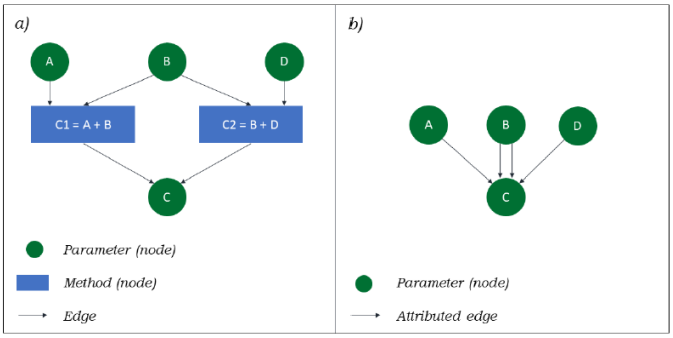

Figure 2.3: Different representations of a multi-methods graph for a) two types of nodes, b) only one type of nodes. Source: [1]

[1] invertible

From a computational point of view, each type of nodes is defined a class: a *Method* class and a *Parameter* class. The attributes of the classes reflect the properties and the metadata of the nodes. As an example, the class *Parameter* has an attribute *value* which stores in an array all the possible values taken by this node. Similarly, the class *Method* has an attribute *formula* which consists of a parsed string of the formula of the method. A comprehensive list of all the attributes is outlined in [1].

A path is defined as a succession of parameter and method nodes to derive one particular destination parameter. It is clear that numerous paths leading to the same destination parameter can coexist. Each path yields a single value that contributes to the array of all the possible values for a given parameter node. The spread of these values is related to the variability of results caused by the human factor: a first engineer would tend to choose one path while the second would pick another one.

2.2 Features of the framework

Generating a graph

When running the automated framework, the first stage processed by the algorithm is the connection of the parameters and the generation of the graph. It links all the nodes, both parameter and method, based on the correlations considered. The user must then provide to the system a set of correlations and a set of parameters that will be appearing in the network. These sets are called the external databases. Two types of external databases are distinguished:

- **Parameter database** which consists of a list of all the parameter nodes of the graph. Some metadata about the parameters are also mentioned there: their unit, and their initial value if applicable.
- **Method database** which consists of a list of all the method nodes of the graph. The literal formula and its input and output parameters are mentioned there.

The external databases specified in tables 2.1 and 2.2 are generating the graph displayed in figure 2.4.

method	formula	input parameter	output parameter
c_method_1	"a+b"	a,b	c
c_method_2	"b+d"	b,d	c

Table 2.1: External method database for the graph 2.4

symbol	unit	value
a	"-"	1
b	"-"	2
d	"-"	3
c	"-"	

Table 2.2: External parameter database for the graph 2.4

Calculating parameter values

Once a graph is generated, the system is able to calculate the values of any parameter[2] based on the value of the source parameters given by the user, and based on the equations formulated in the external database. The values of a parameter are then stored in a 1-D array whose length is equal to the number of paths leading to that particular parameter. A verification step has been performed by van Berkom in [1] for both a test case and a geotechnical case with actual correlations. The automated framework successfully passed the verification test, ensuring that the outputs given by the system were identical to hand calculations.

[2]provided there is a correlation for that parameter

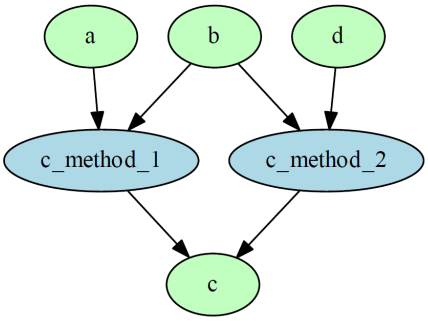

Figure 2.4: Basic graph generated from the external databases 2.1 and 2.2

Adaptability and transparency

The two aspects of adaptability and transparency were key during the development of the framework in order to make it user-friendly and trustworthy. The system is indeed transparent since it only uses the equations specified in the external database, and every intermediate calculation can be manually checked. The user keeps track of the visited parameter and method nodes for each path, and is able to review the attached correlations. The whole structure of the graph is completely governed by the information provided in the external databases. This makes the system highly adaptable as the user only needs to modify the external databases to generate another graph, and does not need to step into the Python code.

2.3 Shortcomings and discussions

The features elaborated in the previous section certainly represent a substantial step forward to the automatic determination of constitutive parameters. However, a number of discussion points mentioned in [1] and shortcomings need to be addressed so that confidence can be built when using this framework.

Interpretation of the outcomes

At this stage, the system solely computes parameter values and leaves their interpretation in the user's hands. Without any validation stage, some chains of correlations could potentially lead to nonsensical, albeit mathematically correct, outlying values. A user could manually chose to discard an outlier, but it would be valuable to integrate a validation procedure to the system in order to make sure that the parameter values make sense from a geotechnical point of view. It is highlighted in the recommendations of the thesis [1] that correlations are valid for a certain type of soil or for an index I_c within a given range. The index I_c is a number combining the cone resistance and the sleeve friction from a CPT to characterize the type of soil of a sample [14]. The table 2.3 outlines the description of the Soil Behavior Types with their range of I_c index. This validity of correlations based on the index I_c is addressed in the chapter 3 of this thesis.

Range of I_c index	Soil Behavior Type	Description
$I_c < 1.31$	7	Gravelly sand to dense sand
$1.31 < I_c < 2.05$	6	Sands: clean sand to silty sand
$2.05 < I_c < 2.60$	5	Gravelly sand to dense sand
$2.60 < I_c < 2.95$	4	Silt mixtures: clayey silt to silty clay
$2.95 < I_c < 3.60$	3	Clays: silty clay to clay
$I_c > 3.60$	2	Organic soils: peats

Table 2.3: Description of the Soil Behavior Types and their associated ranges for the index I_c. Source: [11]

Furthermore, the values of a parameter should be all combined into a single weighted average that will subsequently be used for design. A weighting scheme is already suggested in [1] based on weights assigned by the user to the methods in the external database. Incorporation of the Soil

Behavior Type Index in the weighted process is also advocated. The chapter 5 proposes a different approach based on the parameter predictions.

Incorporating the parameter accuracy

The reference thesis [1] introduced an attribute *accuracy* to the *Parameter* class in order to account for the uncertainty in the parameter values and conceptualize its propagation through the network. However, the notion of accuracy remains quite vague and a rigorous statistical framework must be implemented to define and propagate uncertainties.

Circular connections

Up to now, only acyclic graphs were considered. Circular connections occur when a loop is formed in the network from the information given by the user in the external databases. Such connections are currently not supported by the system which would crash owing to the recursive nature of the code. According to [1], it is the responsibility of the user to prevent such references from occurring by filling the external database appropriately. Unfortunately, this decision limits the adaptability of the system as some reliable methods become purely inoperable. This thesis formulates a few recommendations on how circular connections could be dealt with.

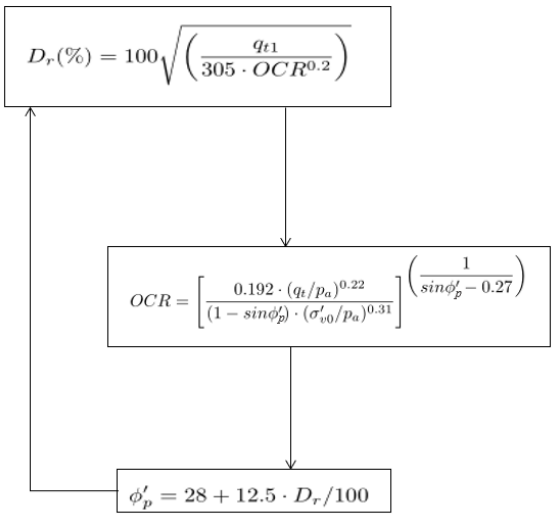

Figure 2.5: Example of a circular connection with geotechnical correlations

Conclusion

The conceptual graph-based framework initiated by van Berkom [1] will be referred as the Automatic Parameter Determination system, or APD, throughout this whole thesis. The Python code being semi-open source, it has been directly re-utilized and refactored here for the addition of new features and the troubleshooting of potential bugs.

Chapter 3

Preliminaries

A few preliminary steps must be undertaken before diving into the construction of a statistical framework for the system. These concern the pre-validation of geotechnical parameter values, and the consideration of circular connections.

3.1 Pre-validation of the APD system

A verification stage has already been performed in [1] which proved that the network can yield correct outcomes from a purely mathematical point of view. The following step is to validate from physical and geotechnical points of view the outcomes provided by the system. In other words, the system must provide realistic parameters values. For instance, it would be unacceptable to obtain a negative friction angle and use this value for further calculations. Although this example might be a bit extreme, it is paramount that the system automatically detects and treats with these outliers and anomalies.

3.1.1 Methodology and dataset

The validation process is performed by comparing parameter values obtained directly from the system with parameter values collected from a recognised software for parameter determination. Raw CPT profile data have been imported and analysed with the software *CPeT-IT* to provide an estimation of several geotechnical parameters for every 2 cm, from 0.18m to 25.42m below ground level. The software *CPeT-IT* uses a particular set of equations to derive the geotechnical parameters from the basic input parameters which are the cone tip resistance, the friction sleeve, and the pore water pressure.

3.1.1.1 Description of the dataset

The cone resistance q_c, the sleeve resistance f_s and the pore water pressure u are recorded for every 2cm depth; they form for our study the input parameters for parameters determination. The dataset includes two sets of parameters: the first is a set of basic intermediate results that are necessary for the interpretation of the CPT profile. The second is a set of actual geotechnical parameters that will be subsequently used for a numerical analysis: they are the destination parameters that we are interested in.

Basic results The basic results mainly consist of a set of parameters which includes the normalised cone resistance Q_{tn}, the soil unit weigth γ_t, along with the Soil Behavior Type (SBT) and its the associated SBT Index I_c. This procedure is done iteratively until convergence of I_c and the stress exponent n (eq 3.1).

$$n = 0.381 \cdot I_c + 0.05(\sigma_v^{'}/p_a) - 0.15 \tag{3.1}$$

For the sake of simplicity and because the system can not cope with loops and iterations at this stage of development, we will assume as a given input all the parameters from the set of basic results. An overview of these input parameters is shown in figure 3.1.

Number	Depth	qc	fs	u	other	qt	Rf	SBT	IcSBT	gamma	sigma_tot	u0	sigma_eff	Qt	Fr	Bq	SBTn	n	Cn	Ic	Qtn	u2
1	0.18	920.0	40	1.50	0	0.92	4.35	3	3.13	17.20	3.10	0.0	3.10	295.95	4.37	0.00	3	0.95	2.0	2.89	18.32	0.48
2	0.20	860.0	41	3.04	0	0.86	4.76	3	3.17	17.20	3.44	0.0	3.44	249.48	4.78	0.00	3	0.97	2.0	2.93	17.16	0.88
3	0.22	830.0	44	4.74	0	0.83	5.27	3	3.21	17.27	3.79	0.0	3.79	219.58	5.29	0.01	3	0.98	2.0	2.97	16.62	1.25
4	0.24	870.0	46	6.20	0	0.87	5.30	3	3.20	17.34	4.13	0.0	4.13	209.12	5.32	0.01	3	0.98	2.0	2.96	17.28	1.50
5	0.26	910.0	49	6.87	0	0.91	5.40	3	3.19	17.43	4.48	0.0	4.48	201.51	5.43	0.01	3	0.98	2.0	2.95	18.06	1.53

Figure 3.1: Sample of the basic results for the first 5 measurements

It is also worth mentioning the following assumptions of this study: ground level is at 0m depth, ground water level is at 0.5m depth, calculated friction angles are peak values and the critical state friction angle ϕ_{cv} is taken as 32 degrees.

Estimated parameters The estimated parameters from the software *CPeT-IT* are shown in figure 3.2. As we focus here only on coarse-grained soils, we are interested in the following parameters: the elastic Young Modulus E_s (kPa), the relative density D_r (%), the state parameter Ψ, the drained friction angle ϕ_p, the 1-D constrained modulus M_{CPT} (kPa), the small strain shear modulus G_0 (kPa) and the shear wave velocity V_s (m/s). The in-situ stress ratio K_0 is also of interest, although it is automatically assigned to 0 by default by the software for coarse-grained materials. The formulas used by the software are described in the appendix A.1.

number	Depth	qc	fs	SBTn	Ksbt	Cv	SPT_N60	M_CPT	Dr	phi	Es	G0	Nkt	Su	Su_ratio	k_OCR	OCR	Vs	psi	K0	Sensitivity	phi_p
1	0.18	0.92	40	3	1.51e-08	1.97e-05	4	12830	0	0	0	31890	14	65.44	21.14	0.33	6.05	134.86	0	1.22	1.6	20
2	0.20	0.86	41	3	1.08e-08	1.33e-05	4	12010	0	0	0	31700	14	61.3	17.82	0.33	5.66	134.45	0	1.19	1.47	20
3	0.22	0.83	44	3	8.22e-09	9.75e-06	4	11640	0	0	0	32280	14	59.37	15.68	0.33	5.49	135.4	0	1.18	1.32	20
4	0.24	0.87	46	3	8.88e-09	1.1e-05	4	12100	0	0	0	33080	14	61.72	14.94	0.33	5.7	136.82	0	1.19	1.31	20
5	0.26	0.91	49	3	9.45e-09	1.22e-05	5	12640	0	0	0	34190	14	64.49	14.39	0.33	5.96	138.72	0	1.21	1.29	20

Figure 3.2: Sample of the estimated parameters for the first 5 measurements

3.1.1.2 Methodology

The methodology for the validation step is described as follows:

- **Case 1:** The exact same set of equations (see appendix A.1) used by the software *CPeT-IT* is entered in the external database of the network. Very similar values between the network outcomes and the software's estimates should be expected.
- **Case 2:** The set of equations is expanded with the additional correlations compiled in the appendix A.2. Several paths are now available for each parameter, and the multiple outcomes are compared with the reference value of the software.

3.1.2 Results

3.1.2.1 Case 1

The parameter values have been calculated at different depths to make sure that the results are consistent for several measurements. The tables 3.1 and 3.2 compare the results provided by the APD system with the reference values provided by the software *CPeT-IT*. The pairs of values should be in theory identical as the same equations and correlations are used in both cases. In practice, we notice a slight difference probably due to rounding errors that propagate through the calculations.[1] The graph can be vizualised in figure 3.3. The APD system is therefore able to produce satisfying results for all parameters. A value for the K_0 has been calculated by APD, even if the software automatically defines it as 0 for coarse-grained soils.
A similar approach has been undertaken for a sandy layer where parameter values have been simply averaged over the whole layer. The table 3.3 sums up the results for a sandy layer between 4.58m and 9.58m below the surface. Once again the system yields pretty satisfying results, especially for the relative density, the friction angle and the shear wave velocity. The difference in terms of stiffness has been slightly amplified.

[1] Python calculations are done at computer's precision, so these errors probably originate from the software *CPeT-IT*

Category	E_s(kPa)	G_0(kPa)	$M_{CPT}(kPa)$	$D_r(\%)$	V_s (m/s)	$\phi(°)$	Ψ	K_0
APD	23 632	29 619	48 030	37.38	134.56	34.05	-0.0427	0.470
CPeT-IT	23 460	29 400	46 920	37	132.38	34	-0.04	0

Table 3.1: Comparison between APD and CPeT-IT values at the depth -4.72m (SBT = 5)

Category	E_s(kPa)	G_0(kPa)	$M_{CPT}(kPa)$	$D_r(\%)$	V_s (m/s)	$\phi(°)$	Ψ	K_0
APD	60 178	75 423	120 3545	66.24	212.25	39.8	-0.1629	0.470
CPeT-IT	59 970	75 160	119 940	67	198.28	40	-0.16	0

Table 3.2: Comparison between APD and CPeT-IT values at the depth -6m (SBT = 6)

Category	E_s(kPa)	G_0(kPa)	$M_{CPT}(kPa)$	$D_r(\%)$	V_s (m/s)	$\phi(°)$	Ψ	K_0
APD	66 276	83 066	134 761	60.30	219.87	39.2	-0.1510	0.470
CPeT-IT	62 150	77 895	122 328	59.05	199.11	38.8	-0.1429	0

Table 3.3: Comparison between APD and CPeT-IT values for a sand layer between 4.58m and 9.58m below ground level.

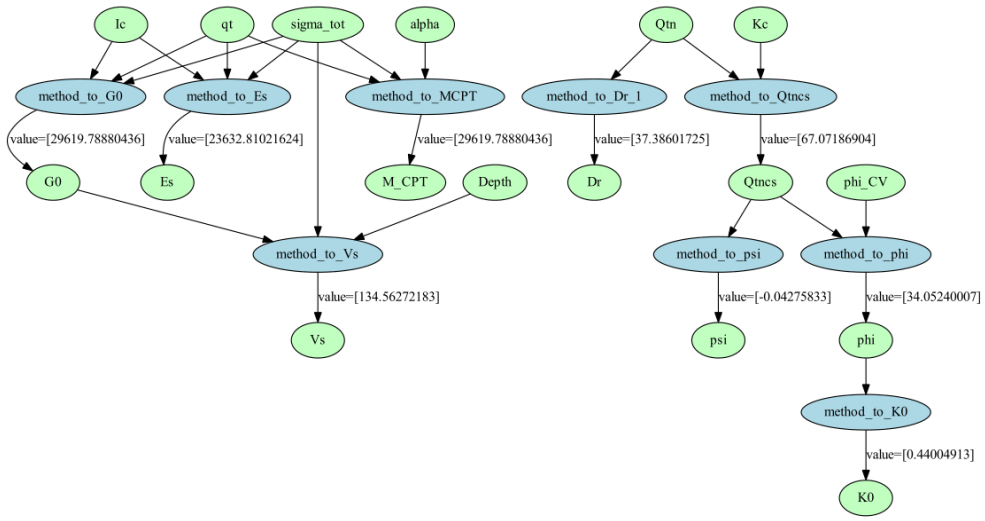

Figure 3.3: Graph of set of methods from the software *CPeT-IT* at depth 4.72m below ground level. Method nodes are in light blue, parameter nodes are in ligth green.

3.1.2.2 Case 2

In this second part, a more complex network is analysed by adding several methods for each parameter (see C). The goal is to observe the deviation of parameters values from the new paths with the reference values given by *CPeT-IT*. The tables below (from 3.4 to 3.11) gather the outcomes given for all the parameters of interest. The reference value is the value given by the software *CPeT-IT*. Each method for a given parameter can yield one or more values depending on whether or not the method's inputs already have multiple paths. An arbitrary depth of 4.72m below ground level is chosen for this study, it corresponds to a sandy material.

The number of outcomes provided by a method is equal to the number of possible combinations of its input parameters occurrences. For instance, the first method that determines the friction angle ϕ (equation A.8) gives two different values because the input parameter of this method, which is the state parameter Ψ, also has two different values.

Parameter: Relative density D_r (%)				
path	method	value	reference value	equation
1	1	37.4	37	A.2
2	2	47.2	37	A.3
3	3	41.6	37	A.4
4	4	28.7	37	A.5
5	5	43.1	37	A.6
6	6	33.4	37	A.7

Table 3.4: Comparison between APD and CPeT-IT values for the relative density D_r at the depth 4.72m below ground level (sand).

Parameter: Friction angle ϕ (°)				
path	method	value	reference value	equation
1	1	34.1	34	A.8
2	1	34.4	34	A.8
3	2	36.2	34	A.9
4	3	38.8	34	A.10
5	4	34.7	34	A.11
6	4	35.9	34	A.11
7	4	35.2	34	A.11
8	4	33.6	34	A.11
9	4	35.4	34	A.11
10	4	34.2	34	A.11
11	4	35.9	34	A.11
12	4	37.7	34	A.11
13	4	36.7	34	A.11
14	4	34.3	34	A.11
15	4	37.0	34	A.11
16	4	35.2	34	A.11
17	5	32.7	34	A.12
18	5	33.9	34	A.12
19	5	33.2	34	A.12
20	5	31.6	34	A.12
21	5	33.4	34	A.12
22	5	32.2	34	A.12

Table 3.5: Comparison between APD and CPeT-IT values for the friction angle ϕ at the depth 4.72m below ground level (sand).

Parameter: State parameter Ψ (-)				
path	method	value	reference value	equation
1	1	-0.0428	-0.04	A.15
2	1	-0.0502	-0.04	A.15

Table 3.6: Comparison between APD and CPeT-IT values for the state parameter Ψ at the depth 4.72m below ground level (sand).

Parameter: Dilatancy angle ψ (°)			
path	method	value	equation
1	1	2.7	A.13
2	1	3.9	A.13
3	1	3.2	A.13
4	1	1.6	A.13
5	1	3.4	A.13
6	1	2.2	A.13
7	2	3.9	A.14
8	2	5.7	A.14
9	2	4.7	A.14
10	2	2.3	A.14
11	2	5.0	A.14
12	2	3.2	A.14

Table 3.7: Dilatancy angle ψ at the depth 4.72m below ground level (sand), no value is provided by the software CPeT-IT

Parameter: Elastic modulus E_s (kPa)				
path	method	value	reference value	equation
1	1	23 632	23 460	A.18
2	2	16 316	23 460	A.19
3	3	17 589	23 460	A.20
4	4	13 001	23 460	A.21
5	5	34 422	23 460	A.22
6	6	23 399	23 460	A.23
7	7	9 468	23 460	A.24

Table 3.8: Comparison between APD and CPeT-IT values for the elastic modulus E_s at the depth 4.72m below ground level (sand)

Parameter: shear wave velocity V_s (m/s)				
path	method	value	reference value	equation
1	1	132.80	132.28	A.34
2	2	158.24	132.28	A.35
3	3	125.74	132.28	A.36
4	4	111.64	132.28	A.37
5	5	129.03	132.28	A.38
6	6	111.51	132.28	A.39

Table 3.9: Comparison between APD and CPeT-IT values for the shear wave velocity V_s at the depth 4.72m below ground level (sand)

Parameter: 1-D constrained modulus M_{CPT} (kPa)				
path	method	value	reference value	equation
1	1	47 265	46 920	A.25
2	2	12 271	46 920	A.28
3	3	22 068	46 920	A.29
4	4	16 255	46 920	A.30
5	4	13 731	46 920	A.30
6	4	15 112	46 920	A.30
7	4	18 892	46 920	A.30
8	4	14 728	46 920	A.30
9	4	17 409	46 920	A.30
10	5	53 124	46 920	A.31
11	5	40 370	46 920	A.31
12	5	47 183	46 920	A.31
13	5	67 839	46 920	A.31
14	5	45 247	46 920	A.31
15	5	59 391	46 920	A.31

Table 3.10: Comparison between APD and CPeT-IT values for the 1-D constrained modulus M_{CPT} at the depth 4.72m below ground level (sand)

Parameter: shear modulus G_0 (kPa)				
path	method	value	reference value	equation
1	1	29 619	29 400	A.32
2	2	42 045	29 400	A.32
3	2	26 523	29 400	A.32
4	2	20 932	29 400	A.32
5	2	27 887	29 400	A.32
6	2	20 882	29 400	A.32
7	3	34 113	29 400	A.33

Table 3.11: Comparison between APD and CPeT-IT values for the small-strain shear modulus G_0 at the depth 4.72m below ground level (sand)

The results are overall rather satisfying since all the calculated values lie within acceptable boundaries with a similar order of magnitude compared to the reference values from the software. The APD system has not produced a single sheer unrealistic outcome, which is very encouraging. As expected, there is a noticeable variability of results for the different paths of a parameter. This variability is expressed in the table 3.12 that shows the mean and the coefficient of variation for each parameter. With the methods imported into the system, the system is able to determine the friction angle and the state parameter with a rather high accuracy. Other parameters like the elastic Young modulus (CoV = 39 %) and the constrained modulus (CoV = 57 %) show a higher variability. The interpretation of the variability of results is certainly parameter-dependent and should be performed by investigating the visited nodes of each path.

Category	E_s(kPa)	G_0(kPa)	$M_{CPT}(kPa)$	D_r(%)	V_s (m/s)	ϕ(°)	Ψ	ψ (°)
Mean value	19 690	28 857	32 727	39	127	34.8	-0.0465	3.4
CoV	39 %	24 %	57 %	16 %	12 %	5 %	8 %	34 %

Table 3.12: Mean value and coefficient of variation for all parameters

1-D constrained modulus M_{CPT} It is important to highlight that the reference value for the 1-D constrained modulus given by the software is actually an unloading-reloading modulus because the in-situ condition of the soil is over-consolidated. The additional methods for the constrained modulus are not necessarily valid for an over-consolidated state of stress, which explains why the modulus calculated by the network show a high variability.

Elastic Young modulus E_s Similarly, the variability for the Young modulus is mainly accounted for by the validity of its associated methods. From the graph A.4, it is easy to see that the value of the elastic modulus directly depends on the state of consolidation, the age and the cementation of the soil. For instance, the value from the seventh path (9468 kPa) stands out and can be classified as an outlier and should be treated carefully. The section 3.2 provides some hindsight on how to deal with such values.

Shear small-strain modulus G_0 The second method for the parameter G0 also shows a rather high variation from 21 MPa (path 6) to 42 MPa (path 2). This spread is mainly accounted for by the high sensitivity of the method 2 with respect to its input variable V_s. The shear modulus is indeed a quadratic function of the shear wave velocity, a small deviation of the input parameter results in an amplified deviation of the output parameter.

Conclusion The variability of results is thus governed by two main factors. Firstly, the sensitivity of the methods visited by a path, which mainly explains the variability between paths of a same method (e.g. G_0). Secondly, the inadequacy of the methods with respect of the soil conditions. Some correlations are indeed only valid for certain types of soil and conditions, and should not be used for a soil that does not match with these conditions.

3.2 Automated validation

The previous section showed that the system was able to yield acceptable outcomes as a first approximation for the given set of methods. To ensure flexibility of the system, it is essential for this validation process to be somewhat automatic, should the user adopt a different set of correlations. As a result, the term 'acceptable outcomes' must be specified and translated into a mathematical and computational framework.

3.2.1 Parameter value boundaries

The first type of validation is to check whether or not the parameter values lie within acceptable boundaries. These boundaries are derived from the geotechnical meaning of the parameters: a relative density cannot be greater than 100% for example. Because the system must remain flexible and because each parameter has its own range of acceptable values, it is up to the user to provide what the boundaries for each parameter are in the parameter external database . Therefore the Python class *Parameter* as defined by van Berkom [1] is now supplemented with a new attribute **constraints** which consists of a list of callable functions that allow for the validation of a computed value. Such functions could be for example:

- *lower_ bound(bound)*: checks if a newly calculated value is greater than the the lower bound.
- *upper_ bound(bound)*: checks if a newly calculated value is lower than the the upper bound.

These basic checks are performed every time a new value is assigned to a parameter. If a newly calculated value is not in compliance with these basic checks, then the value is simply removed from the system so that further calculations do not use this improper value anymore. Alternatively, a cut-off could be applied to the parameter value, should it exceeds the defined boundaries. This approach might be more in line with the current geotechnical practice (see equation A.26 for example), but this choice is left to the user.

The developers of the framework build and implement the basic callable functions for the validation, but it is the responsibility of the users to make use of them properly. The user must provide the expected lower and upper bounds for every parameter in the external database.

3.2.2 A deeper level of validation

The validation for parameter value boundaries is rather easy to perform and to implement, but more complex types of validation could be imagined. The example of the stiffness modulus is a case in point where this kind of relationship between stiffness moduli is expected:

$$E_{50} < E_s < M_{CPT}^{nc} < E_{ur} < E_0 < M_{CPT}^{oc} \tag{3.2}$$

where E_{50} is the secant stiffness at 50% of the ultimate deviatoric stress, E_s is the static secant modulus taken at 0.1% strain, E_{ur} is the unloading/reloading stiffness, E_0 the initial tangent stiffness, M_{CPT}^{nc} and M_{CPT}^{oc} the constrained modulus respectively in a normally consolidated state and an over-consolidated state. This behavior of the soil is explained by the strain dependency of stiffness (figure 3.4): as the shear strain increases during primary loading, the secant Young modulus decreases.

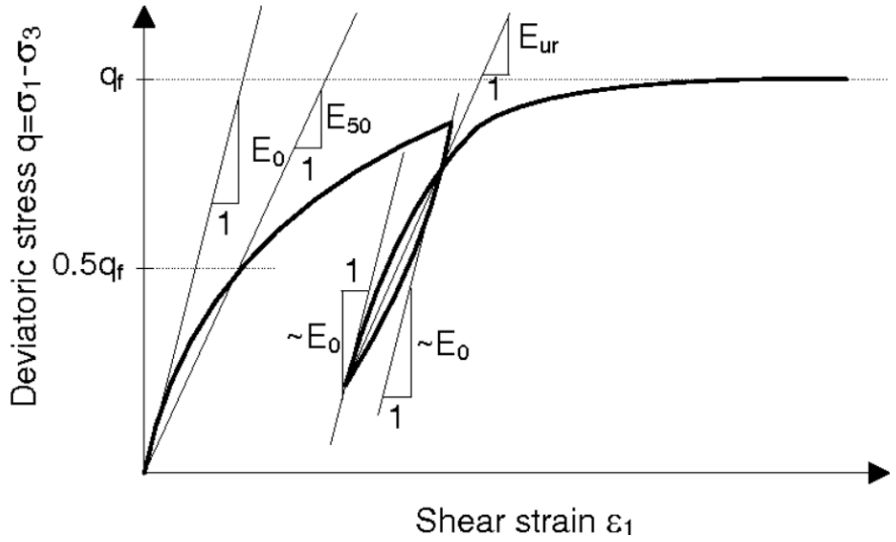

Figure 3.4: Typical stress-strain relationship for soil, the stiffness is directly related to the level of strain and the state of consolidation. Source: [2]

Because of the significant number of possible paths, it is very likely to find a combination of these six parameters for which the inequality 3.2 does not hold. The treatment of such outcome is still an open-question at this stage, but the user should always remain critical towards the values calculated by the network. From a computational point of view, the attribute **constraints** could contain a callable function that reflects the relation 3.2.

3.2.3 Method validity

It has been demonstrated that inadequate correlations sometimes cause an unacceptably large variability. Correlations are usually valid for a limited range of soils and for particular conditions. The range of applicability is most of the time clearly mentioned in the original publication of the correlation, and must be incorporated into the framework.
In a similar manner to the parameter constraints, the class *Method* is also complemented by a new attribute *validity* which consists of a list of callable functions. A non exhaustive inventory of these functions is outlined below:

- *SBT(argument)*: checks if the SBT of the method is consistent with the SBT of the soil tested.
- *Ic_ min(argument)*: checks if the Ic index of the tested soil is greater than the lower bound of the Ic index of the method.
- *Ic_ max(argument)*: checks if the Ic index of the tested soil is lower than the upper bound of the Ic index of the method.
- *consolidation(argument)*: checks if the state of stress of the soil (normally consolidated or over-consolidated) is compatible with the method.

These checks are performed before the graph is connected so that invalid correlations and methods are removed from the system before any calculation is performed. This approach requires knowledge of the SBT and the I_c index beforehand, but these basic specifications are often determined by the CPT interpretation. The state of consolidation is initially left to the user‘s judgment but it can be retroactively modified once the OCR has been computed by the system.

3.3 Dealing with circular connections

Circular connections are another point of interest. They occur when a method for a destination parameter has the same parameter as an input parameter. Since the algorithm for parameter determination is recursive, such circular connections create infinite loops and make the system crash[2]. Two options are then possible: leave the responsibility to the user to avoid creating circular connections when filling the external database, or improve the current algorithm so that it can deal with loops in a systemic manner.

3.3.1 Circular connections in geotechnical engineering

Circular connections are widespread in geotechnical engineering due to the large number of existing correlations. One very common way to deal with these loops is to assume a first initial value for the problematic parameter and perform an iterative process until convergence of that parameter. Iterative procedures are performed by Robertson [14] to compute the stress exponent and the Soil Behavior Type Index, and by Sayed [15] to calculate the friction angle for clay using index properties. The initial value should be either given by the user in the parameter external database or could be calculated by a first iteration of the network with the loops being deactivated. Two algorithms must be coded for that purpose:

- A first algorithm to browse and locate where the circular connections will occur.
- A second one to deal with the loops.

3.3.2 Bijective connections

A particular case is made for bijective connections, that is to say methods or equations that can be reversed. A function f is reversible is there exists a function $g = f^{-1}$ such as:

$$f(x) = y \iff x = g(y) \tag{3.3}$$

Most of the correlations and methods used in the network are mathematically reversible. This means that the associated connections in the graph are undirected: both directions are valid. This is not a desirable situation for parameter determination because the algorithm is designed for directed acyclic graphs. Thus, a critical question is raised: which of the two directions must be chosen? Two types of methods should be distinguished to answer this question:

- Methods defined as regression correlations: These equations were found while fitting a regression function to a database. It seems wise and natural to choose the direction of the method as it has been introduced by the author in the original paper.

  For instance, Brinkgreve et al. (2010)[16] relates the peak friction angle with the relative density such as:

  $$\phi_p = 28 + 12.5\frac{D_r}{100} \tag{3.4}$$

  This method can be reverted to determine the relative density from the peak friction angle:

  $$D_r = \frac{100}{12.5}(\phi_p - 28) \qquad \text{DO NOT USE!} \tag{3.5}$$

  It is highly recommended for the user to use the equation 3.4 instead of 3.5 because the fitting coefficients (28 and 12.5 in this case) were obtained assuming that ϕ_p was the target variable to fit the regression function.

[2] The maximum recursive depth is quickly reached

- Methods based on the theory: The equations that are purely based on physics have no intrinsic prior preferred direction. This is the case for many of the stiffness parameters (see figure 3.5). The 12 equations are in principle all equally valid, but they are also redundant and bijective.

Relationship between E and other stress-strain parameters	$E = 2G(1+\nu)$	$E = 3B(1-2\nu)$	$E = M\frac{(1+\nu)(1-2\nu)}{(1-\nu)}$
Relationship between G and other stress-strain parameters	$G = \frac{E}{2(1+\nu)}$	$G = \frac{3B(1-2\nu)}{2(1+\nu)}$	$G = M\frac{(1-2\nu)}{2(1-\nu)}$
Relationship between B and other stress-strain parameters	$B = \frac{E}{3(1-2\nu)}$	$B = \frac{2G(1+\nu)}{3(1-2\nu)}$	$B = \frac{M}{3}\frac{(1+\nu)}{(1-\nu)}$
Relationship between M and other stress-strain parameters	$M = \frac{E(1-\nu)}{(1+\nu)(1-2\nu)}$	$M = \frac{2G(1+\nu)(1-\nu)}{(1+\nu)(1-2\nu)}$	$M = 3B\frac{(1-\nu)}{(1+\nu)}$

Figure 3.5: Relationship between stiffness parameter for soils: Young Modulus E, shear modulus G, bulk modulus B and constrained modulus M. It is unclear which equations should be chosen. Source: [3]

A few propositions are outlined about how to tackle this situation. Without loss of generality, consider the equation 3.3 between two (geotechnical) parameters x and y:

- In the case where y has only one method attached to calculate this parameter, it seems reasonable to keep the method f and discard the method g. Otherwise y could no longer be determined at all.
- Experienced geotechnical engineers could also know if a direction is preferred in practice, and stick to their current practice by implementing only one of the two possibilities.
- Let us imagine that the parameters x and y can both be determined independently from the methods f and g. If the quality of the estimates of x is much better than the quality of y, then it becomes more beneficial to implement the method f over g: the quality of y improves while the quality of x is unchanged.

This section only provides some food for thought about how circular connections could be dealt with in theory, but these concepts have not been implemented into the APD system. Some bijective functions have been implemented in this thesis, this is the case of the equation A.32 for example, for which the shear stiffness is conventionally determined from the shear wave velocity.

Chapter 4

Statistical framework

The graph-based network has proven itself valuable to provide deterministic estimates of the geotechnical parameter values, however an equally central task is to measure the level of uncertainty of these estimates. This concern is particularly relevant in geotechnical engineering because soil parameters show a high inherent variability, and correlations are merely an approximation of the true complex behavior of the ground. This chapter aims at setting up a statistical framework to properly account for uncertainty in the Automatic Parameter Determination system.

4.1 Uncertainty in geotechnical engineering

4.1.1 Types of uncertainty

Since soil is a very complex and heterogeneous material, uncertainty and variability are part and parcel of geotechnical engineering practices. Uncertainty stems from various origins, Phoon and Kulhawy (1999) [4] [17] identified and distinguished three main types of uncertainty, as displayed in figure 4.1: namely the inherent soil variability, the measurement errors, and the transformation uncertainty.

The inherent soil variability is categorised as an aleatoric uncertainty since it results from natural geological mechanisms that are by definition erratic and unpredictable. Measurement errors relate to the imperfect measure of a physical parameter because of a faulty or inaccurate equipment or a biased measuring procedure for example. It is considered an epistemic uncertainty because the error can always be reduced with better measurement techniques. Most geotechnical parameters are not directly measurable with in-situ tests, therefore models are required to transform the measured parameter (the cone resistance for a CPT test) into a soil property or a soil parameter (the friction angle, for example). The majority of these transformations are actually correlations that try to fit a regression function through a cloud of data points. Therefore, these transformations are merely approximations and introduce as well a degree of uncertainty. This uncertainty relates with the discrepancy between the estimated response from the correlation, and the true unknown response in the field. The transformation uncertainty is also an epistemic uncertainty because it originates from a lack of our scientific knowledge. Moreover the underlying database of the correlations are finite, which entails an additional statistical uncertainty that could be significant for small databases.

4.1.2 Quantification of uncertainty

The agglomeration of these different types of uncertainty constitutes the total uncertainty of the design parameter. The quantification of the parameter's total uncertainty is not as straightforward as the quantification of the parameter values. This study defines the uncertainty either in terms of standard deviation σ, or in terms of coefficient of variation CoV, which is simply the standard deviation normalized by the mean value μ.

$$CoV_X = \frac{\sigma_X}{\mu_X} \tag{4.1}$$

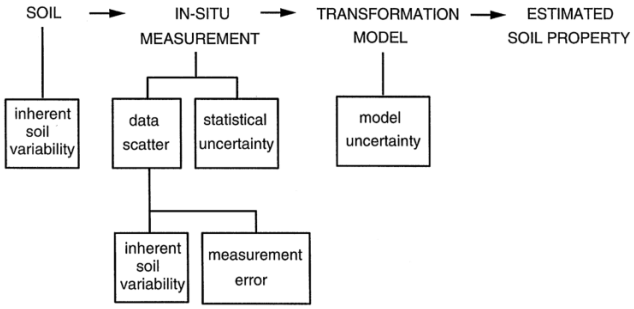

Figure 4.1: General illustration of the types of uncertainties in geotechnical engineering. source: [4]

The coefficient of variation as defined in 4.1 is dimensionless and provides a quick idea of the degree of uncertainty. A CoV around 10% is generally regarded as low in geotechnial engineering, while a CoV of 30 % is considered high [18].

Since our approach to automatic determination of parameters is based on correlations, the task will be to investigate how uncertainties propagate through the different transformation functions and through the graph in general. Multiple approaches and philosophies are available in the literature about the propagation of uncertainties for mathematical functions, and it is important to note that these are very general and not necessarily specific to geotechnical engineering. A few of these methods are applied here for our network of parameters and methods.

4.1.2.1 First Order Second Moment

This First Order Second Moment (FOSM) method relies on the linearization of the transformation function using Taylor-series expansion. Phoon and Kulhawy (1999) [17] explain thoroughly how this principle is applied to various geotechnical correlations. Starting with a design parameter ξ_d determined from measurements ξ_m and a transformation function $T(\cdot)$, they define the total uncertainty of a design parameter as:

$$\sigma^2_{tot}(\xi_d) = (\frac{\partial T}{\partial w})^2\sigma^2_w + (\frac{\partial T}{\partial e})^2\sigma^2_e + (\frac{\partial T}{\partial \epsilon})^2\sigma^2_\epsilon \tag{4.2}$$

where w, e and ϵ are respectively the soil variability of ξ_m, the measurement error and the transformation uncertainty, σ^2_w is the variance of the soil variability, σ^2_e is the variance of the measurement error, and σ^2_ϵ is the variance of the transformation uncertainty.

It should be noted that the equation 4.2 assumes that the sources of uncertainty are all mutually independent. This approach also assumes a pairwise relationship between the design parameter ξ_d and the measured parameter ξ_m while in practice the transformation function $T(\cdot)$ may have multiple variables as explained by van Berkom [1].

4.1.2.2 Monte-Carlo simulation

The Monte-Carlo Simulation (MCS) is a very popular technique used across several fields of engineering to propagate and quantify uncertainty. MCS offers a fully stochastic framework in which the input variables of a transformation function $T(\cdot)$ are no longer considered deterministic but rather as random variables following a specified probability density distribution. Random samples of the input variable are drawn and multiple realizations of the transformation function are computed. The response of a system is evaluated for a large number of times, each realization giving a different outcome. Statistical information like the mean and the variance are then directly derived from the array of values of all the simulations.

Advantages MCS comes down to running the same transformation function over and over again for a large number of times; its implementation is therefore straightforward and easy compared

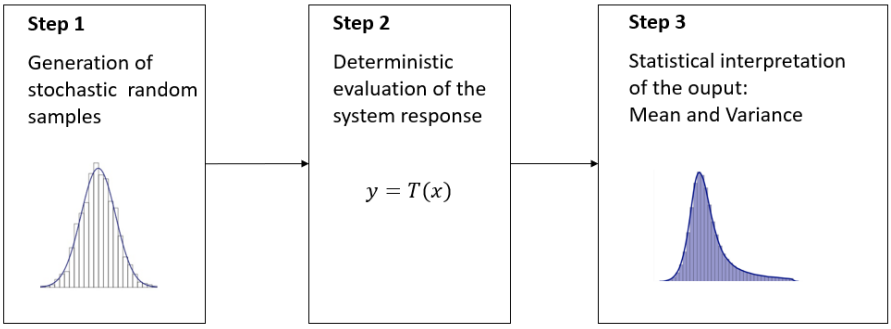

Figure 4.2: Simplified flowchart of the Monte-Carlo Simulation

to FOSM which requires the computation of the derivatives of the transformation function. As its name indicates, FOSM only provides a first order approximation that is only exact for linear functions. Monte-Carlo gives better estimate of the standard deviation when the non-linearity of the transformation function $T(\cdot)$ increases. More importantly MCS not only provide the first two moments of an output (the mean and the variance), but it also generates an histogram of the responses from which a probability distribution can be approximated. Its simplicity and its robustness make it a particularly powerful and attractive tool for engineers.

Limitations MCS requires to run a large number of realizations which can be computationally expensive if this number becomes too large or if the transformation function $T(\cdot)$ takes too much time to evaluate. Several methods have been proposed to remedy this problem: for instance the Latin Hypercube Sampling (LHS) first introduced in [19] reduces the number of required iterations for the MCS. It has been applied in a geotechnical context in [20] to determine the parameter uncertainty of sixty models for the bearing capacity factor of the soil's weight.

How many simulations should be performed? The precision of the estimated mean increases with the number of simulations. Using confidence intervals for the mean and the Central Limit Theorem, it can be proven that the required number n of MC iterations for a level of precision p is [21]:

$$n = \left(\frac{t_{1-\frac{\alpha}{2}} \cdot \sigma}{p} \right)^2 \tag{4.3}$$

where σ is the estimated empiric standard deviation of the population and $t_{1-\frac{\alpha}{2}}$ is the Student t-statistic for a risk α and for $n-1$ degrees of freedom. Assuming that the number n will be quite large, we usually have $t_{1-\frac{\alpha}{2}} = 1.96$ for a risk set at $\alpha = 5\%$ when n tends to infinity. The empirical variance σ^2 is obtained by first running the MCS for a relatively small number of iterations.

4.2 Characterization of uncertainty in the APD system

4.2.1 FOSM

Without loss of generality, we assume here a method node m of the network that is related to n input parameters $x_1, ..., x_n$ and to the single output parameter y, as shown in figure 4.3. The transformation function $f(\cdot)$ of the method m is defined:

$$y = f(x_1, ..., x_n) \tag{4.4}$$

The goal is to derive the total uncertainty of the destination parameter y based on the information we have about the method m and on our prior knowledge of the input parameters. As a result the total variance of the parameter y is decomposed in two terms: the parameter uncertainty $\sigma^2_{para}(y)$ which represents the propagated contribution of the uncertainty of the input parameters, and the method uncertainty $\sigma^2_{met}(y)$ which represents the contribution of the transformation uncertainty.

$$\sigma^2_{tot}(y) = \sigma^2_{para}(y) + \sigma^2_{met}(y) \tag{4.5}$$

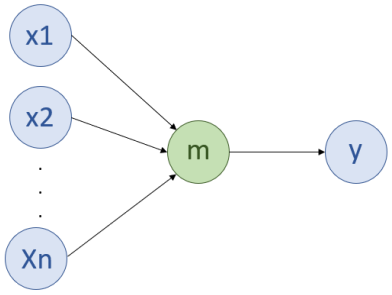

Figure 4.3: Diagram of a multivariate method

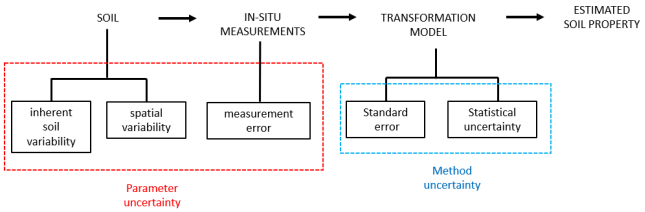

Figure 4.4: Types of uncertainties covered by the parameter uncertainty and the method uncertainty.

It is important to realise that the equation 4.5 is consistent with the formulation 4.2 from Phoon and Kulhawy. A mathematical proof is elaborated in the appendix B.

4.2.1.1 Parameter uncertainty

Each input parameter x_i is characterized with a mean value $\mu(x_i)$ and a standard deviation $\sigma(x_i)$. Applying the concept of linearization of the function $f(\cdot)$ using Taylor-series expansion, it is possible to quantify the propagation of the uncertainty of each individual variable. The parameter uncertainty of y becomes:

$$\sigma^2_{para}(y) = \sum_{i=1}^{n} (\frac{\partial f}{\partial x_i})^2 \sigma^2(x_i) \tag{4.6}$$

The derivatives of $f(\cdot)$ are evaluated at the point $\mu = (\mu(x_1), ..., \mu(x_n))$. It must be noted that equation 4.6 holds only for uncorrelated variables. In case of correlated variables, the covariances $C(x_i, x_j)$ are introduced and the parameter uncertainty of y becomes:

$$\sigma^2_{para}(y) = \sum_{i=1}^{n} (\frac{\partial f}{\partial x_i})^2 \sigma^2(x_i) + 2 \sum_{i=1}^{n-1} \sum_{j=i+1}^{n} (\frac{\partial f}{\partial x_i} \frac{\partial f}{\partial x_j}) C(x_i, x_j) \tag{4.7}$$

From a computational perspective, the derivation of the mathematical functions is required and is made possible by the formula provided in the external database. The user inserts the correlations in the database and the derivatives are automatically calculated. The definition of the standard deviation $\sigma(x_i)$ for the input parameters depends on the type of parameter node:

- **Source parameter:** If a source parameter x_i is an input variable of the method m, the standard deviation $\sigma(x_i)$ is provided by the user in the external parameter database. This standard deviation should cover both the inherent soil variability and the measurement errors of the source parameter. The systematic bias of measurement errors are not covered here. The value for $\sigma(x_i)$ must be carefully chosen to reflect the true uncertainty of the soil and because this uncertainty will propagate through the whole graph. Practical experience and literature review are paramount to determine the source parameter's variability accurately.

- **Intermediate parameter:** If a intermediate parameter x_i is an input variable of the method m, then the standard deviation $\sigma(x_i)$ of the input parameter x_i is simply the total uncertainty of this parameter calculated with the equation 4.5. This principle is similar to a chain rule.

4.2.1.2 Method uncertainty

Since the transformation models are often determined by fitting a regression trend line through a cloud of data points, uncertainty arises. Unlike the parameter uncertainty, there is no clear theoretical framework about how to derive the method uncertainty, which makes it more difficult to define it objectively. A regression function is usually described by a trend line; the scatter of points around the trend line being characterized by a zero-mean random variable with a standard deviation σ (figure 4.5).

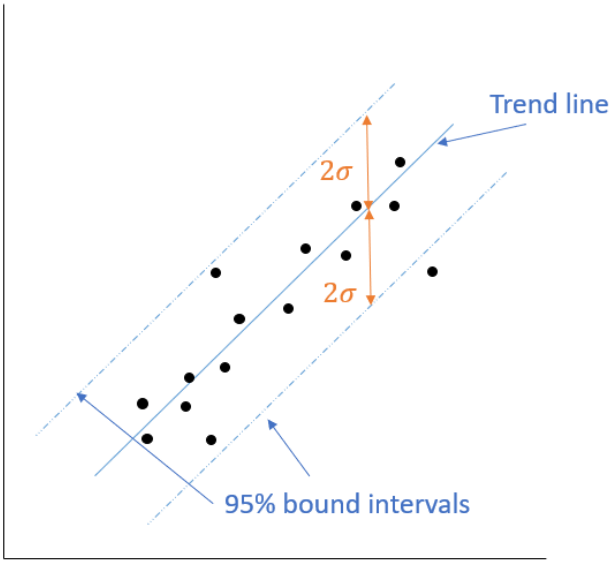

Figure 4.5: Regression trend line with the lower and upper 95% bounds. σ represents the standard error

Phoon and Kulhawy (1999) [17] define the transformation uncertainty as the standard error σ of the regressor, as it illustrates how big the uncertainty of the prediction is. A distinction is made in the statistics literature between the standard error of the prediction and the standard error of the fit, but this difference is usually not mentioned in the geotechnical literature. It is recommended to model the standard error as the **prediction standard error**, for it accounts for both the uncertainty of the mean trend and the data scatter. This method uncertainty is carefully provided by the user in the method external database. Four possibilities are suggested as for determining the right method uncertainty:

- The standard error σ is provided by the author of the correlation in the original publication, along with the number of points of the dataset and the coefficient of correlation R^2.

- A graphical estimation of the standard error is feasible if a graph with the trend line and the scatter of data points is available. This estimation relies on the "4σ" rule: the spread of the 95 % confidence interval is approximately equal to 4σ (figure 4.5). The upper and lower bounds can be drawn on the figure to estimate the standard error. Great care must be taken about the scales of the graph (linear or logarithmic scales).

- If one has access to the original database of the correlation, the standard error could be directly derived.

- In a worst-case scenario where no information is available about the goodness of the regression fit and where the database is not accessible, an arbitrary value must be set for the standard error σ, preferably based on the expert's knowledge.

Unfortunately, this means that the definition of the method uncertainty is not consistent depending on what information is available in the literature about the transformation models. This might be a conceptual problem when it comes to comparing the performance of each method. The ideal situation would be making available the databases of all the methods in order to compute the method uncertainty in a unique manner. This is a particularly time consuming task that falls out of the scope of this research, therefore a combination of the four possibilities detailed above is considered satisfying enough.

Statistical uncertainty The quality of a transformation model does not solely depends on the standard error of the regressor, but also on the number of data points. For an equal standard error, a method based on 1000 data points is arguably more reliable than method based on only 3 points. The definition of the method uncertainty must be slightly adapted to take this size effect into consideration. A characterization of the method uncertainty is proposed by [22] in equation 4.8:

$$\sigma_{met} = \sigma \cdot \frac{k}{u_\alpha} \tag{4.8}$$

where σ is the standard error of the regressor as defined in the previous section, $u_\alpha = 1.645$ for a level of confidence $\alpha = 5\%$. The definition of the factor k depends on which confidence interval is considered. For the prediction interval of the whole population, the factor k is defined by:

$$k = t_{n-1}^{\alpha}\sqrt{1 + \frac{1}{n}} \tag{4.9}$$

where n is the number of data points, and t_{n-1}^{α} is the Student t-statistic for a risk α and for a degree of freedom set at $n - 1$. For the confidence interval of the mean trend, the k becomes:

$$k = t_{n-1}^{\alpha}\sqrt{\frac{1}{n}} \tag{4.10}$$

The type of confidence interval considered is an engineering choice. In the rest of this study, the prediction interval of the population has been selected. To summarize, the statistical uncertainty encompasses several aspects: a level of confidence α typically taken at 5%, a t-Student correction t_{n-1}^{α}, the number of data points and the choice of confidence interval.

Regression technique's uncertainty Depending on which regression technique is used to fit a trend line through a database, different correlation functions can be obtained. This adds another uncertainty linked to the choice of the regression technique (Ordinary Least Squared, Total Least Squared, ...). The type of regression is very rarely mentioned in the original publications, therefore it is totally discarded in this study.

4.2.1.3 Implementation of the total uncertainty in Python

The Python system requires some adaptation to include this description of the statistical framework. The main modifications concern the *Parameter* and the *Method* classes.

Parameter class: The attribute *Accuracy*, which had a vague and general definition, has been refactored into the attribute *sd* [1], which corresponds to the total uncertainty of the parameter as defined in equation 4.5. Hence, both the value and the standard deviation are calculated for every path of the graph. The external parameter database must contain the total uncertainty of the source parameters.

Method class: Two attributes have been added to the *Method* class: *method_sd* and *para_sd*. The method standard deviation for each method is provided by the user in the method external database according to the equation 4.8, while a dedicated Python function computes the parameter deviation according to the equation 4.6 or 4.7. The attribute *output_accuracy* is now returning the outcome of equation 4.5.

[1] sd stands for standard deviation

4.2.1.4 A very basic example

This simple graph shown in figure 4.6 is meant to illustrate how uncertainty propagates through a network using FOSM. The user needs to provide four initial values to the system: the mean value of parameter a and its total uncertainty $\sigma_{tot}(a)$, and the method uncertainty $\sigma_{met}(b)$ and $\sigma_{met}(c)$ of the two methods $m1$ and $m2$. The total uncertainty of parameter b is calculated combining 4.5 and 4.6:

$$\sigma^2_{tot}(b) = \sigma^2_{tot}(a)(\frac{\partial m_1}{\partial a})^2 + \sigma^2_{met}(b) \tag{4.11}$$

The total uncertainty of the destination parameter c is calculated similarly:

$$\sigma^2_{tot}(c) = \sigma^2_{tot}(b)(\frac{\partial m_2}{\partial b})^2 + \sigma^2_{met}(c) = [\sigma^2_{tot}(a)(\frac{\partial m_1}{\partial a})^2 + \sigma^2_{met}(b)] \cdot (\frac{\partial m_2}{\partial b})^2 + \sigma^2_{met}(c) \tag{4.12}$$

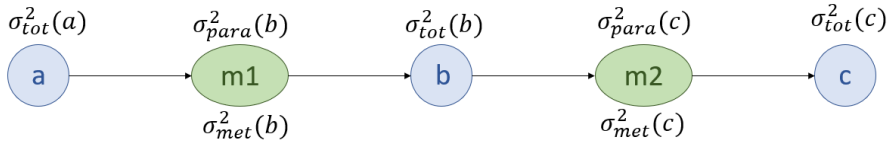

Figure 4.6: Basic graph for two methods and three parameters. a is the source parameter, b is a intermediate parameter and c is the destination parameter.

uid	formula	parameter_in	parameter_out	method_sd
b_method_1	$a+1$	a	b	4
c_method_1	$2b+2$	b	c	8

Table 4.1: External database for the methods of the basic example.

Starting from a parameter a with a value $a = 10$ and a standard deviation $\sigma(a) = 3$, we obtain with hand calculations the following results for the parameters b and c:

$$\sigma^2_{tot}(b) = \sigma^2_{tot}(a)(\frac{\partial m_1}{\partial a})^2 + \sigma^2_{met}(b) = 3^2 \cdot 1 + 4^2 = 25 \tag{4.13}$$

$$\sigma^2_{tot}(c) = \sigma^2_{tot}(b)(\frac{\partial m_2}{\partial b})^2 + \sigma^2_{met}(c) = 5^2 \cdot 4 + 8^2 = 164 \tag{4.14}$$

4.2.1.5 Test case: a less basic graph

The FOSM approach is then applied to a slightly more complex imaginative graph in order to verify that the standard deviations computed by the system are mathematically correct. The tables 4.2 and 4.3 summarize the external dataset of methods and parameters used to generate this test graph.

uid	formula	parameter_in	parameter_out	method_sd
c_method_1	$a+b$	a, b	c	1
c_method_2	$a+2b$	a, b	c	1
d_method_1	$a+c$	a, c	d	1
d_method_2	$a+2c$	a, c	d	1
e_method_1	$c+d$	c, d	e	1
e_method_2	$b+2d$	b, d	e	1

Table 4.2: External database for the methods of the test case.

The figure 4.7 displays the generated graph for the given external database along with the value and the total standard deviation of every path. The table 4.4 compares the total standard deviations of the parameter e with hand calculations. The values match almost perfectly, with minor differences likely due to rounding errors. This assessment confirms that the FOSM has been properly implemented in the system.

symbol	value	std_deviation
a	5	0.8
b	3	0.7
c	-	-
d	-	-
e	-	-

Table 4.3: External database for the parameters of the test case.

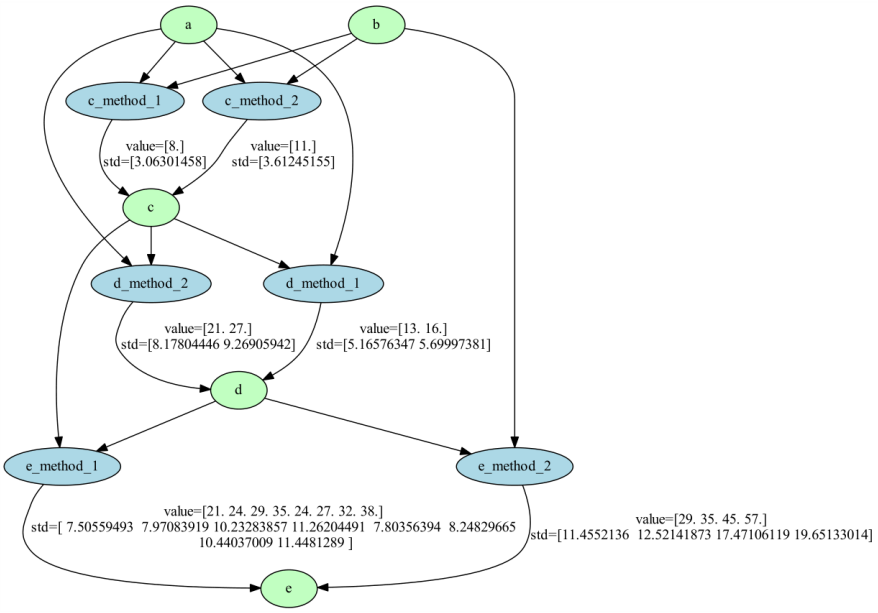

Figure 4.7: Graph of the test case with the external databases defined in tables 4.2 and 4.3.

4.2.1.6 Actual case: with geotechnical correlations

Now that FOSM has been proven to provide the right mathematical standard deviations, it is now tested on a set of geotechnical correlations. The parameters and methods used for the validation of parameter values in chapter 3 are used once again for the validation of the parameter deviations. The annex A.2 describes all the imported methods for this case study and gathers valuable statistical information: the standard deviation of the correlation σ, the number of data points and the coefficient of correlation R.

The source parameters for automatic parameter determination based on CPT correlations are the cone resistance q_c, the sleeve friction f_s, the measured pore pressure u, the depth z, the water unit weight γ_w, the reference pressure p_a taken as the atmospheric pressure, and the cone area ratio a. All the correlations should ideally be established based from these input parameters, but a separate module for CPT interpretation introduces other secondary source parameters: the SBT Index I_c, the vertical total and effective stresses σ_{v0} and σ'_{v0}, the stress exponent n and finally the normalised cone resistance Q_{tn}. These secondary input parameters could be determined in theory from the primary source parameters, but it would require an iterative process that is not supported yet by the system. As a result, all the parameters mentioned above must be provided with a total uncertainty in the external database. The table 4.5 summarizes the input of the system for a given depth. The parameter a, γ_w, and p_a are assumed deterministic, therefore their deviation is equal to 0. It is assumed that the coefficient of variation of the cone resistance q_c and the sleeve friction f_s is set at 40%, which corresponds to the typical range of variation for these parameter [4]. It covers both the inherent soil variability and the measurement errors of the CPT. The standard deviation for the remaining parameters have been approximated by hand calculations, using a propagation law of uncertainty. Finally, the parameters are supposed mutually independent for this case study: their covariances are then reduced to 0.

path	value	system σ_S	hand calculation σ_h
e1	21	2.62679	2.62650
e2	24	2.89310	2.89286
e3	29	3.64554	3.64545
e4	35	4.37836	4.37832
e5	24	2.89310	2.89286
e6	27	3.13688	3.13686
e7	32	3.84187	3.84118
e8	38	4.54313	4.54311
e9	29	4.07062	4.06998
e10	35	4.73814	4.73811
e11	45	6.49076	6.48913
e12	57	8.10247	8.10243

Table 4.4: Comparative table for the parameter e. σ_S is the total standard deviation computed by the APD system, σ_h is the total standard deviation derived by hand calculations

symbol	unit	value	std_deviation	CoV
depth	m	4.72	0	0 %
a	-	0.8	0	0 %
q_c	kPa	2520	1008	40 %
q_t	kPa	2530	1008	40 %
f_s	kPa	15	6	40 %
γ_w	kPa	9.807	0	0 %
p_a	kPa	100	0	0 %
I_c	-	2.05	0.21	10.2 %
n	-	0.65	0.11	16.9 %
σ_{v0}	kPa	75.72	6	7.9 %
σ'_{v0}	kPa	34.42	6	17.4 %
Q_{tn}	-	48.92	19.8	40.5 %

Table 4.5: External database for the source parameters of the geotechnical case. Parameters are given at the depth z = 4.72m.

The results of the system for the friction angle as a destination parameter are detailed in table 4.6. The standard deviation is calculated for all the paths. The coefficient of variation indicates the accuracy of each path.
For visualization purposes, the result of each path is now considered a normally distributed random variable whose mean values and standard deviations are defined as in table 4.6. This assumption needs to be verified to be used in the context of parameter determination for an actual civil engineering project, but it allows to visualise nicely the outcomes of each path (figure 4.9).

In the case of the friction angle (figure 4.9), the variability of results is not very pronounced, as the global mean is fairly close to the value given by the software *CPeT-IT* and the distributions are all superposing each other. Other parameters like the 1-D constrained modulus M_{CPT} are displaying another behavior (figure A.5) with clusters of paths that perform totally differently, the interpretation of such parameter is therefore made more difficult. A close inspection of the paths for the constrained modulus reveals that the clustering effect is explained by the sensitivity of the constrained modulus to the state of consolidation. Some methods are more suitable for a normally consolidated soil (equations A.25 and A.31) and yields a low parameter value compared to the methods adapted to an over-consolidated state (equations A.28 and A.30) The uncertainty of the friction angle remains rather small with a coefficient of variation around 10%, but other parameters like the relative density D_r shows a greater variability of results (figure 4.11) with potential values that could be unrealistic: there is indeed a non-negligible probability for the relative density to be negative. In that case one could consider using a different probability density function like a log-normal distribution to avoid obtaining absurd values for the relative density.

The spider chart in figure 4.8 displays the average COV for several destination parameters based

path	method	value	std_deviation	CoV
1	1	34.05	4.40	13%
2	1	24.41	3.29	10 %
3	2	36.18	3.87	11 %
4	3	38.81	3.48	9 %
5	4	34.67	2.13	6 %
6	4	35.89	2.70	8 %
7	4	35.20	2.48	7 %
8	4	33.59	2.30	7 %
9	4	35.39	1.96	5 %
10	4	34.18	1.96	6 %
11	4	35.92	2.96	8 %
12	4	37.73	3.86	10 %
13	4	36.70	3.50	10 %
14	4	34.31	3.21	9 %
15	4	36.98	2.70	7 %
16	4	35.19	2.69	7 %
17	5	32.67	3.89	12 %
18	5	33.89	4.23	12 %
19	5	33.20	4.08	12 %
20	5	31.59	3.98	12 %
21	5	33.39	3.79	11 %
22	5	32.18	3.79	11 %

Table 4.6: Output values and standard deviation for the friction angle ϕ. 22 paths for 5 methods

on an initial COV of 40 % for the initial parameters. This kind of chart illustrates how the uncertainties propagate through the graph. Some parameters like the friction angle ϕ_p or the the shear velocity V_s are rather insensitive to the initial uncertainty while the stiffness parameters are quite sensitive.

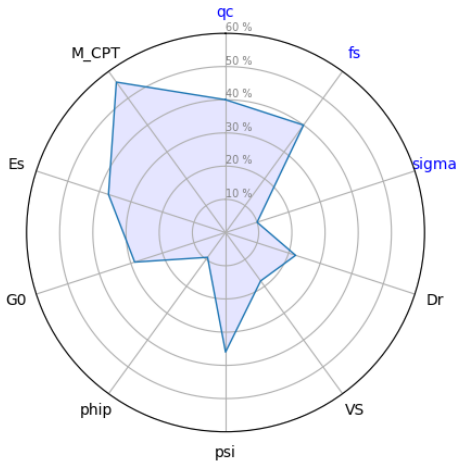

Figure 4.8: Spider chart illustrating the sensitivity of the COV of the destination parameters (in black) to the initial uncertainty of the source parameter (in blue).

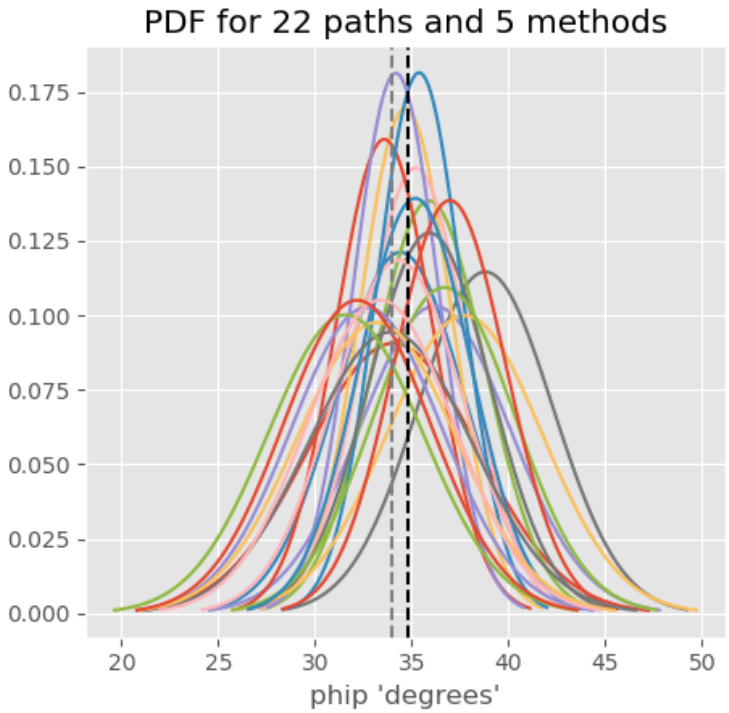

Figure 4.9: Normal probability distributions of the friction angle for all the paths. The black dashed line represents the global mean, the grey dashed line represents the value given by the software *CPeT-IT*.

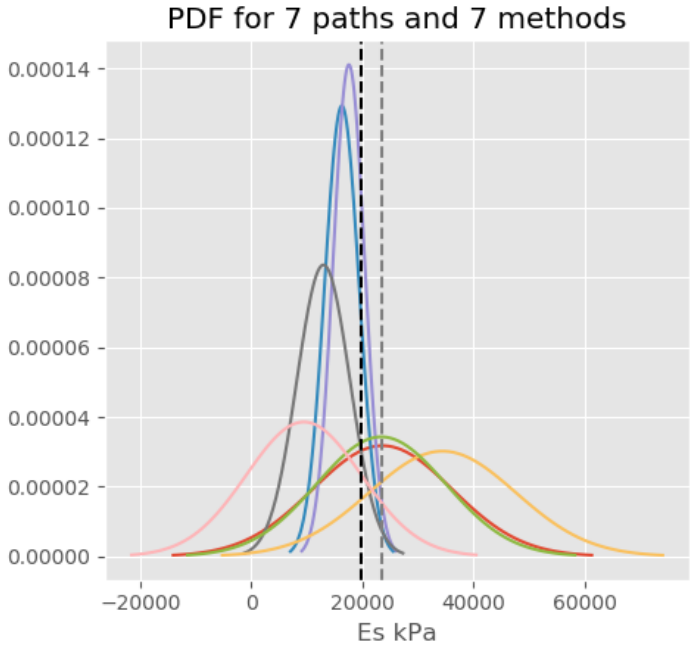

Figure 4.10: Normal probability distributions of the Young modulus for all the paths. The black dashed line represents the global mean, the grey dashed line represents the value given by the software *CPeT-IT*.

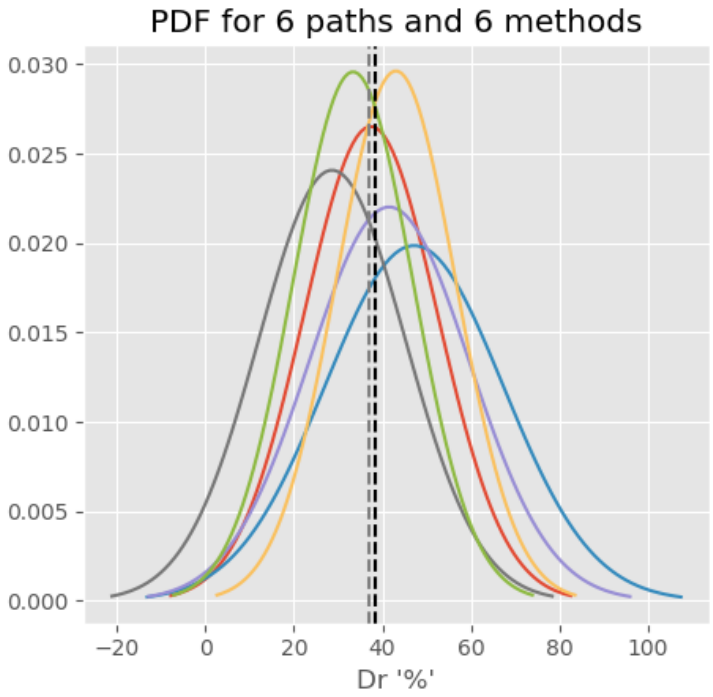

Figure 4.11: Normal probability distributions of the relative density for all the paths. The black dashed line represents the global mean, the grey dashed line represents the value given by the software *CPeT-IT*.

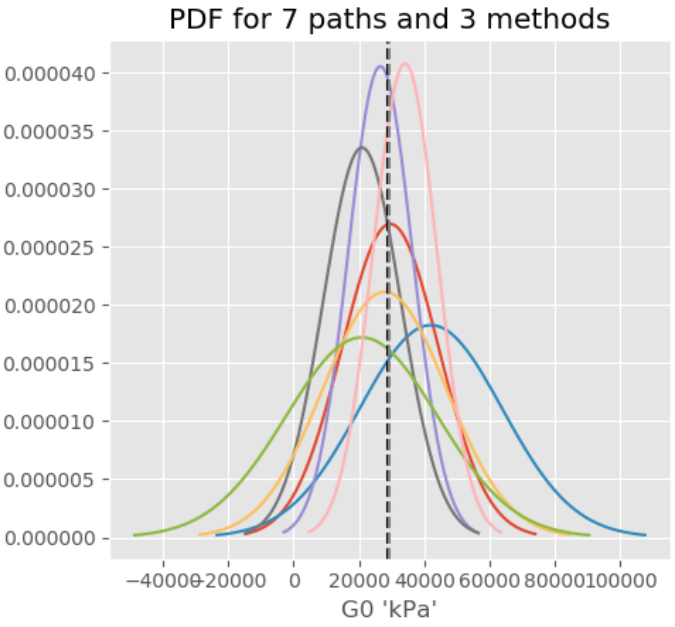

Figure 4.12: Normal probability distributions of the small strain shear stiffness G_0 for all the paths. The black dashed line represents the global mean, the grey dashed line represents the value given by the software *CPeT-IT*.

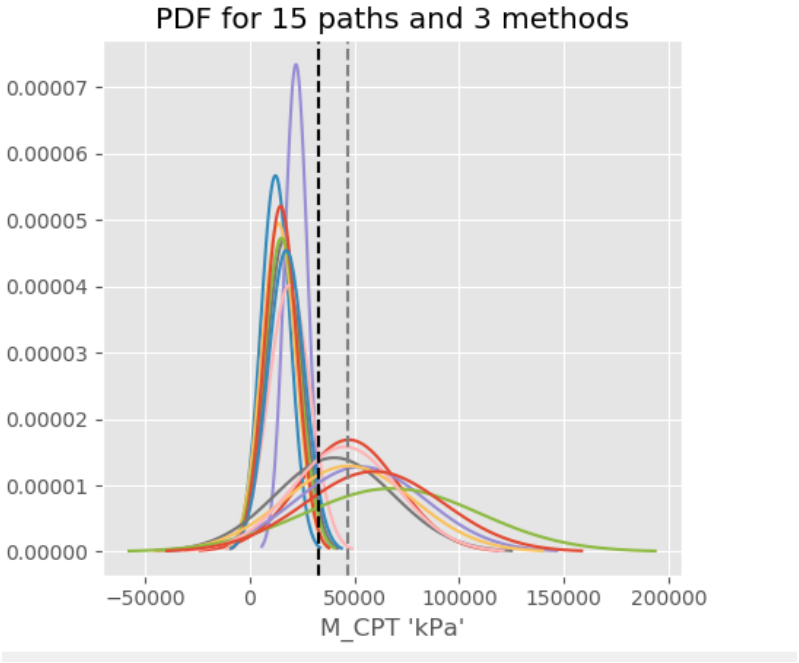

Figure 4.13: Normal probability distributions of the 1-D constrained modulus for all the paths. The black dashed line represents the global mean, the grey dashed line represents the value given by the software *CPeT-IT*.

path	method	value (kPa)	std_deviation (kPa)	CoV	Consolidation state
1	1	47 265	23642	50%	OC
2	2	12 271	7035	57 %	NC
3	3	22 068	5430	25 %	NC
4	4	16 255	8497	52 %	NC
5	4	13 731	8057	58 %	NC
6	4	15 112	8425	55 %	NC
7	4	18 852	9920	52 %	NC
8	4	14 728	7650	52 %	NC
9	4	17 409	8776	50 %	NC
10	4	53 124	31 142	59 %	OC
11	4	40 370	28 717	70 %	OC
12	4	47 183	30 776	65 %	OC
13	4	67 839	41 803	62 %	OC
14	4	45 247	25 198	56 %	OC
15	4	59 391	32 942	55 %	OC

Table 4.7: Output values and standard deviation for the 1-D constrained Modulus M_{CPT}. 15 paths for 4 methods

Conclusion: The FOSM approach has been successfully implemented into the system which is now able to provide both a mean value and a standard deviation of the parameter for every path. Based on this information, the user has a better idea of the accuracy of each method and can choose a single final parameter value accordingly. However it is unclear which type of distribution is the most suitable, and this choice depends on the parameter considered.

4.2.2 Monte-Carlo

Based on the principle explained in section 4.1.2.2, a Monte-Carlo simulation is implemented by simply running the system N times. For each simulation, a random sample is drawn for every source parameters based on the mean value and the standard deviation provided by the user. The Monte-Carlo simulation is applied in this section to a graph of geotechnical parameters and methods. The same external databases as used in section 4.2.1.6 are imported in order to compare the result from FOSM with the Monte-Carlo results. The mean values and standard deviations of the input parameters are therefore described in the table 4.5. For this case study, 2000 simulations were run for normally distributed and uncorrelated source parameters. This number of simulations is high enough to give an appropriate level of precision according to the equation 4.3.

The results of the simulations for the determination of the friction angle are shown in figure 4.14, the histogram of the 2000 simulations and the kernel density estimation (KDE) being displayed for the 22 paths. The KDE is a probability density function that tries to smoothly fit a given histogram [23]. The KDE are rather similar with the densities estimated using the FOSM approach 4.9, as they are all more or less overlaying and centered around the reference value from the software *CPeT-IT*. A statistical test has been performed for every path to verify if a normal distribution fits the histogram of the Monte Carlo simulation. The p-values[2] of this test were all extremely small, which invalidates the normality hypothesis. It should be noted that the p-values shrink to 0 as the number of simulations increases, this means that the assumption of normally distributed variables is wrong.

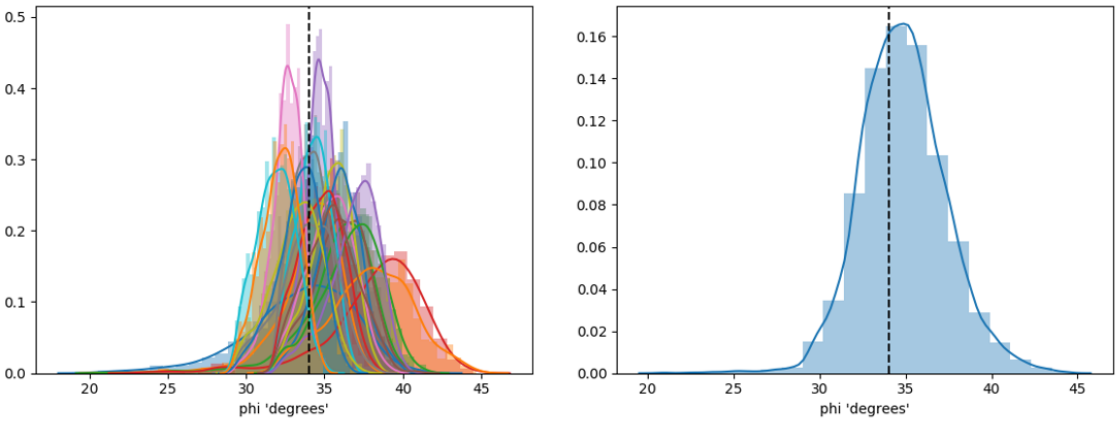

Figure 4.14: Histogram and kernel density estimation of the friction angle ϕ for 22 paths and 5 methods, with 2000 simulations. *Left:* all paths separated. *Right:* all paths cumulated. The black dashed vertical line represents the reference value given by the software *CPeT-IT*

The histograms of other geotechnical parameters are plotted below. They display some similarities with the PDF estimated in the FOSM approach. In particular, the relative density D_r exhibits a quite large variability (figure 4.15) as we already found out with FOSM (figure 4.11). A rectangular distribution seems a more reasonable choice than a normal distribution for the relative density.

Conclusion: The Monte-Carlo simulation (MCS) enables the determination of the probability density function of the parameters, which is an improvement compared to the semi-probabilistic approach FOSM which only provides the first two moments. Although the MCS confirmed the non-normality of the path's densities, the kernel distribution estimations concur rather well with the results of the FOSM approach. Both approaches provide valuable information about the spread of the parameter values in order to make an educated choice for the final parameter value.

[2] if a p-value is below the threshold 0.05, the null hypothesis of a statistical test can be rejected (https://en.wikipedia.org/wiki/P-value)

path	method	p-value	normality
1	1	$4 \cdot 10^{-3}$	No
2	1	$4 \cdot 10^{-17}$	No
3	2	$3 \cdot 10^{-8}$	No
4	3	$1 \cdot 10^{-21}$	No
5	4	$1 \cdot 10^{-67}$	No
6	4	$3 \cdot 10^{-20}$	No
7	4	$1 \cdot 10^{-24}$	No
8	4	$1 \cdot 10^{-19}$	No
9		$5 \cdot 10^{-18}$	No
10	4	$4 \cdot 10^{-19}$	No
11	4	$7 \cdot 10^{-36}$	No
12	4	$1 \cdot 10^{-7}$	No
13	4	$1 \cdot 10^{-28}$	No
14	4	$2 \cdot 10^{-15}$	No
15	4	$2 \cdot 10^{-31}$	No
16	4	$2 \cdot 10^{-12}$	No
17	5	$1 \cdot 10^{-55}$	No
18	5	$1 \cdot 10^{-12}$	No
19	5	$1 \cdot 10^{-15}$	No
20	5	$6 \cdot 10^{-7}$	No
21	5	$4 \cdot 10^{-14}$	No
22	5	$5 \cdot 10^{-17}$	No
all	all	$1 \cdot 10^{-30}$	No

Table 4.8: p-values for the normality test of the friction angle.

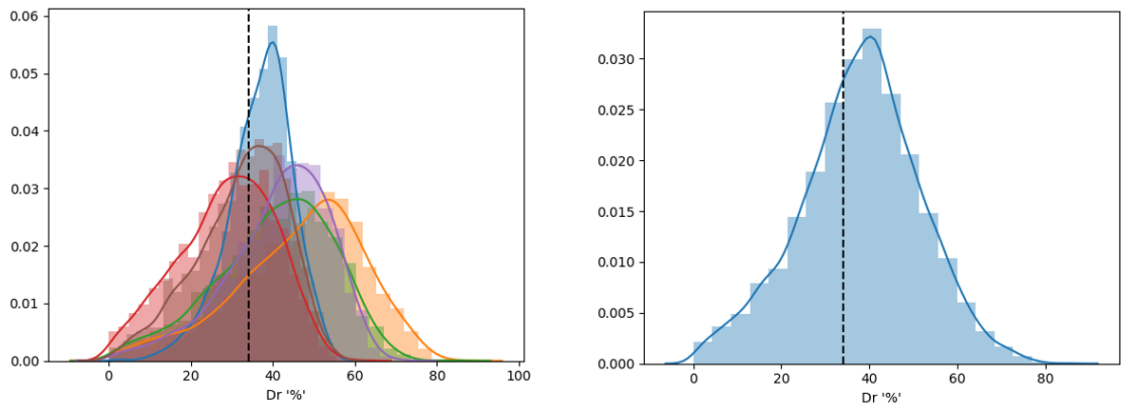

Figure 4.15: Histogram and kernel density estimation of the relative density D_r for 5 paths and 5 methods, with 2000 simulations. *Left:* all paths separated. *Right:* all paths cumulated. The black dashed vertical line represents the reference value given by the software *CPeT-IT*

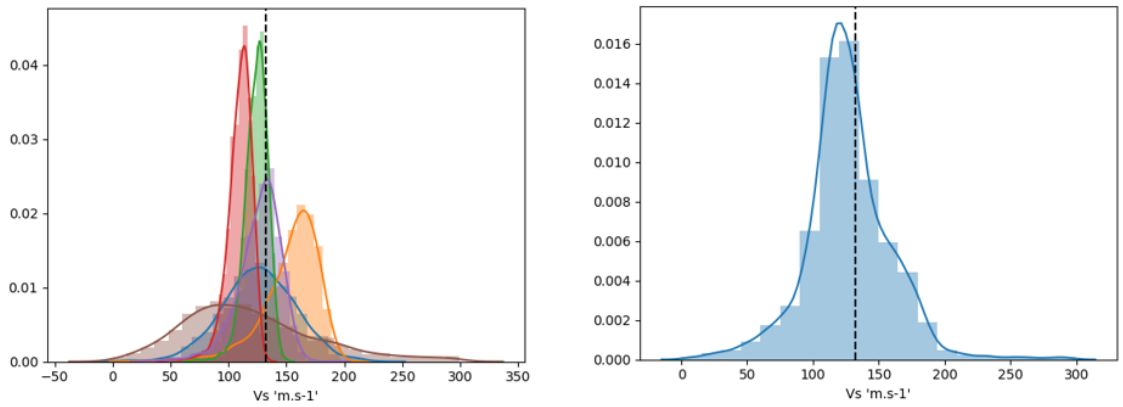

Figure 4.16: Histogram and kernel density estimation of the shear wave velocity V_s for 5 paths and 5 methods, with 2000 simulations. *Left:* all paths separated. *Right:* all paths cumulated. The black dashed vertical line represents the reference value given by the software *CPeT-IT*

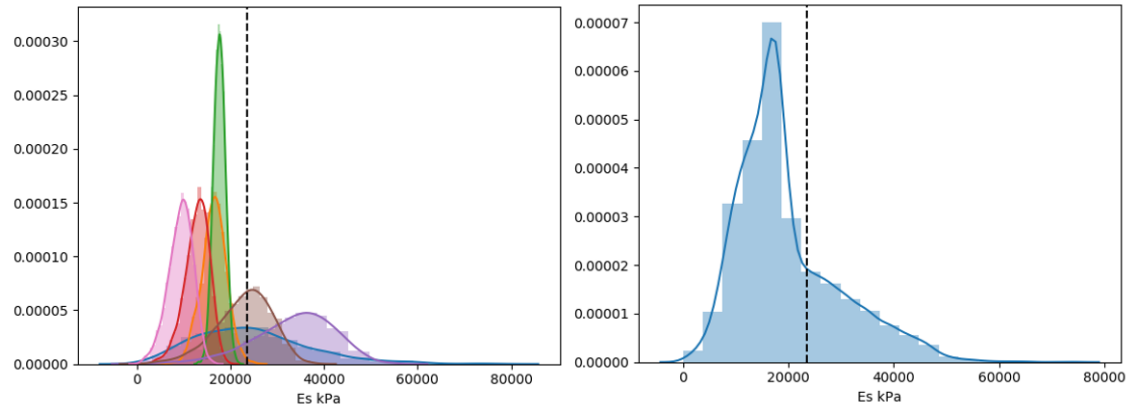

Figure 4.17: Histogram and kernel density estimation of the Young Modulus E_s for 7 paths and 7 methods, with 2000 simulations. *Left:* all paths separated. *Right:* all paths cumulated. The black dashed vertical line represents the reference value given by the software *CPeT-IT*

Chapter 5

Model averaging

The classical approach in geotechnical engineering to parameter determination often boils down to choosing a single correlation that is considered the most appropriate and reliable for that parameter given a certain soil type. In the graphs framework developed here, this is equivalent to choosing the deterministic value from a single path. This strategy completely discards the information given by the remaining paths, and is known as *Model Selection* in statistics. This approach might lead to an underestimation of the parameter uncertainty because the uncertainty related to the choice of the correlation is neglected. Conversely, *Model Averaging* takes into consideration all the correlations specified and presumably provides a better representation of the estimate of a parameter value both in terms of mean value and standard deviation, provided appropriate models are used. The principle of model averaging is elaborated in this chapter and is applied to the graph framework for parameter determination.

5.1 Basics of Model Averaging

Without loss of generality, we aim here at estimating the value of a parameter of interest θ, based on a given set of m models $(M_1, ..., M_m)$. The true value θ^* of the parameter of interest θ is unknown, this is precisely the quantity we want to approximate. Each individual model M_i provides a single estimator $\hat{\theta}_i$ along with his prediction variance $\mathrm{Var}(\hat{\theta}_i)$. We define the prediction error of the estimator $\hat{\theta}_i$ as its Mean Squared Error (MSE):

$$MSE(\hat{\theta}_i) = bias(\hat{\theta}_i)^2 + \mathrm{Var}(\hat{\theta}_i) \tag{5.1}$$

where $bias(\hat{\theta}_i)$ is the bias of the model M_i, that is to say the difference between the estimator $\hat{\theta}_i$ and the true value.

5.1.1 Averaged value

The model averaged estimator $\hat{\theta}$ is the weighted average of the estimator of all contributing models:

$$\hat{\theta} = \sum_{i=1}^{m} w_i \hat{\theta}_i \tag{5.2}$$

with w_i the weight attributed to the model M_i. The weights are naturally normalized so that their sum is equal to one:

$$\sum_{i=1}^{m} w_i = 1 \tag{5.3}$$

5.1.2 Averaged variance

The quality of the estimate $\hat{\theta}$ is quantified by its variance $\mathrm{Var}(\hat{\theta})$. The estimation of the prediction variance is not consensual as several formulations are suggested across the literature. Three averaging strategies are being investigating in this research. They yield different outcomes depending on their underlying assumptions and on the bias and variance of the contributing models.

Convolution

This strategy only considers the prediction variances of the contributing models and the covariances between the models [24] [25]. When averaging we obtain the following averaged variance:

$$\begin{aligned}\hat{\mathrm{Var}}(\hat{\theta}) &= \sum_{i=1}^{m} w_i^2 \mathrm{Var}(\hat{\theta}_i) + \sum_{i=1}^{m} \sum_{i \neq j} w_i w_j \mathrm{Cov}(\hat{\theta}_i, \hat{\theta}_j) \\ &= \sum_{i=1}^{m} \sum_{j=1}^{m} w_i w_j \mathrm{Cov}(\hat{\theta}_i, \hat{\theta}_j)\end{aligned} \tag{5.4}$$

The equation 5.4 does not take into consideration the bias of each individual model, therefore it must not be utilized when bias is expected from the contributing models, which is often the case in geotechnical engineering. We note that a positive correlation between model predictions results in an increase of the averaged variance, and a negative correlation results in a decrease of the averaged variance. The simplified case of independent models is called **Convolution** [25] and is summarised as:

$$\hat{\mathrm{Var}}(\hat{\theta}) = \sum_{i=1}^{m} w_i^2 \mathrm{Var}(\hat{\theta}_i) \tag{5.5}$$

Propagation

Unlike the previous method, **Propagation** allows the contributing models to be biased but assumes that the averaged prediction $\hat{\theta}$ defined in equation 5.2 is an unbiased estimator of the true value. This hypothesis is reasonable for bi-directional bias, that is to say a situation where the individual predictions are spread equally around the true value. Conversely, a uni-directional bias situation would occur when contributing models would consistently underestimate or overestimate the true value. The averaged variance becomes then:

$$\hat{\mathrm{Var}}(\hat{\theta}) = \Big(\sum_{i=1}^{m} w_i (\hat{\theta}_i - \hat{\theta}) \Big)^2 + \sum_{i=1}^{m} \sum_{j=1}^{m} w_i w_j \mathrm{Cov}(\hat{\theta}_i, \hat{\theta}_j) \tag{5.6}$$

It can be noticed that the second term of equation 5.6 is actually equal to the variance from equation 5.4.

Buckland

This third method is a simplification of equation 5.6 and has been derived by Buckland [26]. It assumes that models are all perfectly positively correlated and it still takes into account both the bias and the variance of the contributing models:

$$\hat{\mathrm{Var}}(\hat{\theta}) = \left(\sum_{i=1}^{m} w_i \sqrt{\mathrm{Var}(\hat{\theta}_i) + (\hat{\theta}_i - \hat{\theta})^2} \right)^2 \tag{5.7}$$

Because this formula assumes perfectly correlated models, it will provide a more conservative variance compared to equations 5.4 and 5.6.

5.1.3 Definition of weights

The definition and the determination of weights naturally influence the outcome of the averaging process. Several possibilities are available to define the weights.

Equal weights The most simple way to average values is to consider that the weights are all equal. This approach, albeit crude, can provide reasonable results if the models are all equally satisfying or if the user has no prior information on the quality of the contributing models. The weights are therefore simply defined:

$$\forall i \in [\![1, m]\!], w_i = \frac{1}{m} \tag{5.8}$$

User-defined An expert user can use his own knowledge and expertise to define himself the weights. This approach is obviously very subjective and situation-dependent. Therefore, a set of weights assigned for a specific soil should not be taken as a universal rule for another soil. The only requirement here is to normalize the sum of weights to the unity.

Bates-Granger inverse variance and inverse MSE This approach is inspired from Bates and Granger who are the pioneers of model averaging and the combination of forecasts. In their paper [27], they use the inverse of the prediction variance of the individual models as weights:

$$\forall i \in [\![1, m]\!], w_i = \frac{1/\mathrm{Var}(\hat{\theta}_i)}{\sum_{j=1}^{m} 1/\mathrm{Var}(\hat{\theta}_j)} \tag{5.9}$$

However this approach relies on the assumption that the models are unbiased, which is not necessarily the case. To deal with this shortcoming, a modification is advocated here by replacing the prediction variance by the MSE defined in equation 5.1:

$$\forall i \in [\![1, m]\!], w_i = \frac{1/MSE_i}{\sum_{j=1}^{m} 1/MSE_j} \tag{5.10}$$

Since the true value is unknown, a reference value is required to compute the MSE of the contributing models. As a first approximation, a simple average with equal weights is taken as reference value. It should be noted that the Root Mean Squared Error (RMSE) can also be used instead of the MSE in equation 5.10, which would lead to different weights.

Bayesian posterior weights (BMA) This approach is particularly valuable if a reference value is considered or if an observation of the parameter of interest is provided subsequently (from laboratory tests for example). Most [28] applies Bayesian Model Averaging using the simple mean value as the reference value. The weights are then defined:

$$\forall i \in [\![1, m]\!], w_i = \frac{\Pr\left(\bar{\theta}|M_i\right) \cdot \Pr(M_i)}{\sum_{j=1}^{m} \Pr\left(\bar{\theta}|M_j\right) \cdot \Pr(M_j)} \tag{5.11}$$

where $\Pr(M_i)$ are the prior probabilities (or prior weights) of the model M_i, and $\Pr\left(\bar{\theta}|M_i\right)$ is the likelihood of observing the value $\bar{\theta}$ given the model M_i which is formulated as:

$$\Pr\left(\bar{\theta}|M_i\right) = \frac{1}{\sqrt{2\pi \cdot V}} \exp\left(-\frac{1}{2}(\hat{\theta}_i - \bar{\theta})V^{-1}(\hat{\theta}_i - \bar{\theta})\right) \tag{5.12}$$

The drawback of this method is that not only a reference value $\bar{\theta}$ is needed, but also an estimated variance of this reference value V.

5.1.4 Conclusion

The weighted averaged value and variance result from a complex process including several components: the prediction covariances and bias of the models, the weights, and the strategy used to average the variance. This research will compare the influence of the choice of weights and strategies in the context of a graph-based determination of geotechnical parameters.

5.2 Building confidence or distrust using model averaging

5.2.1 Desired benefits of model averaging

In the context of parameter determination, the graph generates several paths for each parameter. These paths are regarded as the models in the vocabulary of model averaging. The network is able to produce for each path a single estimator of the parameter, but also its prediction variance (chapter 4). Model averaging is then applicable to the system and an averaged estimator and variance can be computed for every parameter of the network.

The goal of model averaging is to take into account the results of all the paths but also the spread of these outcomes to come up with a more reliable averaged value and variance. This approach aims at building confidence in the final parameter value in a situation where all the outcomes are roughly similar. Conversely, if the contributing paths give inconsistent results, then some distrust in the averaged value should be expected. The figure 5.1 illustrates this principle. In the first case, a single method leads to the parameter x and a single standard deviation $\sigma_{x,I}$ is calculated. The second situation introduces several models[1] from which an averaged standard deviation $\sigma_{x,II}$ is determined for the parameter x. We want model averaging to meet the following requirements:

- If the models $m_1, ..., m_M$ all give somewhat similar results, we say that the models are consistent or well aligned and the following inequality holds:

$$\sigma_{x,II} < \sigma_{x,I} \tag{5.13}$$

  This means that the averaged standard deviation is lower than the standard deviation of the individual models. In other words, we have built confidence in the value of the parameter x because all the models give more or less the same outcomes.

- If the models $m_1, ..., m_M$ all give quite different results, we say that the models are inconsistent or poorly aligned and the following inequality holds:

$$\sigma_{x,II} > \sigma_{x,I} \tag{5.14}$$

  In that case, the averaged standard deviation is greater than the standard deviation of the individual models. In other words, there is distrust in the value provided for the parameter x because the contributing models are not consistent.

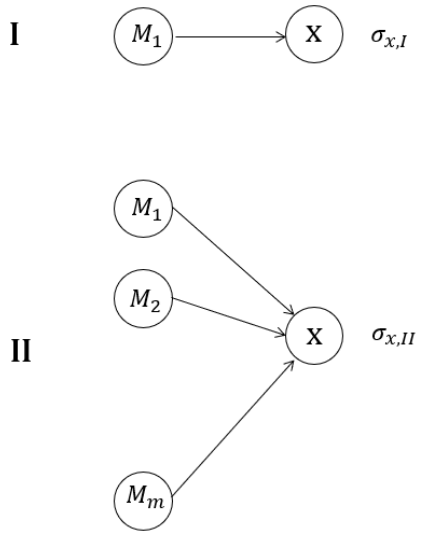

Figure 5.1: Case I: only one model is calculating the parameter x and its single standard deviation $\sigma_{x,I}$. Case II: the m models are contributing to the parameter x and an averaged standard deviation $\sigma_{x,II}$ is produced.

These desired features for our model averaging framework are examined in two examples in the following sections: one imaginary case study to illustrate the principle (section 5.2.2), and an actual case with geotechnical parameters (section 5.3).

5.2.2 Variance versus bias

As described in equation 5.1,the prediction error of an estimator is decomposed into two terms: the bias and the variance. These two components can be used to distinguish between the consistent and

[1] replace "model" by "path" in the context of graph-based parameter determination

the inconsistent models. As suggested in figure 5.2, three conceptual test cases are then identified depending on which term is dominant between the bias and the variance of the individual models. A situation where the models are poorly aligned is described by a lower variance and a greater bias, we can clearly see that the density distributions of the contributing models are all well separated. As the variance increases, or the bias decreases, the density distributions start superposing each other and the models become well aligned.

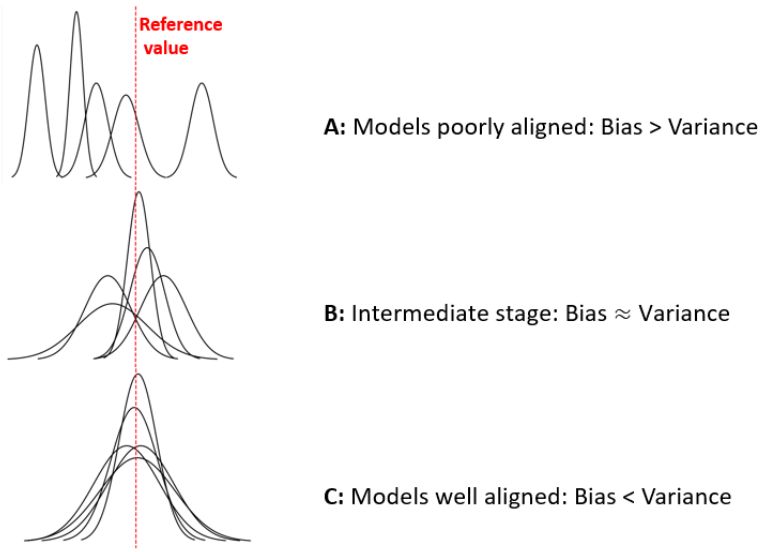

Figure 5.2: Qualitative representation of the three test cases. The contributing models are described in table 5.1.

Model averaging is then applied to these three test cases in order to investigate the effects of the choice of weights as well as the three formulas for the prediction of the variance. The three test cases consist in 5 contributing models whose characteristics are detailed in table 5.1.

Cases	Array of values	Array of standard deviations	Combined mean	Combined sd
Case A	$[97, 82, 70, 88, 120]$	$[4, 2, 2.5, 3.5, 3.5]$	91	13
Case B	$[100.140, 101.2, 98.8, 99, 100.5]$	$[0.5, 1, 1, 1.5, 0.75]$	99.9	0.937
Case C	$[100.140, 100.2, 99.8, 99, 100.5]$	$[4, 2, 2.5, 3.5, 3.5]$	99.9	1.48

Table 5.1: Description of the test cases A, B and C. A common reference value is taken as 100 for the three cases. The combined mean and standard deviation were calculated according to the *Propagation* formula.

Case A: poorly aligned models In this first case, the clear separation of the probability densities indicates a poor alignment of the models. The figure 5.3 shows the result of the averaging process for four different types of weights, and compares the averaged prediction variance. The distributions obtained using the strategies *Propagation* and *Buckland* are very similar if not identical and provide a much wider distribution (that is to say a larger variance) than the contributing models, which meets the requirement enacted in the previous section. The strategy *Convolution* is not satisfactory as the averaged distribution is even more narrow than the models themselves. It can be observed that the choice of weights has little influence on the mean value of the averaged distributions, but it has a significant impact on its variance. The equal weights approach seems to yield a very large averaged variance compared to the other methods. The weights obtained by BMA give very unsatisfying results as it consistently overfits the closest distribution to the reference value and fails to comply with the requirements.

Case B: intermediate stage The second intermediate case shows a clear decrease of the bias as the distribution densities are superposing in figure 5.4. The averaged distributions for *Convolution*, *Propagation* and *Buckland* can be distinguished. The strategy *Convolution* gives a very narrow

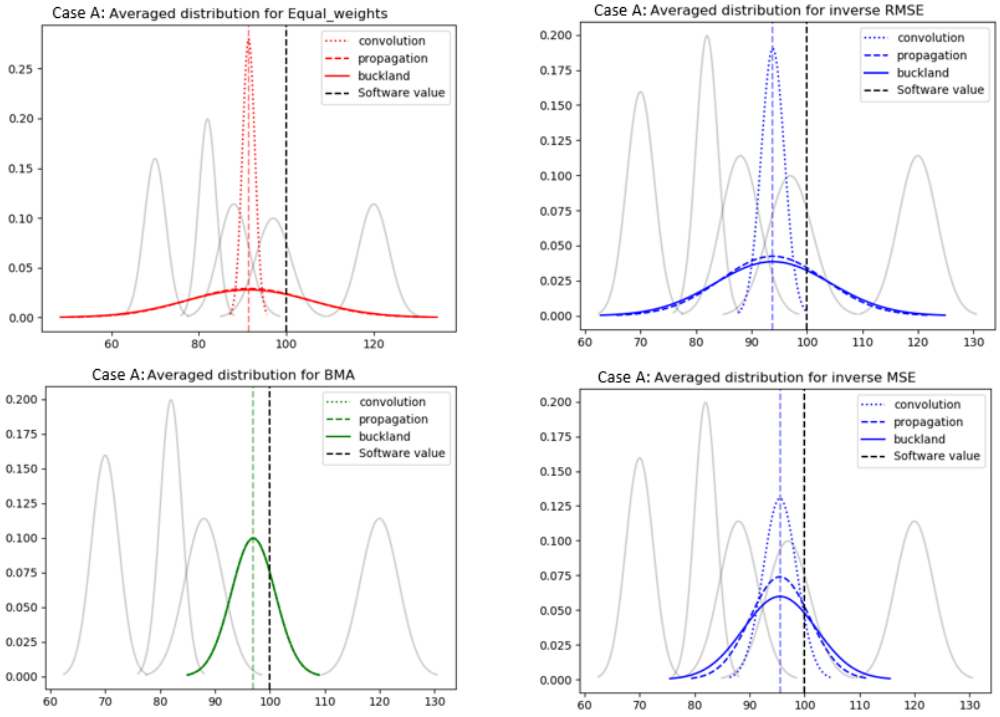

Figure 5.3: Case A: contributing and combined distributions for four types of weights and three averaging methods. The reference value is taken as the simple average. Consistency ratio $R_c = 28$. The weighting scheme BMA and the averaging strategy *Convolution* yields unsatisfying resutls.

distribution that is probably overconfident as there is still a significant fraction of bias in the contributing models. The method *Buckland* for case B is much less flat than for A but it still provides an averaged variance that is lower than the variance of the individual models. It is difficult to state if this distribution is simply conservative or over-pessimistic. The third approach *Propagation* provides an averaged distribution that is realistically confident with a variance that is slightly lower than the contributing models.

Case C: well aligned models This case depicts a situation where the models are all very well aligned as the distributions superpose almost identically in figure 5.5. As the bias is very low compared to the variance, the averaged distribution from *Convolution* and *Propagation* are identical and provide a lower averaged variance compared to the contributing models, which meets the requirement stated in the previous section. These two strategies help building confidence in the determination of the parameter of interest. There is no benefit from using *Buckland* as it gives a distribution very similar to the individual models.

The distinction between the cases A, B and C is at this stage purely qualitative and frankly subjective. The position and the width of the peaks were carefully chosen here to obtain three dissimilar cases but it could be harder in practice to determine which situation applies. In an attempt to quantitatively describe the alignment of models and reduce subjectivity when investigating the bias-variance trade-off, we define here a consistency ratio R_c as the variance of the mean values of the contributing models divided by the average of their variances:

$$R_c = \frac{\dfrac{\sum_{i=1}^{M}(\hat{\theta}_i - \hat{\theta})^2}{M}}{\dfrac{\sum_{i=1}^{M}\mathrm{Var}(\hat{\theta}_i)}{M}} = \frac{\sum_{i=1}^{M}(\hat{\theta}_i - \hat{\theta})^2}{\sum_{i=1}^{M}\mathrm{Var}(\hat{\theta}_i)} \tag{5.15}$$

A consistency ratio R_c much greater than 1 implies that the spread of the means is greater than the width of the distribution densities, and that the models are poorly-aligned. Conversely, a

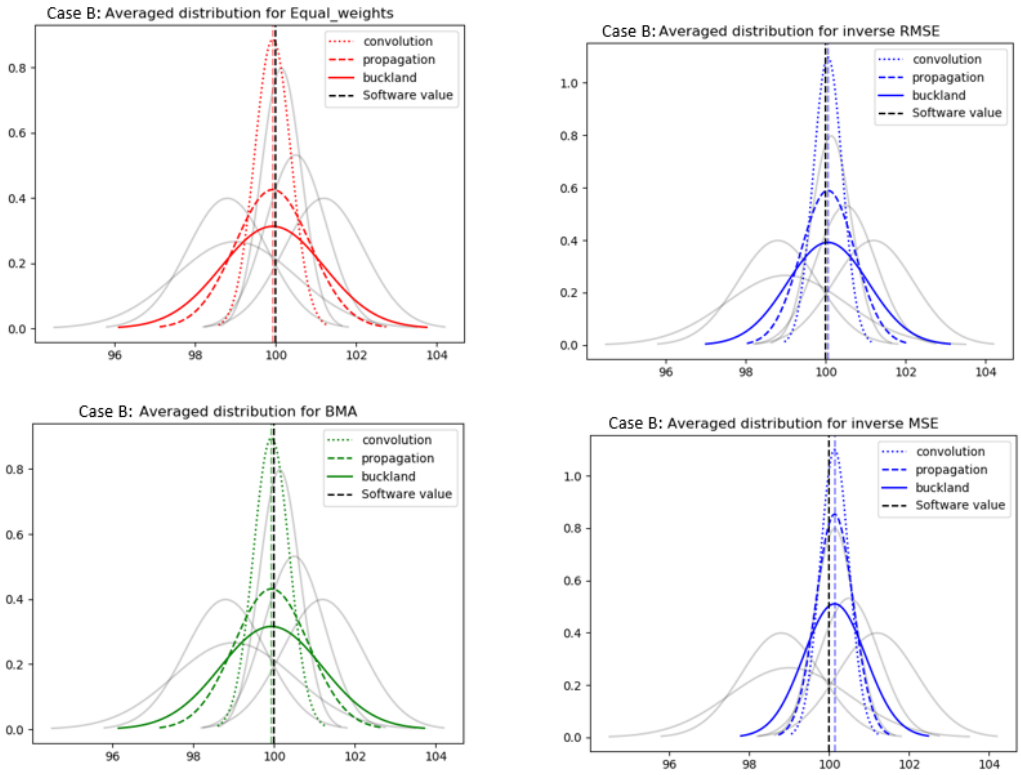

Figure 5.4: Case B: contributing and combined distributions for four types of weights and three averaging methods. The reference value is taken as the simple average. Consistency ratio $R_c = 0.81$

consistency ratio much lower than 1 would indicate that the distributions superpose and that the models are very well aligned. The intermediate stage is characterized by a consistency ratio around 1. Although this consistency ratio produces a scalar to quantitatively account for the alignment of models, it is unclear how to evaluate the quality of consistency for values of R_c between 10^{-1} and 10^{1}. Similarly, a consistency ratio for the individual model $R_{c,i}$ is defined as the ratio between the bias and the variance of the model considered, with the bias considered as first approximation as the squared distance between the model prediction $\hat{\theta}_i$ and the average $\hat{\theta}$. This could be a useful unit of measure to detect outlier models with either a very strong bias or an usual variance.

$$R_{c,i} = \frac{(\hat{\theta}_i - \hat{\theta})^2}{\mathrm{Var}(\hat{\theta}_i)} \tag{5.16}$$

5.2.3 Conclusion

This comparison has shown that the behavior of the averaged distributions depends on which term between the bias or the variance of the models is dominant. The averaged mean seemed rather insensitive to the choice of weights but the averaged variance highly depends on it. The strategy *Propagation* produced satisfying results for the three test cases as it was able to build confidence when the models were consistent, and build distrust when the models were inconsistent.

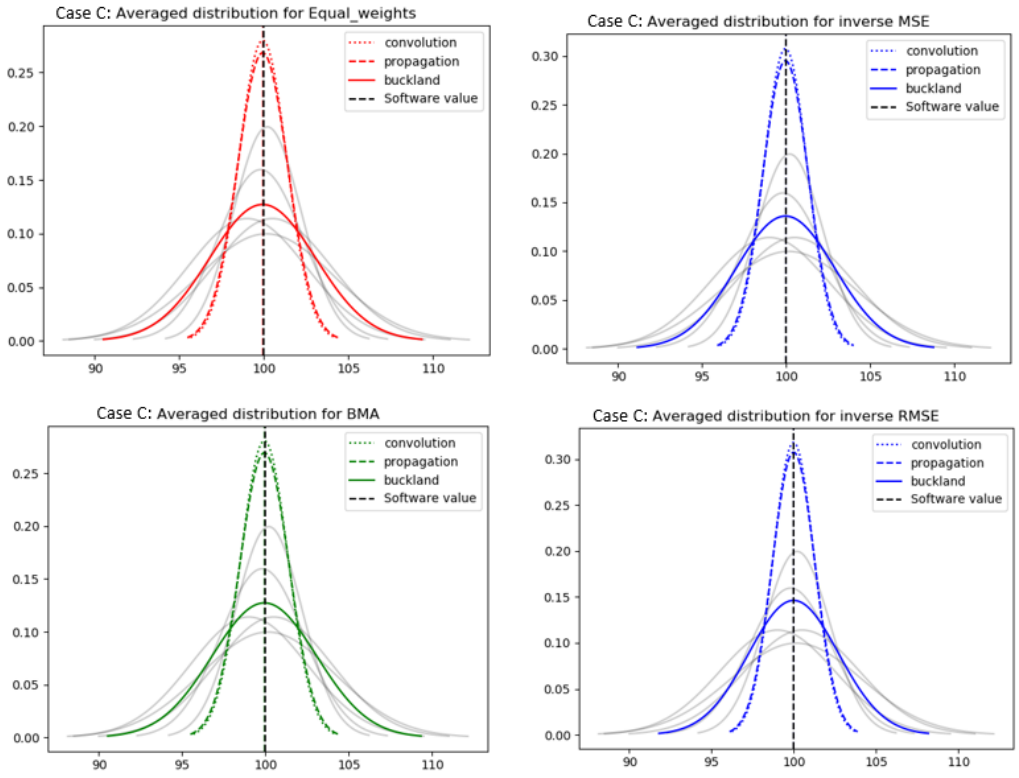

Figure 5.5: Case C: contributing and combined distributions for four types of weights and three averaging methods. The reference value is taken as the simple average. Consistency ratio $R_c = 0.0260$. The strategy *Buckland* gives unsatisfying results.

5.3 Application to geotechnical parameters

The principle of model averaging introduced in this chapter is then applied to a network of geotechnical parameters and correlations. As we have seen in the previous chapters, each parameter of the graph is characterized with an array of values and an array of standard deviations, these arrays are directly used to compute a final averaged value and variance. While applying model averaging to the graph, one should bear in mind that the paths of the network are the actual 'models' M_i we have introduced in this chapter.

This section is reusing the results obtained in chapter 4 with the standard deviations of the paths calculated from FOSM. An averaged distribution has been calculated for the three strategies (*Convolution*, *Propagation* and *Buckland*) and for four types of weights: equal weights, inverse MSE, inverse RMSE, and Bayesian Model Averaging (BMA). An arbitrary reference value was assumed for the test cases of the previous section but in practice this true reference value is unknown and taken as the simple average as a first approximation.

The results are displayed in following figures 5.6 to 5.11 for several geotechnical parameters. It is complicated to say whether or not the contributing paths are well aligned for the other geotechnical parameters, except for the relative density (figure 5.7) which has a relatively low consistency ratio $R_c = 0.14$. Indeed, the consistency ratio R_c lies between 0.2 and 0.8 for most parameters, which makes it hard to clearly distinguish between a case C of well aligned models, and a case B of intermediate models. The elastic Young modulus E_s is the only parameter that has shown a consistency ratio above 1 which is explained by the incorporation of methods that are valid for a too wide range of soils. Except from this exception, the correlations used in the system are in accordance **in general**.

The choice of weights seems to have little influence on the final averaged value, probably because the contributing paths are more or less equally satisfying and the resulting weights are not sharply contrasting with the equal weights. Nonetheless, the averaged variance slightly depends on the weights. Based on the figures 5.6 to 5.11, the density from equal weights seems to be a bit more conservative with a flatter curve compared to inverse MSE and RMSE. The table 5.2 compares the value initially provided by the software CPeT-IT, with the value obtained when applying model averaging. This table basically highlights the difference between model selection to model averaging.

The averaging strategy *Convolution* is once again not suitable as it consistently yields an over-optimistic distribution, and should be therefore discarded. For all parameters except the 1-D constrained modulus (figure 5.8), *Propagation* builds confidence in the parameter value with a lower averaged variance than the contributing paths. The approach *Buckland* remains conservative as the new distribution is flatter than the individual paths, this originates from the assunmption that the contributing models are all perfectly correlated. A special mention can be made for the 1-D constrained modulus. As mentioned earlier, the presence of the two clusters is due to methods applicable for either over-consolidated or normally consolidated soils. It makes then little sense to try averaging the paths for this parameter as the in-situ soil condition is either one or the other. In future works, the over-consolidated and normally consolidated constrained modulus must be decoupled into two distinct parameters.

parameter	paths	R_c	Software value	Equal weights	inverse MSE	inverse RMSE
ϕ (°)	22	0.28	34	34.82	34.85	34.84
D_r (%)	6	0.14	37	38.55	38.25	38.37
M_{CPT} (kPa)	15	0.72	46 920	32 726	32 597	32 482
E_s (kPa)	4	0.30	23 460	17 635	16 821	16 862
G_0 (kPa)	14	0.53	29 400	33 261	33 269	33 375
V_s (m/s)	6	0.17	132	126	125	126

Table 5.2: Comparison between values from the software CPeT-IT and the averaged means for different types of weights.

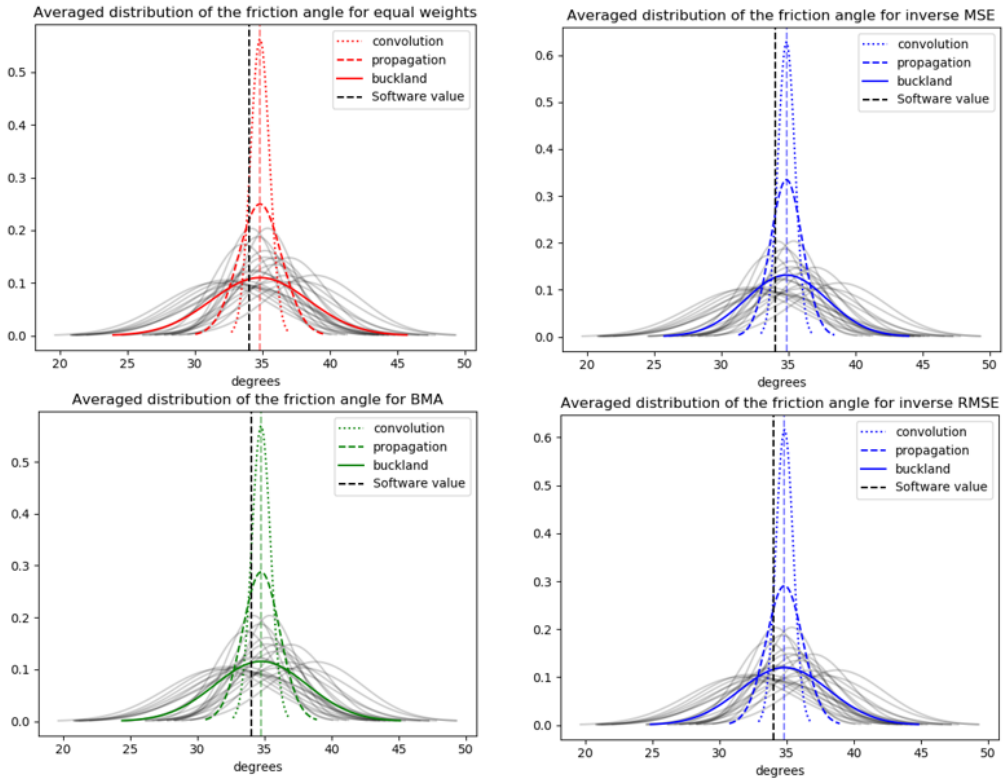

Figure 5.6: Averaged density distributions for 22 paths of the friction angle ϕ. The black dashed line represents the value given by the software CPeT-IT, set here at 34 degrees. Consistency ratio $R_c = 0.28$

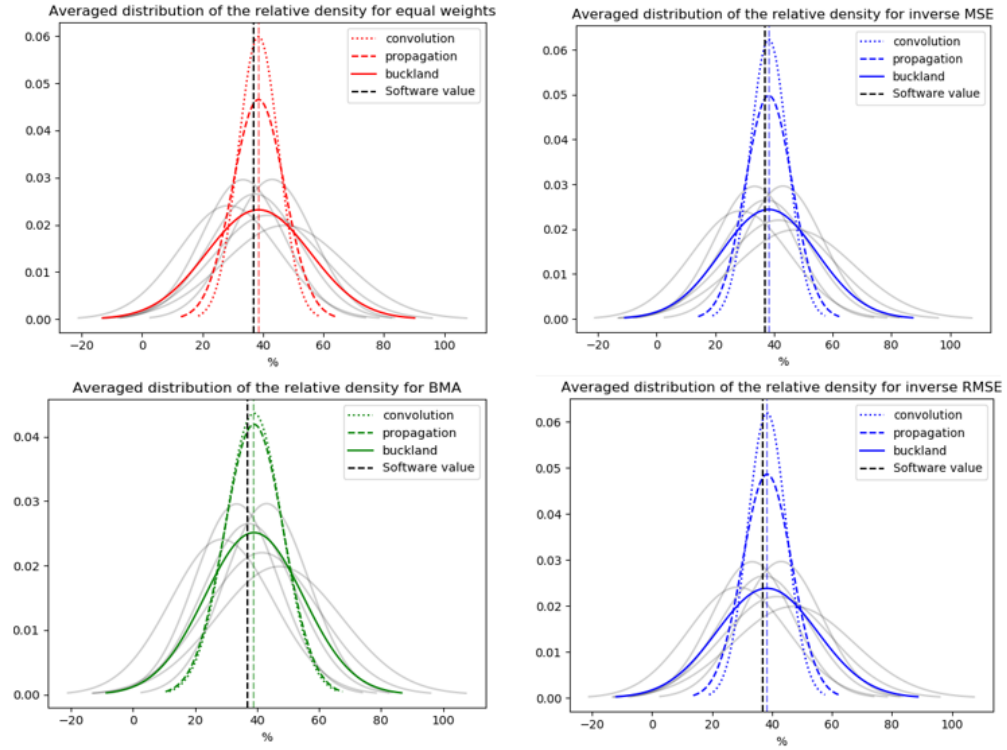

Figure 5.7: Averaged density distributions for 6 paths of the relative density D_r. The black dashed line represents the value given by the software CPeT-IT, set here at 37%. Consistency ratio $R_c = 0.14$

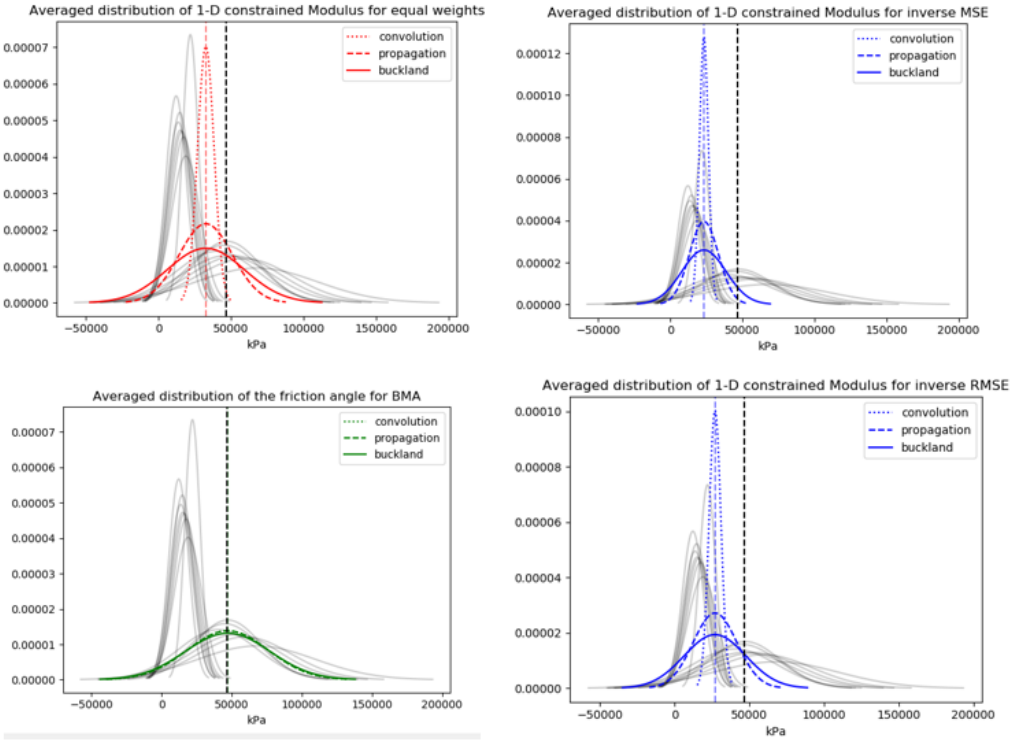

Figure 5.8: Averaged density distributions for 15 paths of the 1-D constrained modulus M_{CPT}. The black dashed line represents the value given by the software CPeT-IT, set here at 46 920 kPa. Consistency ratio $R_c = 0.72$

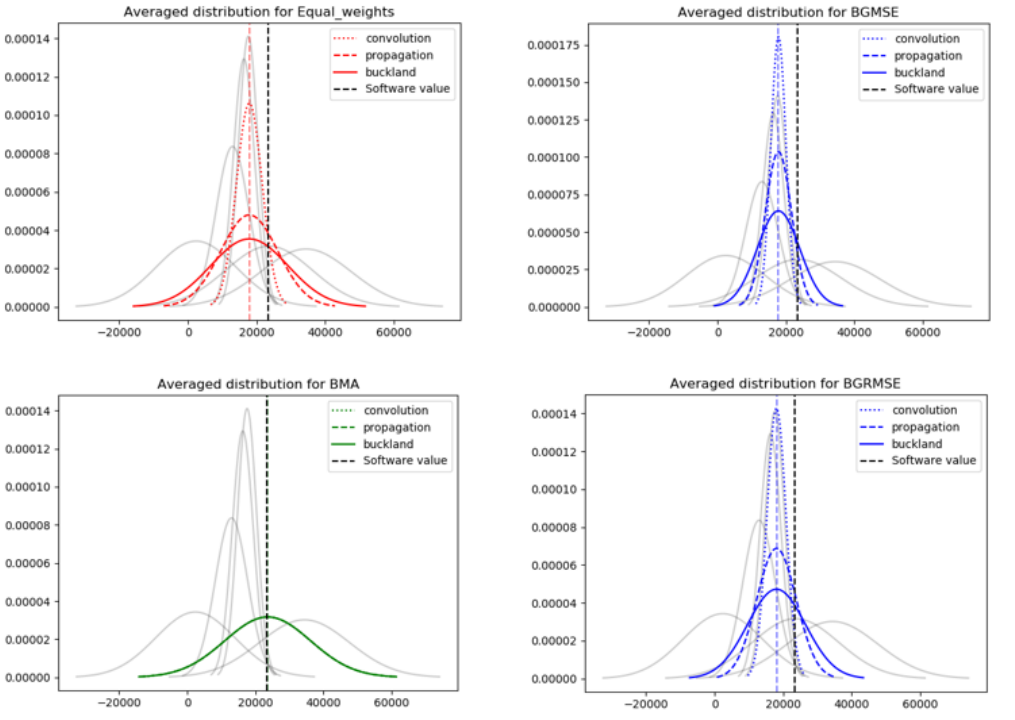

Figure 5.9: Averaged density distributions for 6 paths of the Elastic modulus E_s. The black dashed line represents the value given by the software CPeT-IT, set here at 23 460 kPa. Consistency ratio $R_c = 1.49$

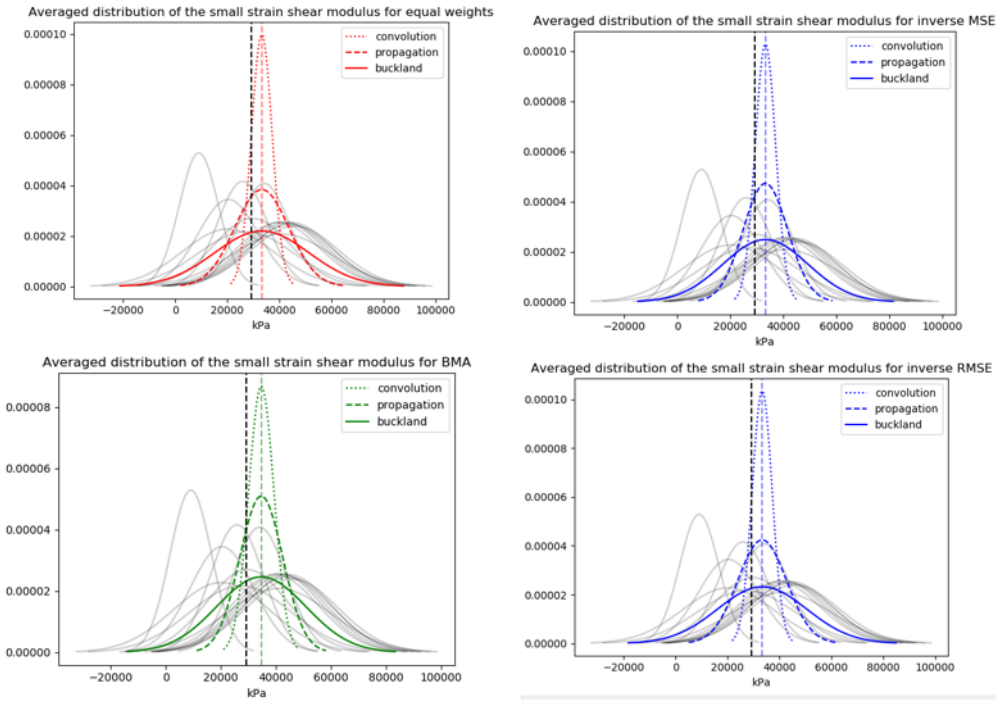

Figure 5.10: Averaged density distributions for 14 paths of the small strain shear modulus G_0. The black dashed line represents the value given by the software CPeT-IT, set here at 29 400 kPa. Consistency ratio $R_c = 0.53$

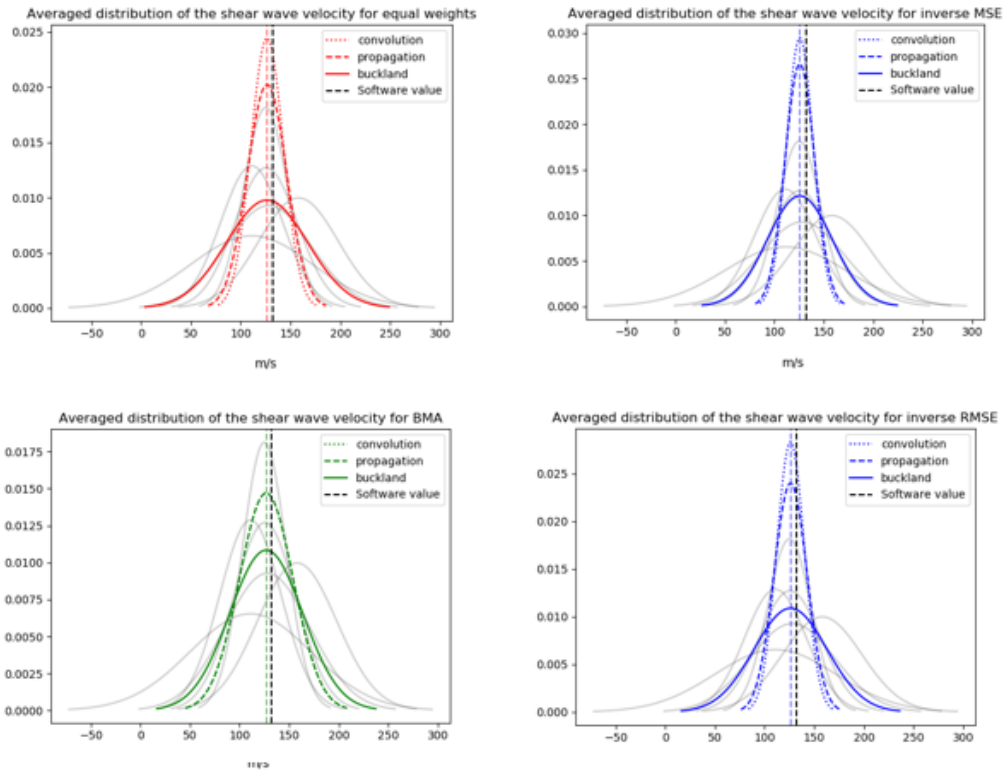

Figure 5.11: Averaged density distributions for 6 paths of the shear velocity wave V_s. The black dashed line represents the value given by the software CPeT-IT, set here at 132 m/s. Consistency ratio $R_c = 0.17$

5.4 Incorporating the Soil Behavior Type in model averaging

5.4.1 Generalities

The principles of model averaging elaborated so far are remarkably general, in a sense that it can be implemented for a wide range of applications. Indeed, the determination of weights and the averaging strategies are purely based on theoretical and mathematical concepts. However, the type of soil is a critical component in geotechnical engineering and it is paramount to incorporate this aspect in the averaging process. It is clear that some correlations are more suitable for a certain type of soils, and this aspect should be reflected in the weights. The expert knowledge about the methods and correlations included in the network and their range of applicability can be incorporated into the system through user-defined weights. If a method is considered particularly reliable for the soil considered, then the method should be assigned with a higher weight.

Three variants of this approach are proposed below:

- The user defines himself the weights based on his expertise and his familiarity of the correlations, heedless of any of the mathematical considerations underlined in this chapter. The only restraint is of course the normalization of the weights. This procedure leaves a lot of room for subjectivity, as the final outcome can changed dramatically based on the selection of weights, it is not recommended for those without a lot of experience with the applied methods. However, the interpretation of results by the user may become easier and more straight-forward and the process feels a little bit more transparent.

- An hybrid technique encompassing both user-defined and theoretically-defined weights could be a reasonable compromise. A single array of weights is obtained from the combination of these two arrays of weights. The figure 5.12 shows an example of how two arrays of weights can be combined and normalized. Other combination techniques can be considered: arithmetic mean, geometric mean, harmonic mean.

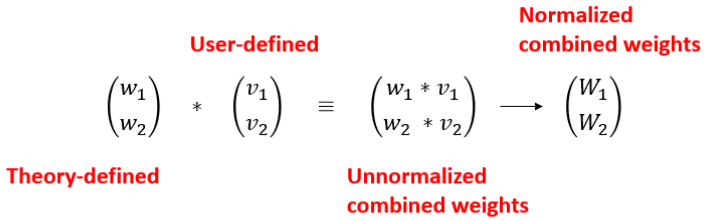

Figure 5.12: Example of the combination of two arrays of weights.

- Multiple averaging techniques require a reference value, as detailed previously. So far, the simple average has been chosen as a reference value but it would be worthwhile to pick the average determined with user-defined weights instead.

5.4.2 Characterization of the method weights

The customized method weights are incorporated into the system via the external database where the user can define for each model what the weight should be. In that case a single value for the weight is attributed to the method, preferably a number between 0 and 1. At this stage, the weights are not necessarily normalized and represent the overall validity of the method as defined by the user for a specific soil layer: the closer to 0, the less valid the method is, and conversely the closer to 1, the more suitable the method is. It is recommenced to assign a weight equal to 1 for analytical methods as they are assumed unconditionally correct, and a weight lower than 1 to the methods based on empirical correlations.

So far, this characterization only describes constant piecewise weights for the methods, as shown in figure 5.13. Additionally, weights can also be interpolated for any value of the I_c index provided

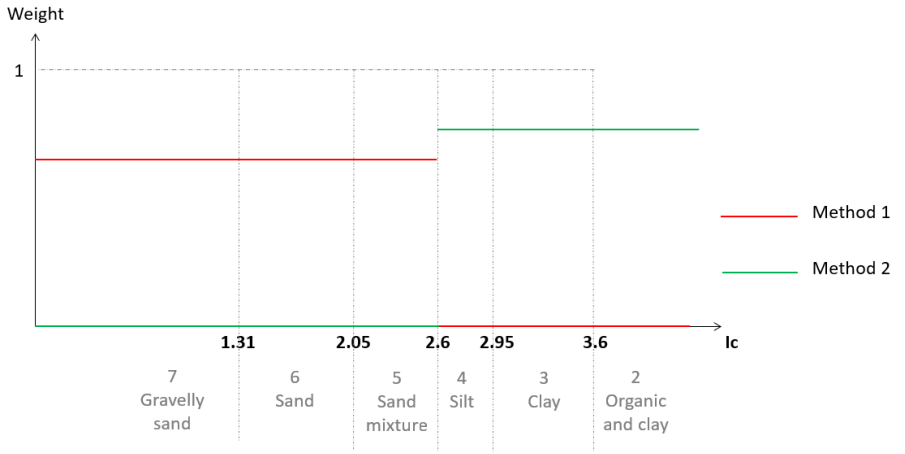

Figure 5.13: Example of user-defined constant weights for a method. The method 1 is only valid for coarse-grained soils with a I_c index below 2.6. Conversely, the method 2 is only valid for fine-grained soils.

the weights are given by the user for two reference points (figure 5.14). Both linear and logarithmic interpolations have been made available to enable an increase or decrease of the weights with the I_c index. Linear interpolations allows for a smooth and gradual transition between two points, whereas the transition in the logarithmic case can be much sharper. As it is not possible to interpolate between 0 and 1 with a logarithmic function because log(0) is undefined, an arbitrary number close to 0 must be chosen instead. As can be seen on figure 5.15, the closer to 0 this number is, the sharper the transition between 1 and 0 becomes. This number can be seen as a tuning factor for the user to control how the weights should vary with the I_c index. In other words, this tuning factor controls the steepness of the transition. To summarize, there is plenty of room for subjectivity on how the user can define and tweak the weights of the method, based on his own knowledge and expertise.

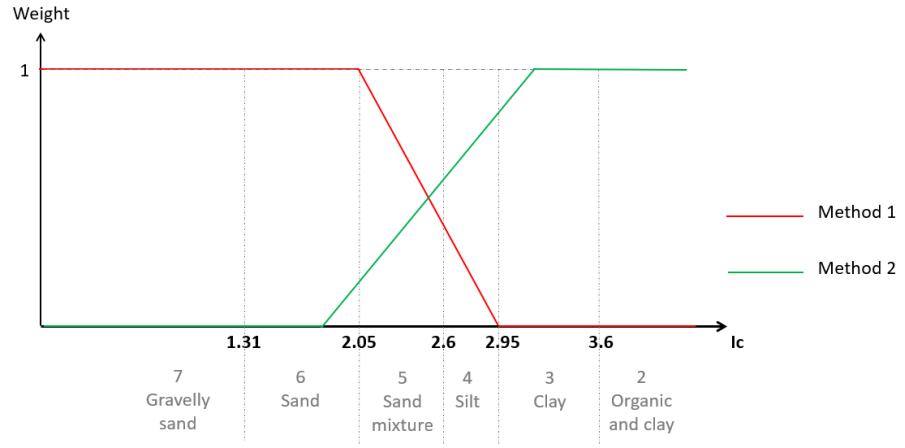

Figure 5.14: Example of linearly interpolated weights for a method, based on the I_c index. The method 1 is generally valid for coarse-grained soils, and the method 2 is generally valid for fine-grained soils.

5.4.3 From method weights to path weights

The averaging framework detailed in this chapter assumes that the paths to a parameter are the contributing models $M_1, ..., M_m$. However, the user can only define the weights for the methods and not for the paths directly. Moreover, the number of paths is much larger than the number of methods. As a result, is it required to convert the user-defined method weights into the path weights that are actually used in the averaging process.

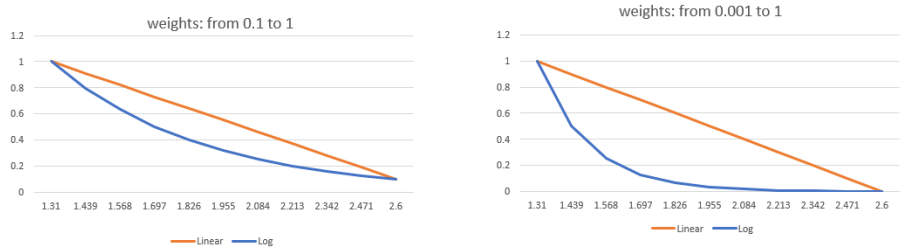

Figure 5.15: Comparison of linear and logarithmic interpolations for between 1 and a number close to 0. The closer to 0, the sharper the transition.

A path can be summarized as a succession of visited methods, although its characterization is made more difficult owing to the branching phenomenon. The final outcome of the path results from all the intermediate calculations that occurred within the path. The validity of a path is then a function of the validity of its underlying methods. The non-normalized weight of a path is therefore defined as the product of the weights for all the visited nodes of the path:

$$w_{path} = \prod_{method \in path} w_{method} \tag{5.17}$$

Once the weights are determined for all the paths of a parameters, they are then normalized and the equation 5.2 can be used.

Conclusion Input into the system based on geotechnical considerations is made possible via user-defined weights. The weighting scheme can include a dependency on either the SBT or the I_c index, but the characterization of the weights can be quite subjective with many decisions left to the user. This means that a set of weights will be highly dependent of the case considered and the preferences of the user, and this set should not be copied-pasted from one project to another. Calibration of the weights based on a large dataset could also be an option, but maybe at the expense of a reduced transparency.

Chapter 6

Application of automatic parameter determination with HSsmall model

The Hardening Soil model is an advanced constitutive model often used in geotechnical engineering for numerical analysis. The main advantages of this model is the stress dependency of the stiffness, and the inclusion of both shear hardening and compaction hardening [29]. A modified version of this model called Hardening Soil small strain (HSsmall) accounts for the strain dependency of stiffness at a very low level of strain. The apparent complexity of this model compared to more basic models like Mohr-Coulomb, requires to determine a larger number of model parameters from soil investigations. In this chapter, the APD system is applied to a geotechnical project from Witteveen-Bos using the HSsmall model. The aim is to compare the parameter values calculated by the framework developed in this thesis, with values determined by geotechnical experts for an actual case study.

6.1 Model parameters

A comprehensive list of parameters required for the HSsmall is detailed in the PLAXIS Material Models Manual [29]. The present study focus mainly on the strength and stiffness parameters of this model, namely: the peak friction angle angle ϕ_p, the dilatancy angle ψ, the reference secant stiffness E_{50}^{ref}, the tangent reference stiffness for primary oedometer loading E_{oed}^{ref}, the unloading-reloading reference stiffness E_{ur}^{ref}, the power of stress-level dependency of stiffness m, the reference shear modulus at very small strains G_0^{ref}, the threshold shear strain $\gamma_{0.7}$, the failure ratio R_{fail} and the stress ratio for normal consolidation K_0^{nc}. As cohesionless coarse-grained soils are only considered in this study, the cohesion is assumed to be $c = 0\,\text{kPa}$. The unloading-reloading Poisson's ratio is supposed constant at $\nu_{ur} = 0.2$, and the reference stress is set at $p_{ref} = 100\,\text{Pa}$. The stress ratio for a normally consolidated state K_0^{nc} is by default defined according to Jaky's formula: $K_0^{nc} = 1 - \sin\phi_{cv} = 0.470$.

Various methods from the appendix A.2 have already been incorporated to the system in the previous chapters to derive a few soil properties, some of which are already model parameters for the HSsmall models: the peak friction angle and the dilatancy angle. The remaining model parameters require to add new methods to the external database, these methods are detailed below:

K_0 : The stress ratio K_0 is related to the overconsolidated ratio OCR with the following relation (Mayne 2007 [10]):

$$K_0 = 0.192 \cdot \left(\frac{q_t}{p_{ref}}\right)^{0.22} \cdot \left(\frac{p_{ref}}{\sigma_v^{'}}\right)^{0.31} OCR^{0.27} \tag{6.1}$$

OCR: The overconsolidation ratio is approximated using the following correlation (Mayne 2007 [10]):

$$OCR = \left(\frac{0.192(q_t/p_{ref})^{0.22}}{K_0^{nc}(\sigma_v^{'}/p_{ref})}\right)^{\frac{1}{\sin\phi_p - 0.27}} \tag{6.2}$$

$\boldsymbol{E_{50}^{ref}}$ **:** The secant reference stiffness can be calculated using the analytical formula:

$$E_{50}^{ref} = E_{50}\Big(\frac{c\cos\phi_p + p_{ref}\sin\phi_p}{c\cos\phi_p - \sigma_3\sin\phi_p}\Big)^m = E_{50}\Big(\frac{p_{ref}}{K_0\sigma_v^{`}}\Big)^m \tag{6.3}$$

The secant Young modulus E_s is often given for a level of strain of 0.1%, which is lower than the level of strain for which the secant stiffness E_{50} is defined, in the range 0.2 % to 0.6 % [30]. This means that E_{50} is likely to be lower than E_s. However according to Lengkeek [30], sands are often aged and slightly overconsolidated even if they are supposed normally consolidated, which leads to an underestimation of the stiffness E_{50}. In other words, the secant Young modulus E_s defined at 0.1 % strain for normally consolidated sands can replace the E_{50} stiffness in the equation 6.3 for the HSsmall model. A correlation by [30] has been proposed to estimate directly the reference secant stiffness based on the relative density:

$$E_{50}^{ref} = \frac{60}{100}D_r \tag{6.4}$$

where E_{50}^{ref} is expressed in MPa and D_r in %.

$\boldsymbol{E_{oed}^{ref}}$ **:** The oedometer reference stiffness can be calculated using the analytical formula:

$$E_{oed}^{ref} = E_{oed}\Big(\frac{c\cos\phi_p + p_{ref}\sin\phi_p}{c\cos\phi_p - \frac{\sigma_3}{K_0^{nc}}\sin\phi_p}\Big)^m = E_{oed}\Big(\frac{p_{ref}}{\sigma_v^{`}}\Big)^m \tag{6.5}$$

where the oedometer stiffness E_{oed} can be assimilated to the 1-D constrained modulus M_{CPT} in the normally consolidated state [30] determined from CPT interpretation. As E_{oed}^{ref} is defined for primary loading, it is important to realise that values for M_{CPT} are only valid for the normally-consolidated case. Additionally, the oedometer reference stiffness E_{oed}^{ref} can be estimated from the reference secant stiffness E_{50}^{ref} according to [29] and [30]:

$$E_{oed}^{ref} = E_{50}^{ref} \tag{6.6}$$

This formulla is generally valid for young deposit.

$\boldsymbol{E_{ur}^{ref}}$**:** The unloading-reloading reference stiffness can be calculated using the analytical formula:

$$E_{ur}^{ref} = E_{ur}\Big(\frac{c\cos\phi_p + p_{ref}\sin\phi_p}{c\cos\phi_p - \sigma_3\sin\phi_p}\Big)^m = E_{ur}\Big(\frac{p_{ref}}{K_0\sigma_v^{`}}\Big)^m \tag{6.7}$$

The level of strain in unloading-reloading condition is often lower than 0.1 %, therefore Lengkeek [30] advocated that the secant Young modulus E_s in unloading-reloading conditions[1] can serve as a lower boundary for the unloading-reloading stiffness E_{ur}. For many situations, the unloading-reloadin reference stiffness can also be conveniently determined from the E_{50}^{ref} stiffness [29]:

$$E_{ur}^{ref} = 3E_{50}^{ref} \tag{6.8}$$

$\boldsymbol{G_0^{ref}}$ **:** The small strain shear reference stiffness can be calculated using the analytical formula:

$$G_0^{ref} = G_0\Big(\frac{c\cos\phi_p + p_{ref}\sin\phi_p}{c\cos\phi_p - \sigma_3\sin\phi_p}\Big)^m = G_0\Big(\frac{p_{ref}}{K_0\sigma_v^{`}}\Big)^m \tag{6.9}$$

where G_0 is the small strain shear stiffness as described and calculated by the equations **??**, A.32 and A.33. An additional correlation from Brinkgreve et al [16] links the reference stiffness G_0^{ref} in MPa with the relative density:

$$G_0^{ref} = 60 + \frac{68}{100}D_r \tag{6.10}$$

where G_0^{ref} is expressed in MPa and D_r in %.

[1] understand over-consolidated state

m: The power for stress dependency of the stiffness is often take as a constant value equal to 0.5 for coarse-grained soils. Alternatively, a correlation with the relative density is provided by [16]:

$$m = 0.7 - \frac{Dr}{320} \tag{6.11}$$

where D_r is expressed in %.

$\gamma_{0.7}$: The threshold shear strain $\gamma_{0.7}$ can be approximated according to [29] as:

$$\gamma_{0.7} = \frac{1}{9G_0}(\sigma_v^{'}(1 + K_0)\sin 2\phi_p) \tag{6.12}$$

A correlation from Brinkgreve et al [16] links the threshold $\gamma_{0.7}$ with the relative density expressed in %.

$$\gamma_{0.7} = (2 - \frac{D_r}{100}) \cdot 10^{-4} \tag{6.13}$$

***R_f* :** The failure ratio is conventionally equal to 0.9, but a correlation with the relative density expressed in % can be found in [16]:

$$R_f = 1 - \frac{D_r}{800} \tag{6.14}$$

6.2 Description of the case study

The case study consists in the determination of the soil properties and the parameters for the HSsmall model the based on two CPT performed in the region of Utrecht. The raw CPT data includes the measurements of the cone resistance q_c, the sleeve friction f_s and the pore pressure u_2 for every two centimeters. A pre-processing stage has decomposed the soil profile into consistent layers. Therefore the source parameters considered in this case study are: the average cone resistance q_c of the layer, the average friction ratio R_f, and the average effective and total stresses σ_v and $\sigma_v^{'}$. The layers considered in this case study and the corresponding values for the source parameters are described in the table 6.1. Layers made of fine-grained materials may lie between the sandy layers and have not been studied here.

Layer	depth[2]	q_c(MPa)	R_f (%)	σ_v(kPa)	$\sigma_v^{'}$ (kPa)	pore pressure (kPa)
1 Antropogeen Zand	0.9	8.99	0.79	18.62	18.62	0
2 Holoceen Zand	5.1	3.53	1.09	92.85	56.95	35.9
3 KR Zand_a	11.4	8.30	0.50	196.49	105.59	90.9
4 KR Zand_b	12.5	19.11	0.47	281.99	147.59	134.4
5 UR Zand	23.4	22.18	0.49	499.56	256.16	243.4
6 ST Zand	37.4	39.60	0.49	744.98	380.54	364.44

Table 6.1: Description of the source parameters for the sandy layers of the case study. The values presented here are averages and are considered representative of the whole layer.

Based on these source parameters, basic soil properties and model parameters for HSsmall are determined. Two different approaches are contemplated here: the first one analyses all the individual paths for every parameter and proceed to the averaging operation once all the parameter values are calculated. The second approach is a staged process where a first step calculates and averages the intermediate parameters before proceeding to a second step to determine the destination parameters. The distinction between source, intermediate and destination parameters is detailed in the table 6.2. The external database for the methods used in this case study is provided in the appendix (tables C.1 and C.2).

The initial values for the source parameters are given in table 6.1. A coefficient of variation of 5% has been arbitrary chosen for the four source parameters.

[2]average depth of the layer

Symbol	type of parameter	Nb of methods	Nb of paths	definition
q_c (kPa)	source	0	0	cone tip resistance
R_f (%)	source	0	0	friction ratio
σ_v (kPa)	source	0	0	total vertical stress
$\sigma_v^{'}$ (kPa)	source	0	0	effective vertical stress
D_r (%)	intermediate	6	6	relative density
V_s (m/s)	intermediate	6	6	shear wave velocity
ψ (°)	intermediate	2	12	dilatancy angle
Ψ (-)	intermediate	2	2	state parameter
ϕ_p (°)	intermediate	5	22	peak friction angle
G_0 (MPa)	intermediate	2	7	small strain shear modulus
$E_{s,NC}$ (MPa)	intermediate	5	12	elastic Young modulus (normally-consolidated)
$E_{s,OC}$ (MPa)	intermediate	3	9	elastic Young modulus (over-consolidated)
M_{NC} (MPa)	intermediate	3	8	constrained modulus (normally-consolidated)
M_{OC} (MPa)	intermediate	2	7	constrained modulus (over-consolidated)
OCR (-)	intermediate	1	22	Over consolidation ratio
K_0^{nc} (-)	intermediate	1	1	Stress ratio (normally consolidated)
K_0 (-)	intermediate	1	22	Stress ratio
m (-)	intermediate	1	6	stress exponent of stiffness
R_{fail} (-)	intermediate	1	6	failure ratio
E_{oed}^{ref} (MPa)	destination	2	1638	reference oedometer stiffness
E_{50}^{ref} (MPa)	destination	3	1584	reference secant stiffness
E_{ur}^{ref} (MPa)	destination	2	2772	reference unloading/reloading stiffness
G_0^{ref} (MPa)	destination	2	930	reference shear small strain stiffness
$\gamma_{0.7}$ (-)	destination	2	3394	threshold small strain

Table 6.2: Description of the soilparameters

6.3 Results

6.3.1 First approach

For the first approach, all the paths to the intermediate and destination parameters are considered, and the averaging process is performed once all the values are calculated. The averaging technique *Propagation* has been chosen since we have seen it provides the most satisfying outcomes, and the weights have been calculated according to the inverse RMSE of the path values in order to account for both the bias and the variance of the contributing models. The probability densities of the parameter's paths are assumed here normally distributed as a first approximation, even if this we have seen that this assumption is incorrect. The global mean has been taken as a reference value. The table 6.2 indicates the number of methods and the number of paths for every parameter. The number of paths for the destination parameters may seem astonishingly high. There are for example 3394 paths for the threshold $\gamma_{0.7}$, 6 of which come from the equation 6.13, and 3388 of which come from the equation 6.12. Indeed the equation 6.12 uses several input parameters which already have many paths: G_0 (7 paths), K_0 (22 paths) and ϕ_p (22 paths), thus $22 \cdot 22 \cdot 7 = 3388$.

The results obtained from the APD system for the layer "2- Holoceen Zand" are summarized in the table 6.3. A consistency ratio below 1 is found for most of the parameters, except for the shear wave velocity V_s for which the models are rather poorly aligned. This inconsistency of the paths then propagates to the shear stiffnesses G_0 and G_0^{ref}, and the threshold $\gamma_{0.7}$. Therefore, distrust has been built for these parameters. Conversely, confidence has been built for the two strength parameters ϕ_p and ψ, for which the averaged distribution is narrower than the contributing models (see figure 6.1). The remaining graphs for the other parameters are displayed in the appendix C.3.

parameter	q_c [kPa]	R_f [%]	σ_V [kPa]	σ'_V [kPa]	Dr [%]	Vs [m/s]	ψ [deg]	Ψ [-]
value	3530	1.09	93	57	40	160	3.44	-0.55
σ	176	0.0545	4.65	2.85	6.3	23	0.92	0.024
R_c	-	-	-	-	0.32	1.47	0.3	0.005
parameter	ϕ_p [deg]	G0 [MPa]	$E_{s,NC}$ [MPa]	$E_{S,OC}$[MPa]	M_{NC} [MPa]	M_{OC} [MPa]	OCR [-]	K0nc [-]
value	35	45.3	18.7	57.8	21.7	70	1.23	0.47
σ	1.2	10.2	2.1	10.7	3.1	9.5	0.09	0
R_c	0.31	1.56	0.24	0.58	0.18	0.27	0.0019	-
parameter	K0 [-]	m [-]	R_Fail [-]	E50ref [MPa]	Eoedref [MPa]	Eurref [MPa]	G0ref [MPa]	$\gamma_{0.7}$ [-]
value	0.53	0.57	0.95	37.1	36.9	112.3	90.4	2.01E-04
σ	0.011	0.02	0.008	3.6	3.7	14.1	19.4	3.67E-05
R_c	0.0018	0.32	0.32	0.23	0.24	0.35	1.44	0.59

Table 6.3: Description of the results from APD for the layer "2-Holoceen Zand". The parameter value and standard deviation σ result from the averaging scheme. R_c is the consistency index as defined in 5.15

The comparison between the parameter values provided by APD and the values obtained from Witteveen+Bos are detailed in the table 6.4 for the second layer "Holoceen Zand". Mean parameter values calculated from APD are provided as well as upper and lower values, which correspond to a deviation of 1.96 times the standard deviation from the average. There is a strong similarity for the reference stiffness parameters E_{50}^{ref}, E_{oed}^{ref} and E_{ur}^{ref} between APD and WB, however the small strain shear stiffness G_0^{ref} tends to be underestimated by APD. The oedometer stiffness is overestimated by APD for both the normally-consolidated and over-consolidated case, but this apparent discrepancy does not transfer to the reference stiffness. Comparison of parameters values for the other layers can be seen in table C.1. The quality of the estimates from APD depends of the layer considered. The shallow layer "1 Antropogeen Zand" has a calculated OCR of 5, which is not realistic because this layer is the most recent and has probably been remolded by human's activity. The OCR for shallow layer should be manually overwritten to 1.0 as Witteveen+Bos did. This error in the OCR value has propagated to the other parameters K_0 and the reference stiffness parameters. The consistency of the whole parameter set has been checked by filling the parameter values calculated by APD into a PLAXIS material set, which did not return any warning or error message.

parameter	RD [%]		M_NC [MPa]		M_OC [MPa]		OCR [-]		K0 [-]		php [deg]		psi [deg]	
	APD	WB	APD	WB	APD	WB	APD	WB	APD	WB	APD	WB	APD	WB
lower	27.6	-	15.6	-	51	-	1.04	-	0.51	-	32.7	-	1.63	-
avg	40	37	21.7	14.1	70	48.7	1.23	1.00	0.53	0.47	35.0	36.5	3.44	4.00
upper	52.4	-	27.8	-	89	-	1.43	-	0.55	-	37.3	-	5.25	-
parameter	E50ref [MPa]		Eoedref [MPa]		Eurref [MPa]		G0ref [MPa]		gamma0.7 [-]		m [-]		Rf [-]	
	APD	WB	APD	WB	APD	WB	APD	WB	APD	WB	APD	WB	APD	WB
lower	29.9	29.4	29.4	21.5	84.6	80.5	52.3	81.12	1.29E-04	-	0.54	-	0.935	-
avg	37.1	36.8	36.9	30.6	112.3	114.3	90.4	115.1	2.01E-04	1.59E-04	0.57	0.50	0.95	0.9
upper	44.2	44.2	44.2	39.6	140.1	148.2	128.5	149.2	2.74E-04	-	0.61	-	0.965	-

Table 6.4: Comparative table for the layer "2-Holoceen Zand" of the parameters values between APD and Witteveen+Boss.

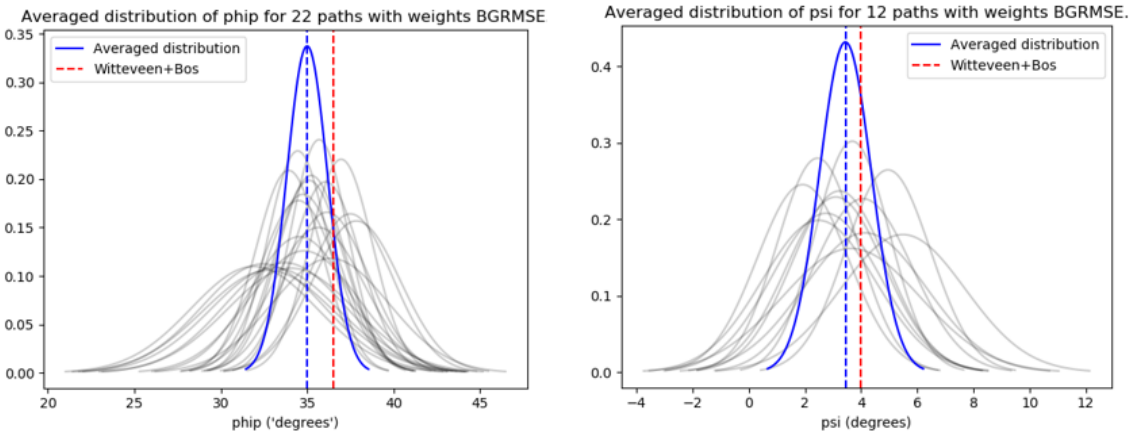

Figure 6.1: Averaged distributions for the strength parameters ϕ_p ($R_c = 0.31$) and ψ ($R_c = 0.30$). The vertical red dotted line is the average value from W+B

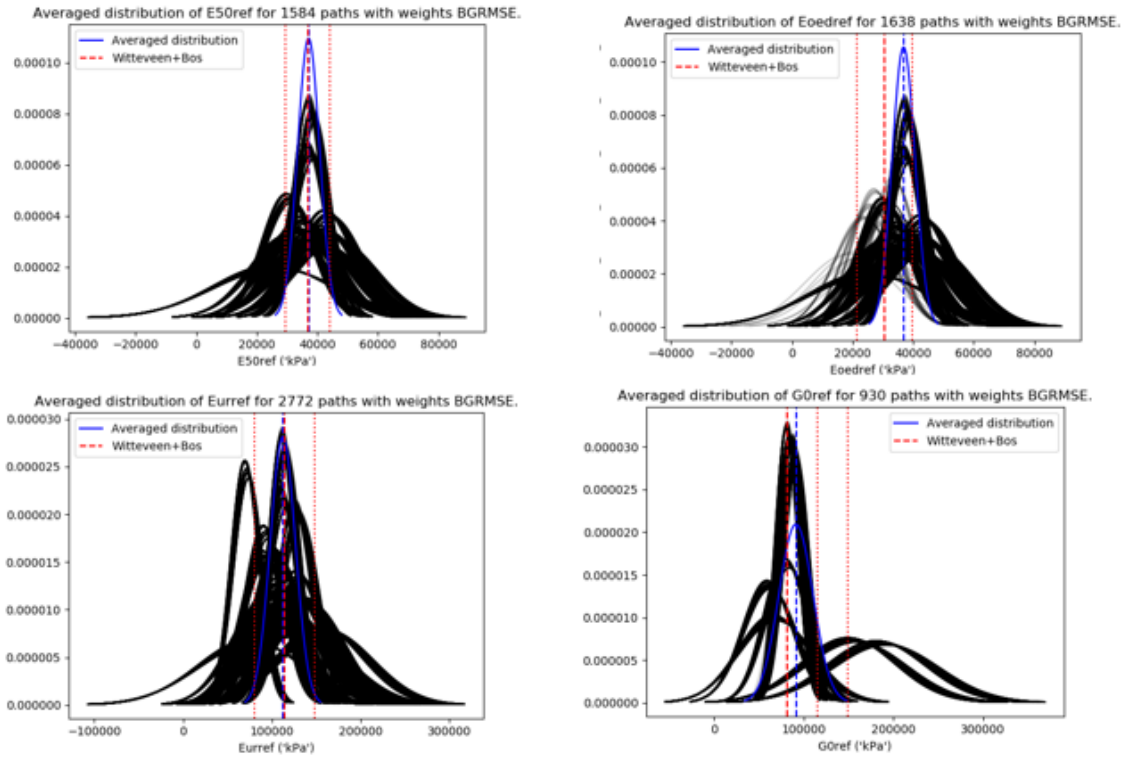

Figure 6.2: Averaged distributions for the reference stiffness parameters E_{50}^{ref} ($R_c = 0.23$), E_{oed}^{ref} ($R_c = 0.24$), E_{ur}^{ref} ($R_c = 0.36$) and G_0^{ref} ($R_c = 1.44$). The vertical red dotted lines represent the lower, average and upper values from W+B. There is a rather strong similarity between the averaged distribution from APD and the span from W+B.

6.3.2 Second approach

For the second approach, the intermediate parameters as defined in the table 6.2 were averaged before proceeding to the determination of the destination parameters. The results of the intermediate parameters are thus identical to the first approach. The differences in the destination parameters are highlighted in the table 6.5 where the parameter values from the first and second approaches are displayed along with the parameter values from Witteveen+Bos for the second layer "2-Holoceen Zand". The second approach returns reasonable results in the range of the expected values with only minor discrepancies compared to the first approach, at least for this second layer. A larger difference up to a factor 2 is sometimes noticeable in other layers (annexe C.3), but it is quite difficult to draw general conclusions to characterize the variation between the two approaches.

parameter	**E50ref [MPa]**			**Eoedref [MPa]**			**Eurref [MPa]**			**G0ref [MPa]**			$\gamma 0.7[-]$		
	APD1	APD2	WB	APD1	APD2	WB	APD1	APD2	WB	APD1	APD2	WB	APD1	APD2	WB
lower	29.4	22.2	23.1	29.4	17.2	21.5	84.6	70.5	80.5	52.3	65.3	81.12	1.30E-04	1.29E-04	-
avg	37.1	32.6	31.5	36.9	28.3	30.6	112.4	101.3	114.3	90.4	88.9	115.1	2.02E-04	1.71E-04	1.59E-04
upper	44.2	43	40	44.2	39.3	39.6	140.2	132	148.2	128.5	112.4	149.2	2.74E-04	2.12E-04	-

Table 6.5: Comparative table for the layer "2-Holoceen Zand" of the parameter values between the first and second approaches of APD and Witteveen+Bos.

One remarkable aspect about this staged procedure is the reduction of the number of paths for the destination parameters. In the first approach, the number of paths of a destination parameter depended on its depth in the graph, but also on the complexity of its associated methods and on their number of input parameters. This led for example to a large number of paths for the reference stiffness E_{ur}^{ref} which had 2880 paths. The readability and the interpretation of the graph 6.2 was then harder, and the system becomes overall less transparent. The staged approach improves the readability of such graph (see figure 6.3) but it also significantly alters the averaging process of the destination parameters. From the 930 paths of the reference small strain shear stiffness G_0^{ref}, 6 originated from the equation 6.10 while the remaining 924 originated from 6.9. This means that n the case of equal weights, the method 6.10 accounts for less than 1% of the weights for the first approach, but it now accounts for exactly 50 % of the weights for the second staged approach. This phenomenon directly influences both the averaged value and standard deviation of the parameters, and could potentially lead to absurd values in some cases.

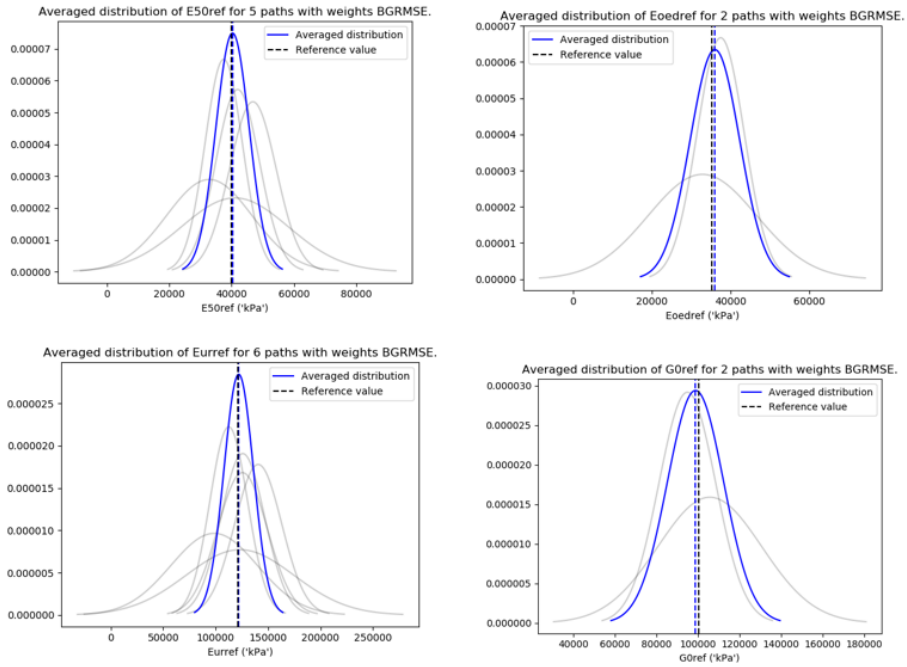

Figure 6.3: Averaged distributions for the reference stiffness parameters E_{50}^{ref} , E_{oed}^{ref} , E_{ur}^{ref} and G_0^{ref} for the second approach.

An argument can be made to limit the number of possible outcomes for consistency reasons for certain parameters. In that case, intermediate averaging would be a reasonable and valuable approach. The stress exponent m or the soil unit weight γ_s are cases in point. It as generally agreed that the same exponent m should be used for the reference stiffness parameters. In that case, it is preferable not to have too many values for the m exponent and to have a single fixed value.

6.4 Conclusion

The APD system proved to be able to provide a consistent parameter set for the HSsmall model with values that were in general in accordance with the parameters determined by Witteveen+Bos. It is difficult at this stage to draw reliable general conclusion about the quality of APD's outcomes as it would sometimes overestimate a parameter value compared to W+B for a particular layer, and underestimate that same parameter for another layer. Two approaches were compared to investigate the influence of an intermediate averaging procedure before assessing the final destination parameters. It is recommended not to proceed to an intermediate averaging as the model averaging framework for the determination of weights was not tailored to support such a procedure.

Chapter 7

Conclusions and discussions

7.1 Conclusions

This thesis elaborated on the development of a system designed to determine geotechnical model parameters based on in-situ tests and various correlations found in the literature. The plurality of correlations, charts and rules-of-thumb contributes to the total uncertainty in the determination of model parameters and may result in scepticism or distrust in the use of complex constitutive models for numerical analysis. A first major milestone towards an automated system for parameter determination has been reached by van Berkom [1] and has served as a basis on which the present study has expanded and improved. The emphasis was put on CPT correlations for coarse-grained soils, but the principles established in this thesis are quite general and could be easily applied to other types of soil and in-situ tests. The goal of this thesis throughout the chapters was to answer the main research question formulated in introduction: *"How to combine results from multiple correlations and chains of correlations to estimate geotechnical parameter values and how to assess the quality of these estimates ?"*. To answer this question, several sub-objectives were defined and are re-enacted below:

- **Designing and implementing validation of parameters:** Before setting-up any statistical framework, it was critical to make sure that the values provided by the system made sense from a geotechnical point of view. Chapter 3 presented a case study based on actual CPT data to show that the system was able to produce reasonable outcomes. Absurd values and outliers are now taken care of and removed thanks to an automatic validation of the calculated values.

- **Dealing with circular connections:** A few ideas were developed in chapter 3 about how circular connections could be be incorporated into the APD system. However the concepts elaborated in this study were not implemented and have not been validated.

- **Characterizing and propagating uncertainty:** A statistical framework has been conceptually developed in chapter 4 and implemented to the system to account for the uncertainty and its propagation into the graph. The uncertainty is now clearly expressed in terms of standard deviation and includes both the uncertainty from the input parameters and the uncertainty from the empirical transformation functions of the network. The propagation of the uncertainty is made possible either by the FOSM approach or with Monte-Carlo simulations. This framework has been verified on a imaginary test case and then validated for geotechnical parameters.

- **Comparing Methods selection and Method averaging:** The concept of model averaging has been described in chapter 5 to combine results from multiple paths into one averaged distribution. This enabled the comparison between method selection where only a single path is considered and method averaging where all the contributing paths are accounted for. The behavior of the combined model depends heavily on the consistency or the alignment of the contributing models: confidence in a parameter value is built when the paths are well aligned and distrust is built when the paths are poorly aligned. In both cases, method averaging always provides a more accurate description of the true variability for the model parameters, provided the methods are appropriate for the soil type and the applicable conditions.

- **Validity of correlations:** The of validity of the empirical correlations hinges on several aspects: the Soil Behavior Type, the I_c index, the state or consolidation, and even sometimes on the chemical composition of the soil. Inadequate correlations are deactivated in the system in order to avoid obtaining outliers or values with little significance. Moreover, user-defined weights with a linear or logarithmic interpolation of weights based on the I_c index enables the inclusion of geotechnical knowledge about the validity of correlations.
- **Validation of the system:** The system has been applied to an actual civil engineering project in chapter 6 and the parameter values calculated by APD were compared with the values determined by the engineers from Witteveen+Bos. The system was able to produce a satisfying and consistent parameter set with outcomes in the expected range, and had a rather decent similarity with the values from Witteveen+Bos. The difference mainly depended on the layer considered, therefore it is difficult to state if APD is more accurate and closer to the truth than W+B or not.
- **Transparency of the system:** As the system became more complex with the addition of new features for the uncertainty framework and model averaging, the verification of intermediate results has become more difficult but is still possible. This verification can even become more tedious as the number of paths quickly rises to a thousand in some cases. When determining an averaged distribution, it is highly recommended to look at the distributions of all the contributing models to have a good feeling of how the system proceeded. Each value calculated by the system is now also associated to its path containing all the visited method nodes to obtain that value. This is an important step towards a better transparency and an efficient verification of the results.

In practice, it is recommended to choose a model averaging strategy over the uni-method selection. The averaging process should be preferably hybrid, taking into account both geotechnical and statistical inputs in the determination of weights. The averaging technique *Propagation* is advocated here as it provides the most satisfying results, but the technique *Buckland* is also acceptable if one chooses to be a bit more on the conservative side. It is not recommended at this stage of development to proceed to an intermediate averaging of the parameters, but this approach is worth investigations provided some modification in the averaging scheme. To conclude, the APD system is a promising tool that successfully passed the first validation stage. Engineers are encouraged to confront the outputs of the APD system with their current practice.

7.2 Discussions

This thesis constitutes another step forward towards an automatic procedure for the determination of model parameters based on in-situ tests. However the system needs some maturity to be legitimized as a valid and reliable tool. The following bullets points highlight a few facet of the system that require additional investigations:

- As this study solely focused on coarse-grained soils, the whole framework needs to be applied and validated for fine-grained soils too. The collection of methods must then be extended to include various correlations valid for clayey soils. Mixed-soils like silts must be studied with great care as correlations from both coarse and fine-grained materials could apply. We have seen in this thesis that user-defined and interpolated weights based on the I_c index could be a possibility when dealing with mixed soils. The main challenge here would be to calibrate the weights of the methods appropriately. The calibration of the weights is still at this stage an open question and could originate either from the experience of geotechnical experts, or from machine learning algorithms.
- When building the statistical framework, it was supposed that the parameters were all mutually independent, but this hypothesis is not necessarily realistic as strong correlations may be expected between parameters. This implies that the cross-correlation coefficients between all the parameters, or the covariance matrix must be specified by the user. It would be valuable in further studies to investigate the influence of the contribution of the cross-correlations in the determination of the paths' variance. The inclusion of the cross-correlation is rather straightforward from a conceptual and software points of view, but the difficulty here lies in the specifications of the covariance coefficients.

- Quite similarly, the cross-correlation between the models has been neglected in the model averaging framework. This affects the results of the averaged variance determined from the strategy *Propagation* as its formula includes the covariance between each contributing model. From a theoretical point of view, a negative covariance results in a decrease of the averaged variance and a positive covariance results in an increase of the averaged variance. The strategy *Buckland* can be regarded as an upper bound for the averaged variance since it assumes perfectly correlated models, but this assumption might be too pessimistic in practice. The determination of the cross-correlation between the models is not a straightforward task but might be possible with the combination of a Monte-Carlo analysis and bootstrapping techniques.

- The definition of the transformation uncertainty is not constant for all the methods as it greatly depends on what information is provided by the author of a correlation. The total uncertainty of certain paths might then be either under-estimated or over-estimated. Moreover, it was assumed that the standard error around the trend line was constant for all parameter values, but it might not be the case. These issues could be easily solved if the database from which a correlation has been estimated was made available. The uncertainty of the transformation function could be then accurately measured.

- For simplification purposes, it was assumed throughout this thesis that the variables were normally distributed. This assumption is acceptable for some cases, situations arose where a non-negligible fraction of the density distribution was cover absurd (negative) values. The Monte-Carlo analysis was able to provide empirical distributions with the determination of the Kernal Density Estimation, but the KDE is a non parametric distribution that is difficult to incorporate in the model averaging framework. Further research should be made about which type of distribution is most suitable for each parameter.

- This study was based on CPT-based correlations. It would be interesting to validate the system for other types of in-situ test: DMT, SPT or pressuremeter test. Ideally, two different in-situ tests executed at the same location should yield very similar results. Different weights may apply depending of the user's judgment about the reliability and the quality of the in-situ tests.

- For large networks, the graphs generated by the system become difficult to read and to interpret. Assigning a value with its path is visually complex and is not an automated task. It would be valuable to make the graph dynamic and user interactive in order to increase the transparency and the usability of the framework.

- Finally, the case study for the validation of the HSsmall model parameters showed that the results from APD varied notably depending on which layer was considered. In order to legitimize the benefits of APD, the system should be applied to a larger number of projects and cases to clear global trends about the performance of the system. This thesis concluded that APD was able to provide reasonable parameters values with supposedly a better description of the parameter's accuracy and quality, but this remains to be verified on a much larger scale.

Appendix A

Collection of correlations

A.1 Correlations used by the software CPeT-IT

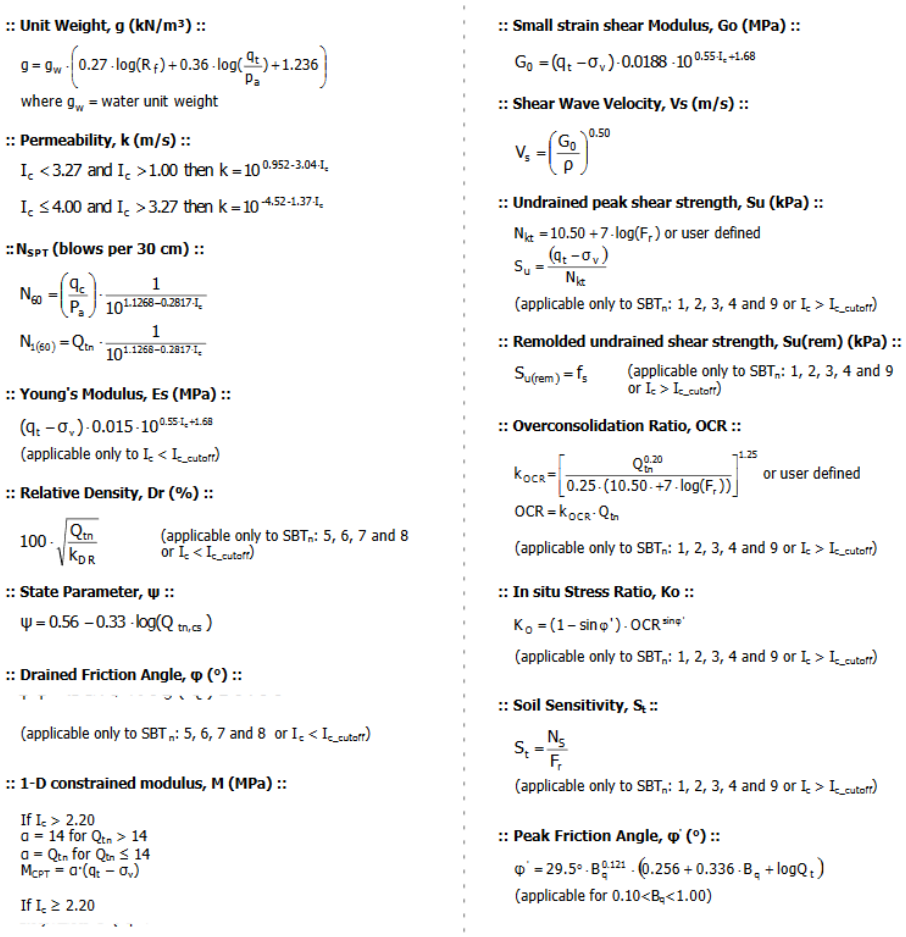

:: Unit Weight, g (kN/m³) ::

$$g = g_w \cdot \left(0.27 \cdot \log(R_f) + 0.36 \cdot \log\left(\frac{q_t}{p_a}\right) + 1.236 \right)$$

where g_w = water unit weight

:: Permeability, k (m/s) ::

$I_c < 3.27$ and $I_c > 1.00$ then $k = 10^{0.952 - 3.04 \cdot I_c}$

$I_c \leq 4.00$ and $I_c > 3.27$ then $k = 10^{-4.52 - 1.37 \cdot I_c}$

:: N_{SPT} (blows per 30 cm) ::

$$N_{60} = \left(\frac{q_c}{P_a}\right) \cdot \frac{1}{10^{1.1268 - 0.2817 \cdot I_c}}$$

$$N_{1(60)} = Q_{tn} \cdot \frac{1}{10^{1.1268 - 0.2817 \cdot I_c}}$$

:: Young's Modulus, Es (MPa) ::

$$(q_t - \sigma_v) \cdot 0.015 \cdot 10^{0.55 \cdot I_c + 1.68}$$

(applicable only to $I_c < I_{c\_cutoff}$)

:: Relative Density, Dr (%) ::

$$100 \cdot \sqrt{\frac{Q_{tn}}{k_{DR}}}$$

(applicable only to SBT_n: 5, 6, 7 and 8 or $I_c < I_{c\_cutoff}$)

:: State Parameter, ψ ::

$$\psi = 0.56 - 0.33 \cdot \log(Q_{tn,cs})$$

:: Drained Friction Angle, φ (°) ::

(applicable only to SBT_n: 5, 6, 7 and 8 or $I_c < I_{c\_cutoff}$)

:: 1-D constrained modulus, M (MPa) ::

If $I_c > 2.20$
$\alpha = 14$ for $Q_{tn} > 14$
$\alpha = Q_{tn}$ for $Q_{tn} \leq 14$
$M_{CPT} = \alpha \cdot (q_t - \sigma_v)$

If $I_c \geq 2.20$

:: Small strain shear Modulus, Go (MPa) ::

$$G_0 = (q_t - \sigma_v) \cdot 0.0188 \cdot 10^{0.55 \cdot I_c + 1.68}$$

:: Shear Wave Velocity, Vs (m/s) ::

$$V_s = \left(\frac{G_0}{\rho}\right)^{0.50}$$

:: Undrained peak shear strength, Su (kPa) ::

$N_{kt} = 10.50 + 7 \cdot \log(F_r)$ or user defined

$$S_u = \frac{(q_t - \sigma_v)}{N_{kt}}$$

(applicable only to SBT_n: 1, 2, 3, 4 and 9 or $I_c > I_{c\_cutoff}$)

:: Remolded undrained shear strength, Su(rem) (kPa) ::

$S_{u(rem)} = f_s$ (applicable only to SBT_n: 1, 2, 3, 4 and 9 or $I_c > I_{c\_cutoff}$)

:: Overconsolidation Ratio, OCR ::

$$k_{OCR} = \left[\frac{Q_{tn}^{0.20}}{0.25 \cdot (10.50 \cdot +7 \cdot \log(F_r))}\right]^{-1.25}$$ or user defined

$OCR = k_{OCR} \cdot Q_{tn}$

(applicable only to SBT_n: 1, 2, 3, 4 and 9 or $I_c > I_{c\_cutoff}$)

:: In situ Stress Ratio, Ko ::

$$K_O = (1 - \sin\varphi') \cdot OCR^{\sin\varphi'}$$

(applicable only to SBT_n: 1, 2, 3, 4 and 9 or $I_c > I_{c\_cutoff}$)

:: Soil Sensitivity, S_t ::

$$S_t = \frac{N_S}{F_r}$$

(applicable only to SBT_n: 1, 2, 3, 4 and 9 or $I_c > I_{c\_cutoff}$)

:: Peak Friction Angle, φ' (°) ::

$$\varphi' = 29.5° \cdot B_q^{0.121} \cdot (0.256 + 0.336 \cdot B_q + \log Q_t)$$

(applicable for $0.10 < B_q < 1.00$)

Figure A.1: Extract from the manual of the software CPeT-IT. This is the set of correlations used by the software.

A.2 Extra correlations and methods for soil properties

A.2.1 Relative density

1. **Kulhawy & Mayne (1990)** This formulation relates the relative density with the normalised cone tip resistance $Q_{tn} = (q_t/p_a)/(\sigma'_{v0}/p_a)^{0.5}$. A correcting factor Q_f accounts for the compressibility and the stress state of the sample [12]. The table A.1 compiles the statistical data of the relationship A.1 for different cases.

$$D_r^2 = \frac{Q_{tn}}{Q_f} \tag{A.1}$$

Case	Q_f	n	r^2	σ
NC-high comp.	280	59	0.796	0.14
NC-med comp.	292	145	0.885	0.10
NC-low com.	332	190	0.711	0.14
NC-average	305	404	0.776	0.13
low OCR (<3)	390	34	0.711	0.14
med OCR (3-8)	403	56	0.849	0.10
high OCR (>8)	443	50	0.859	0.12

Table A.1: Statistical data of the correlation A.1. SOurce: [12]

The software *CPeT-IT* uses the approximation from Robertson and Cabal [14], which is actually the average value of Q_f. The pooled variance of these datasets for D_r^2 is then $\sigma = 0.13$.

$$D_r = 100 \cdot \sqrt{\frac{Q_{tn}}{350}} \qquad (\%) \tag{A.2}$$

2. **Baldi et al (1986)** The form of the equation is inspired by Schmertmann (1976). The fitting coefficients are $C_0 = 15.7$ and $C_2 = 2.41$ for normally consolidated sands [14].

$$D_r = 100 \cdot (\frac{1}{C_2}) \ln \frac{Q_{tn}}{C_0} \qquad (\%) \tag{A.3}$$

No standard deviation is reported for this formula, an arbitrary value has been set at $\sigma = 11\%$.

3. **Lunne and Christoffersen (2003)** The form of the equation is also inspired by Schmertmann (1976). The fitting coefficients are $C_0 = 61$, $C_1 = 0.71$ and $C_2 = 2.91$ [8].

$$D_r = 100 \cdot (\frac{1}{C_2}) \ln \frac{q_c}{C_0(\sigma'_{v0})^{C_1}} \qquad (\%) \tag{A.4}$$

where q_c and σ'_{v0} are both given in kPa. No standard deviation is reported for this formula, an arbitrary value has been set at $\sigma = 11\%$.

4. **Jamiolkowski, Presti and Manassero (2001)** The form of the equation is also inspired by Schmertmann (1976). The fitting coefficients are $C_0 = 17.68$, $C_1 = 0.50$ and $C_2 = 3.10$ [31].

$$D_r = 100 \cdot (\frac{1}{C_2}) \ln \frac{q_c/p_a}{C_0(\frac{\sigma'_{v0}}{p_a})^{C_1}} \qquad (\%) \tag{A.5}$$

The standard deviation for this correlation is $\sigma = 10\%$ for 180 data points and a correlation coefficient $R = 0.89$.

5. **Lancellotta (1983)** Applicable for normally consolidated, unaged and uncemented sands.

$$D_r = -98 + 66 \log \frac{q_c}{\sqrt{\sigma'_{v0}}} \qquad (\%) \tag{A.6}$$

in which q_c and σ'_{v0} are given in t/m^2. The standard deviation for this correlation is $\sigma = 6.6\%$ for 144 data points and a correlation coefficient $R = 0.96$ [32].

6. **Jamiolkowski (2001)** For quartz and silica sands, the following relation inspired by Lancellotta (1983) relates the relative density with the normalised cone tip resistance for several state of compressibility:

$$D_r = 100 \cdot [0.268 \ln \frac{Q_{tn}/p_a}{\sqrt{\sigma'_{v0}/p_a}} - b_x] \qquad (\%) \tag{A.7}$$

in which $b_x = 0.675$ for sands with a medium compressibility, $b_x = 0.525$ for highly compressible sands, and $b_x = 0.825$ for sands with a low compressibility. The standard deviation for this relation is $\sigma = 7.9\%$ for 456 data points and a correlation coefficient $R = 0.887$ [31].

A.2.2 Friction angle

1. **Jefferies & Been (2006)** This is the reference equation used by the software *CPeT-IT*, it relates the peak friction angle with the critical state friction angle and the state parameter Ψ. This relation was found in [14] (Robertson and Cabal) but is based on publications by Jefferies and Been [5] [33] [34].

$$\phi' = \phi'_{cv} - 48\Psi \tag{A.8}$$

No standard deviation is reported for this formula, it has been estimated graphically to be equal to $\sigma = 2°$ for 154 data points, based on the figure A.2.

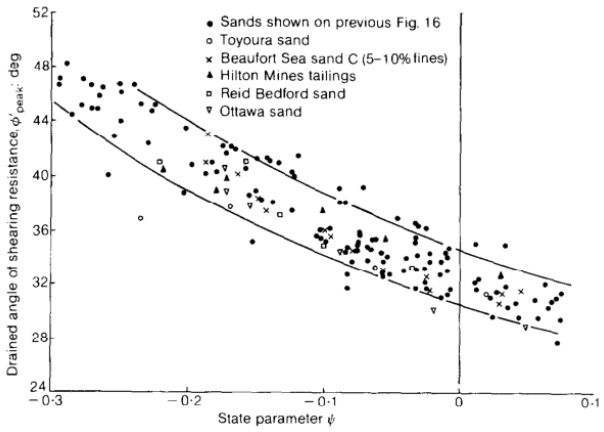

Figure A.2: Drained angle of friction as a function of state parameter for several sands. Source: [5].

2. **Kulhawy & Mayne (1990)** This relation is valid for a clean, rounded quartz sand [14], for both normally consolidated and overconsolidated states.

$$\phi' = 17.6 + 11 \log Q_{tn} \tag{A.9}$$

The standard deviation for this correlation is $\sigma = 2.8°$ for 633 data points, with a correlation coefficient $R = 0.640$ [12].

3. **Robertson & Campanella (1983)** This relation is usually valid for moderately compressible quartz sands according to [14] and [6].

$$\phi' = \arctan\left(\frac{1}{2.28}[\log \frac{q_c}{\sigma'_{v0}} + 0.29]\right) \tag{A.10}$$

No standard deviation is reported for this formula, it has been estimated graphically to be equal to $\sigma = 2°$ for 48 data points, based on the figure A.3.

4. **Peak friction angle and dilatancy angle** The peak friction angle is the sum of the friction angle at critical state and the dilatancy angle ψ.

$$\phi' = \phi'_{cv} + \psi \tag{A.11}$$

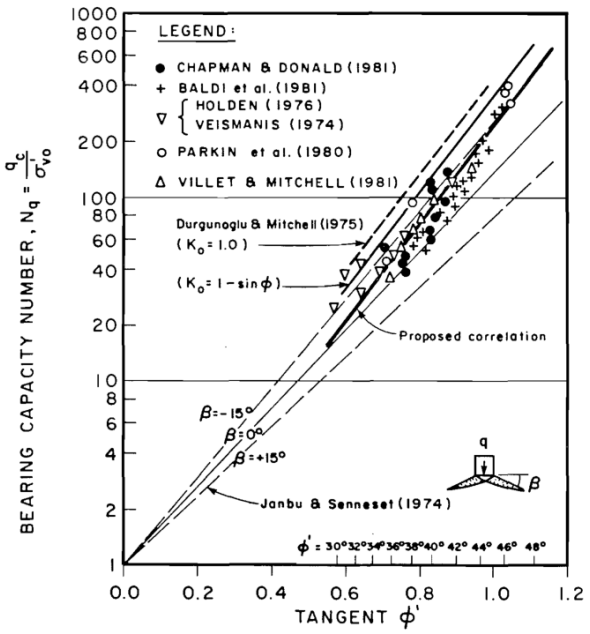

Figure A.3: Peak friction angle as a function of the bearing capacity number. Source: [6].

This relation is considered theoretical, therefore the standard deviation of this relation is reduced to 0.

5. **Brinkgreve, Engin and Engin (2010)** In drained conditions, the friction angle can be estimated from the relative density [16]:

$$\phi^{'} = 28 + 12.5\frac{D_r}{100} \tag{A.12}$$

No standard deviation is reported in the original publication, an arbitrary deviation $\sigma = 3°$ is chosen.

A.2.3 Dilatancy angle

1. **Brinkgreve, Engin and Engin (2010)** In drained conditions, the dilatancy angle can be estimated from the relative density [16]:

$$\psi = -2 + 12.5\frac{D_r}{100} \tag{A.13}$$

No standard deviation is reported in the original publication, an arbitrary deviation $\sigma = 1°$ is chosen.

2. **Lee et al. (2008)** This formula is inspired from Bolton 1986 ([35]) but here the mean effective stress is replaced with $\frac{100q_c}{p_a}$ [36]. R and Q are functions of the silt content and were taken as 1 and 14 respectively. The m parameter is a dilatancy ratio varying between 3 for triaxial conditions and 5 for plane-strain conditions. A value m=3 has been chosen.

$$\psi = m[D_r(Q - \ln\frac{100q_c}{p_a}) - R] \tag{A.14}$$

The standard deviation for this correlation is $\sigma = 0.9°$ [36].

A.2.4 State parameter

1. **Robertson (2010)** The state parameter for a wide variety of sands can be estimated from the equivalent normalized cone resistance [37]:

$$\Psi = 0.56 - 0.33\log Q_{tn,cs} \tag{A.15}$$

where $Q_{tn,cs}$ is a corrected cone resistance taking into account the fine content, the mineralogy and the plasticity. The correcting factor K_c is function of the I_c valiue.

$$Q_{tn,cs} = K_c Q_{tn} \tag{A.16}$$

No standard deviation is reported in the original publication for the correlation A.15, an arbitrary deviation $\sigma = 0.04$ is chosen.

2. **Sadrekarimi (2016)** The relation in inspired from Been et al (1987), thus Sadrekarimi [38] proposed k=27.6 and m =11.4 as fitting coefficients. It can be noted that the coefficients k and m depend on the slope of the critical state line.

$$\Psi = -\frac{\ln \frac{Q_{tn}}{k}}{m} \tag{A.17}$$

The standard deviation for this correlation is $\sigma = 0.03$ for 42 data points [38]. The author mentions that this precision for the state parameter is satisfying.

A.2.5 Young Modulus

1. **Robertson (2009)** This is the reference relation used by the software *CPeT-IT*. The Young modulus is defined as the mobilized modulus at 0.1% strain [14]. The following relation is valid for uncemented silica sands . The ratio $E_s/(q_t - \sigma_{v0})$ is sometimes referred as α_E [39].

$$E_s = (q_t - \sigma_{v0}) 0.015 \cdot 10^{0.55 I_c + 1.68} \tag{A.18}$$

No standard deviation is reported in the original publication, however α_E ranges between 3 and 12 for normally consolidated sands, and between 5 and 20 for overconsolidated sands [39]. An arbitrary standard deviation for α_E is then set at $\sigma = 2$.

2. **Melnikov & Boldyrev (2016)** A unified regression equation for both the Young Modulus of sandy and clayey soils is given by [40]:

$$E_s = 24.60 - 6.005 I_c - 0.5811 I_c^2 + q_c(1.084 - 1.511 I_c + 1.090 I_c^2) \tag{A.19}$$

with q_c and E_s both in MPa.

The standard deviation for this correlation is $\sigma = 1.67\,\text{MPa}$ with a correlation coefficient $R^2 = 0.872$.

3. **Melnikov & Boldyrev (2016)** From the same paper as the previous equation, a regression equation specifically for sands is given [40]:

$$E_s = 14.429 + 1.2454 q_c \tag{A.20}$$

with q_c and E_s both in MPa.

The standard deviation for this correlation is $\sigma = 2.53\,\text{MPa}$ with a correlation coefficient $R^2 = 0.817$.

4. **Massarsch (2015)** The elastic modulus for cohesionless soils can be determined for various compaction levels (governed by the a coefficient). A value $a = 28$ has been chosen for compact sands [41].

$$E_s = 74 a (\frac{q_c}{p_a})^{0.5} \tag{A.21}$$

with E_s in kPa

No standard deviation is reported in the original publication for the correlation A.15, an arbitrary deviation $\sigma = 4000\,\text{kPa}$ is chosen.

5. **Baldi (1989)** The secant Young modulus E_s at a level if strain of 0.1% can be estimated based on the chart figure A.4 for various states of consolidation. However, no correlation is provided by the author, which makes it hard to incorporate the chart into the system. Three equations have been graphically estimated for the three areas defined in the chart. These correlations are quite rough and custom, and have not been validated. They have been implemented into this work for the sake of comparison and should not be used in any actual project.

   The correlation for the over-consolidated sand is:

$$E_s = q_c(45 - 11.9 \log\left(\frac{q_c}{\sigma_v^{'}}\right)) \qquad \text{(Do not use!)} \tag{A.22}$$

   The correlation for the aged normally-consolidated sand is:

$$E_s = q_c(30.17 - 7.93 \log\left(\frac{q_c}{\sigma_v^{'}}\right)) \qquad \text{(Do not use!)} \tag{A.23}$$

   The correlation for the recent normally-consolidated sand is:

$$E_s = q_c(10.71 - 2.64 \log\left(\frac{q_c}{\sigma_v^{'}}\right)) \qquad \text{(Do not use!)} \tag{A.24}$$

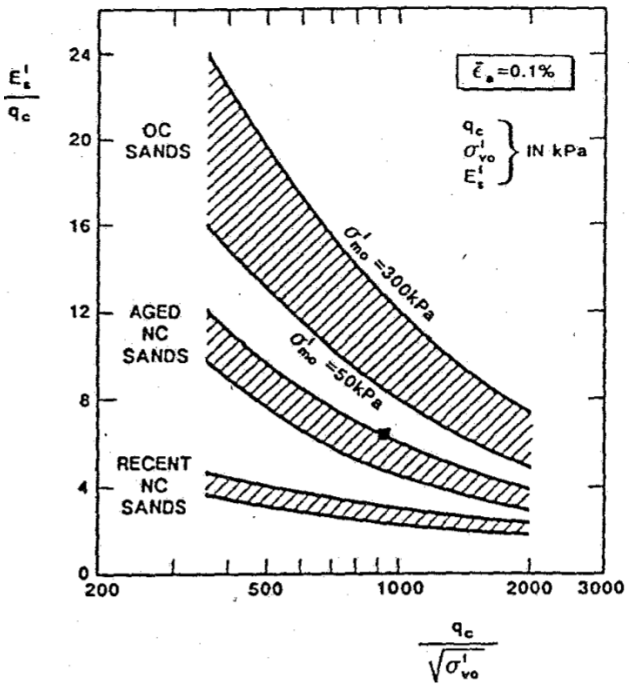

Figure A.4: Secant Young modulus against the normalised cone resistance. Source [7].

A.2.6 1-D Constrained Modulus

1. **Robertson (2009)** This is the reference relation used by the software *CPeT-IT*. The 1-D constrained modulus is defined as

$$M = \alpha_M \cdot (q_t - \sigma_{v0}) \tag{A.25}$$

   The value of α_M usually lies in the range 2-14 [14], Robertson [39] proposes a correlation based on I_c: $\alpha_M = 0.03[10^{0.55I_c+1.68}]$ for coarse-grained soils. It should be noted that Robertson and Cabal (2015)[14] advocates a coefficient 0.0188 for α_M but it has been overruled here by the coefficient 0.03 instead based on the paper from Robertson 2009 [39]. The coefficient α_M must be cut-off for high values of the normalized cone resistance Q_{tn}.

For $I_c > 2.2$:

$$\begin{aligned} \alpha_M &= Q_{tn} \qquad \text{when } Q_{tn} < 14 \\ \alpha_M &= 14 \qquad \text{when } Q_{tn} > 14 \end{aligned} \tag{A.26}$$

For $I_c < 2.2$:

$$\alpha_M = 0.03[10^{0.55 I_c + 1.68}] \tag{A.27}$$

However with this definition for α_M, there is strange jump at the threshold $I_c = 2.2$. A suggestion would be to apply a cut-off for α_M that is valid for all the I_c values. No standard deviation is reported in the original publication, an arbitrary standard deviation for α_M is then set at $\sigma = 2$.

2. **Mayne (2001)** Mayne proposes a constant value $\alpha = 5$ [14], which is only valid for normally consolidated sands.

$$M = 5 \cdot (q_t - \sigma_{v0}) \tag{A.28}$$

No standard deviation is reported in the original publication, an arbitrary standard deviation for α_M is then set at $\sigma = 2$.

3. **Lunne & Christoffersen (1983)** Various correlations fro the constrained modulus are collected in the paper [8]. Results from the NGI suggests that for normally consolidated sands:

$$M = 2.17 q_c + 16.6 \tag{A.29}$$

where q_c is in MPa.

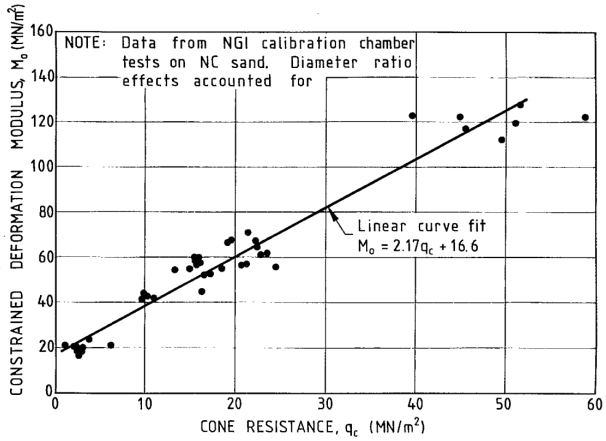

Figure A.5: 1D Constrained Modulus against the cone resistance q_c. Source: [8].

No standard deviation is reported for this formula, it has been estimated graphically to be equal to $\sigma = 4.97\,\text{MPa}$ for 40 data points, based on the figure A.5.

4. **Robertson & Mayne (1990)** A relationship between the ratio $\frac{M_{CPT}}{q_c}$ and the relative density D_r has been studied for normally consolidated sands:

$$M = q_c 10^{1.09 - 0.0075 * D_r} \tag{A.30}$$

where D_r is expressed in %. The standard deviation for the ratio M/q_c correlation is $\sigma = 1.38$ for 118 data points, with a correlation coefficient $R = 0.678$ [12].

A similar expression for overconsolidated sands exists:

$$M = q_c 10^{1.78 - 0.0122 * D_r} \tag{A.31}$$

The standard deviation for the ratio M/q_c correlation is $\sigma = 1.51$ for 94 data points, with a correlation coefficient $R = 0.734$ [12].

A.2.7 Small-strain Shear modulus

1. **Elastic theory** The shear modulus can be directly determined from the shear wave velocity V_s using the theory of elasticity:

$$G_0 = \rho V_s^2 \tag{A.32}$$

This relation is considered as theoretical, therefore the standard deviation of this relation is reduced to 0.

2. **Tanaka & Tanaka (1999)** The net cone tip stress can be related to the small strain shear modulus with the equation [9]:

$$G_0 = 50 p_a \left(\frac{q_t - \sigma_{v0}}{p_a}\right)^m \tag{A.33}$$

with the approximation $m = 0.6$ for sandy soils.

No standard deviation is reported in the original publication, an arbitrary standard deviation for α_M is then set at $\sigma = 5\,\text{MPa}$.

A.2.8 Shear wave velocity

1. **Robertson Cabal (2014)** This is the reference equation used by the software *CPeT-IT* to compute the shear wave velocity [14]:

$$V_s = \sqrt{(\alpha_{V_s}(q_t - \sigma_v)/p_a)} \tag{A.34}$$

with $\alpha_{V_s} = 10^{0.55 I_c + 1.68}$. No standard deviation is reported in the original publication, an arbitrary standard deviation for α_{V_s} is set at $\sigma = 60$.

2. **Mayne (2006)** The shear wave velocity can be computed directly from the sleeve friction f_s in kPa for both sands and clays: [9]

$$V_s = 51.6 \ln f_s + 18.5 \tag{A.35}$$

with f_s in kPa and V_s in m/s.

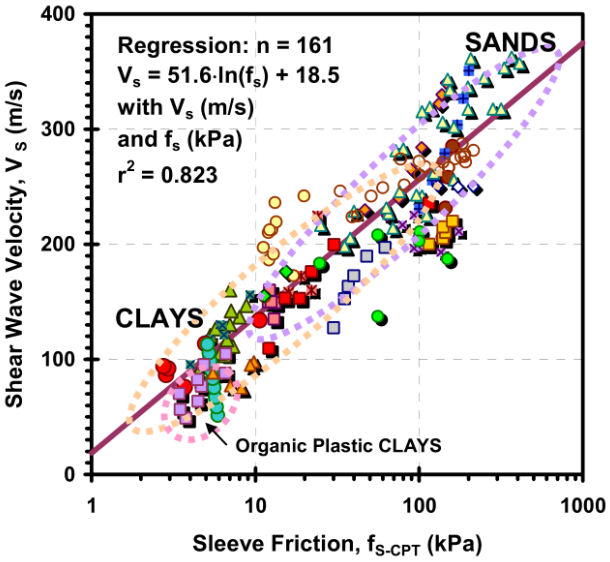

Figure A.6: Shear wave velocity against sleeve friction of SCPTU observations. Source: [9].

No standard deviation is reported for this formula, it has been estimated graphically from figure A.6 to be equal to $\sigma = 35\,\text{m}\,\text{s}^{-1}$ for 161 data points and a correlation coefficient $R^2 = 0.823$.

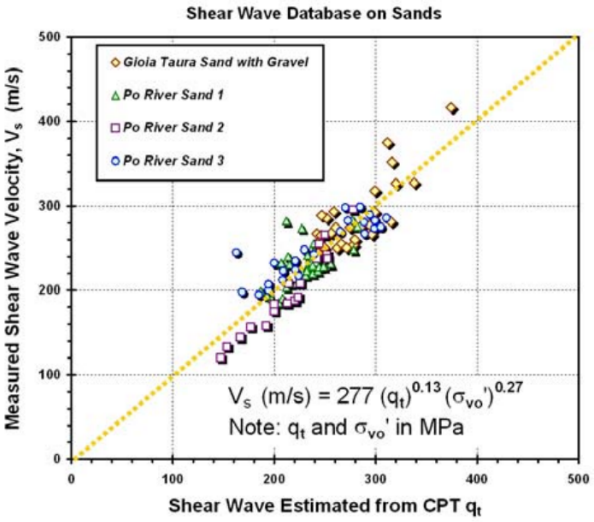

Figure A.7: Shear wave velocity against cone resistance q_t. Source: [10].

3. **Baldi et al (1989)** The following correlation is valid for uncemented unaged quartz sands [10]:

$$V_s = 277(q_t)^{0.13}(\sigma_{v0}^{'})^{0.27} \tag{A.36}$$

No standard deviation is reported for this formula, it has been estimated graphically from figure A.6 to be equal to $\sigma = 21\,\mathrm{m\,s^{-1}}$.

4. **Hegazy and Mayne (1995)** Three correlations are provided by Hegazy and Mayne [42] to estimate the shear wave velocity for sandy material:

$$V_s = 13.18(q_c)^{0.192}(\sigma_{v0}^{'})^{0.179} \tag{A.37}$$

with q_t and $\sigma_{v0}^{'}$ both in kPa.

No standard deviation is reported on the original publication [42], an arbitrary value is set to $\sigma = 30\,\mathrm{m\,s^{-1}}$. However, the original publication provides the correlation coefficient $R^2 = 0.684$ for 133 data points.

$$V_s = 12.02(q_t)^{0.319}(f_s)^{-0.0466} \tag{A.38}$$

with q_t and f_s both in kPa.

No standard deviation is reported on the original publication [42], an arbitrary value is set to $\sigma = 40\,\mathrm{m\,s^{-1}}$. However, the original publication provides the correlation coefficient $R^2 = 0.574$ for 92 data points.

The following formula is more general and is also valid for clayey soils, it can also be found in [43] and [10]:

$$V_s = [10.1\log(q_t) - 11.4]^{1.67} \cdot (100\frac{f_s}{q_t})^{0.3} \tag{A.39}$$

with q_t and f_s both in kPa.

No standard deviation is reported on the original publication [42], an arbitrary value is set to $\sigma = 30\,\mathrm{m\,s^{-1}}$. However, the original publication provides the correlation coefficient $R^2 = 0.695$ for 323 data points.

%

Appendix B

Characterization of the total uncertainty according to APD and Phoon & Kulhawy

Chapter 4 introduced the characterization of the uncertainty in geotechnical practices according to Phoon and Kulhawy [4] [17] who defined the total uncertainty of a design parameter ξ_d (equation 4.2). The definition of the uncertainty in the APD framework developed in this thesis (equation 4.5) slightly differs from Phoon and Kulhawy but is actually congruous with their previous publications. This appendix provides a mathematical proof that the two approaches are consistent, based on a particular example. The two approaches are compared for the correlation:

$$\phi^{'} = 17.6 + 11 \log \frac{q_c/p_a}{\sqrt{(\sigma_v^{'}/p_a)}} \tag{B.1}$$

This correlation has been chosen because it is explicitly studied by Phoon and Kulhawy in [17].

B.1 Approach from Phoon and Kulhawy

We reuse here the notations from the publications [4] and [17]. The friction angle ϕ is considered to be the design parameter ξ_d, and the cone resistance q_c is the measured parameter ξ_m. The measured parameter is split into three component: the trend t, the inherent variability w and the measurement error e:

$$q_c = \xi_m = t + w + e \tag{B.2}$$

The design parameter is the result of a transformation function $T(\cdot)$ such as:

$$\phi = \xi_d = T(q_c, \epsilon) = T(t + w + e, \epsilon) = 17.6 + 11 \log \frac{q_c/p_a}{\sqrt{(\sigma_v^{'}/p_a)}} + \epsilon \tag{B.3}$$

where ϵ is the transformation error of the function $T(\cdot)$. Note that the function $T(\cdot)$ is considered uni-variate here with respect of the geotechnical parameters q_c, p_a and $\sigma_v^{'}$.
The total uncertainty of the design parameter is defined according to the equation [6b] from [17] as:

$$SD_{\xi_d}^2 = \left(\frac{\partial T}{\partial w}|_{(t,0)}\right)^2 SD_w^2 + \left(\frac{\partial T}{\partial e}|_{(t,0)}\right)^2 SD_e^2 + \left(\frac{\partial T}{\partial \epsilon}|_{(t,0)}\right)^2 SD_\epsilon^2 \tag{B.4}$$

After evaluating the partial derivatives, it holds:

$$SD_{\xi_d}^2 = \frac{22.8}{t^2}\left(SD_w^2 + SD_e^2\right) + SD_\epsilon^2 \tag{B.5}$$

where SD_ϵ^2 is the standard deviation of the transformation error, SD_w^2 the standard deviation of the soil inherent variability, and SD_e^2 the standard deviation of the measurement error.

B.2 Approach from APD

Uni-variate and independent case

The total uncertainty of the friction angle ϕ is composed of the parameter uncertainty σ_{para} and the method uncertainty σ_{met}:

$$\sigma^2_{tot}(\phi) = \sigma^2_{para}(\phi) + \sigma^2_{met}(\phi) \tag{B.6}$$

The parameter uncertainty is calculated using the formula:

$$\sigma^2_{para}(\phi) = \sum_{i=1}^{n}(\frac{\partial f}{\partial x_i})^2\sigma^2(x_i) + 2\sum_{i=1}^{n-1}\sum_{j=i+1}^{n}(\frac{\partial f}{\partial x_i}\frac{\partial f}{\partial x_j})C(x_i, x_j) \tag{B.7}$$

In the case of a single variable q_c, the total uncertainty for the friction angle becomes:

$$\sigma^2_{tot}(\phi) = \frac{22.8}{q_c^2}\sigma^2(q_c) + \sigma^2_{met} \tag{B.8}$$

The total uncertainty as defined in APD (eq B.8) is then quite similar to the formulation from Phoon and Kulhawy (eq B.5). In practice, the value for the cone resistance q_c in equation B.8 would be equal to the trend t in equation B.5. The two approaches are identical if the input uncertainty $\sigma^2(q_c)$ encompasses the inherent variability SD^2_w and the measurement error SD^2_e. The standard deviation of the transformation error SD^2_ϵ is taken as the standard error of the regression function [17], while a correcting factor is applied in the framework APD (equation 4.8).

Multivariate and independent case

In practice, the correlation B.1 is not consider uni-variate by the APD system, but is actually a multivariate function with respect of the cone resistance q_c, the reference pressure p_a and the effective stress $\sigma_v^{'}$. These variables are still considered mutually independent such as their covariances are all equal to 0. In this case, the total uncertainty of the friction angle becomes:

$$\sigma^2_{tot}(\phi) = \frac{22.8}{q_c^2}\sigma^2(q_c) + \frac{22.8}{2p_a}\sigma^2(p_a) + \frac{22.8}{2\sigma_v^{'}}\sigma^2(\sigma_v^{'}) + \sigma^2_{met} \tag{B.9}$$

In this case, the approaches from APD and Phoon & Kulhawy are slightly different, in a sense that APD includes the variability of all the parameters present in the correlation B.1. Throughout this thesis, the uncertainty has been calculated using the multivariate and independent approach from APD.

Appendix C

Annexes to the chapter 6

C.1 External database for the methods

The external methods database used for the validation of the HSsmall model in chapter 6 is detailed in the two tables C.1 and C.2.

C.2 Graphs of the parameters for first approach

The averaged distributions and their contributing paths are displayed in the graphs below for all the parameters. They are valid for the second layer "2- Holoceen Zand".

C.3 Results of the APD system for several layers

The tables C.1 and 6.4 gathers the results from APD and WB for all several layers.

C.4 Graph generated

The graph generated by the system for the HSsmall case study is displayed here.

		RD [%]		M_NC [MPa]		M_OC [MPa]		OCR [-]		K0 [-]		[deg]		[deg]		E50ref [MPa]		Eoedref [MPa]		Eurref [MPa]		G0ref [MPa]		0.7 [-]		m [-]	
		ADP	WB	ADP	WB	ADP	WB	ADP	WB	ADP	WB	ADP	WB	ADP	WB	ADP	WB	ADP	WB	ADP	WB	ADP	WB	ADP	WB	ADP	WB
3[2]*1: Antropogeen Zand	lower	66	-	15.2	-	22.6	-	3.9	-	1.26	-	37.5	37.2	6.5	5.8	34.3	29.3	34.3	27.8	63.4	113.5	44.6	108.3	2.82E-05	-	0.376	-
	avg	85	83	29.5	36	53.9	99.1	5.03	1.00 (8.62)	1.35	0.48	40.5	40.4	9.1	8.2	45.7	41.4	46	40.9	115	167	111.6	156.2	8.41E-05	7.71E-05	0.433	0.5
	upper	-	-	43.9	-	85.388	-	6.22	-	1.43	-	43.6	43.7	11.6	10.7	57.1	53.5	57.7	53.9	166.4	220.6	178.6	204.1	1.40E-04	-	0.49	-
3[2]*2: Haloceen Zand, zwak siltig	lower	27.6	-	15.6	-	51	-	1.04052	-	0.506508	-	32.67	-	1.63	-	29.4	23.1	29.4	21.5	84.6	80.5	52.3	81.12	1.30E-04	-	0.536283	-
	avg	40	37	21.7	14.1	70	48.7	1.23363	1.00 (1.66)	0.530084	0.47	34.992	36.5	3.4425	4	37.1	31.5	36.9	30.6	112.4	114.3	90.4	115.1	2.02E-04	1.59E-04	0.57494	0.5
	upper	52.4	-	27.8	-	89	-	1.426744	-	0.553661	-	37.3	-	5.2543	-	44.2	40	44.2	39.6	140.2	148.2	128.5	149.2	2.74E-04	-	0.613599	-
3[2]*3: KR_Zand siltig, matig	lower	41.148	-	27.2	-	72.8	-	1.030351	-	0.503	-	34.45636	35.6	3.174471	-	30.3	42.6	30.3	34.1	88.5	132.2	64.5	122.3	1.81E-04	-	0.486194	-
	avg	54.8	49	38.6	37.6	110.3	113	1.204406	1.41 (1.28)	0.5251	0.5	36.6404	37.5	5.006478	5	42	46.8	41.8	38.6	125.8	148.3	90.1	137	2.60E-04	1.18E-04	0.528802	0.5
	upper	68.41787	-	50	-	147.8	-	1.378462	-	0.546871	-	38.82448	-	6.838485	-	53.7	51.1	53.4	43	163	164.5	115.8	141.6	3.39E-04	-	0.57141	-
3[2]*4: KR_Zand siltig, vast	lower	60.2	-	41	-	80.9	-	1.276828	-	0.5773	-	36.44031	37.7	4.95813	-	34.7	62	34.8	54.4	98.3	192.7	81.7	167.4	1.62E-04	-	0.41919	-
	avg	75.07	71	64.7	58.2	150.2	195.8	1.4795	1.78 (1.34)	0.601	0.51	38.82971	39.5	6.864877	4.5	53.1	67.3	53.1	62.4	149.45	217.9	114.7	178.4	2.41E-04	1.47E-04	0.46538	0.5
	upper	89.85814	-	88.3	-	220.8	-	1.68233	-	0.624826	-	41.21912	-	8.771622	-	71.4	72.6	71.3	70.4	200.5	243.12	147.7	189.3	3.20E-04	-	0.511572	-
3[2]*5: UR_Zand, siltig, latig	lower	54.72	-	48.7	-	120.6	-	0.8694	-	0.453275	-	35.63	37	4.0494	3.3	34.5	36.6	34.7	27.8	109.3	117	86.2	128	2.22E-04	-	0.438991	-
	avg	69.122	47	81.3	48.3	206.8	191	1.00569	1.01 (1.10)	0.471722	0.46	37.88	38.6	5.97051	4.4	56	43.7	55.8	33.7	164.4	144.3	117.2	147.7	3.20E-04	2.06E-04	0.483	0.5
	upper	83.5	-	113.9	-	293.3	-	1.14	-	0.49	-	40.12877	40.3	7.891609	5.6	77.4	50.8	76.8	39.5	219.6	171.7	148.2	167.4	4.18E-04	-	0.528993	-
3[2]*6: ST_Zand, siltig, vast	lower	65.2255	-	71.1	-	141	-	0.885801	-	0.457636	-	36.004	39.2	3.9401	3.3	44.8	49.4	44.9	38.6	129.2	175.6	129.3	177.1	2.44E-04	-	0.404637	-
	avg	79.87092	75	123	99.2	279	395.8	1.019071	1.14	0.47567	0.46	38.7372	40.4	6.524816	5.5	70.8	54.1	70.6	43.9	201.1	197	184	202.2	3.39E-04	1.72E-04	0.450403	0.5
	upper	94.5	-	175.8	-	417	-	1.1523	-	0.493709	-	41.4701	41.6	9.10951	6.4	96.7	58.7	96.2	49.3	273	218.5	238.7	227.3	4.34E-04	-	0.49617	-

Table C.1: Comparison of model parameters and soil properties between values from Witteveen+Bos (WB) and Automatic Parameter Determination (APD)

		E50ref [MPa]			**Eoedref [MPa]**			**Eurref [MPa]**			**G0ref [MPa]**			**0.7 [-]**		
		APD1	APD2	WB	APD1	APD2	WB	APD1	APD2	WB	APD1	APD2	WB	APD1	APD2	WB
1: Antropogeen Zand	lower	34.3	36.8	29.3	34.3	32.9	27.8	63.4	91	113.5	44.6	86.7	108.3	2.82E-05	5.88E-05	-
	avg	46.4	58.1	41.4	59.2	56	40.9	117.2	160	167	111.4	116	156.2	9.00E-05	1.00E-04	7.71E-05
	upper	58.7	79.4	53.5	83	79	53.9	169.5	229	220.6	179.1	145.9	204.1	1.68E-04	1.42E-04	-
2: Holoceen Zand, zwak siltig	lower	29.4	22.2	23.1	22.6	17.2	21.5	83.8	70.5	80.5	54.1	65.3	81.12	7.70E-05	1.29E-04	-
	avg	36.9	32.6	31.5	29.5	28.3	30.6	111.9	101.3	114.3	91.4	88.9	115.1	1.94E-04	1.71E-04	1.59E-04
	upper	44.2	43	40	36.3	39.3	39.6	139.9	132	148.2	128.8	112.4	149.2	3.12E-04	2.12E-04	-
3: KR_Zand siltig, matig	lower	30.4	29.9	42.6	28.6	23.7	34.1	88.8	84.5	132.2	64.2	72.7	122.3	1.50E-04	7.74E-05	-
	avg	42	40.3	46.8	37	36	38.6	125.7	112	148.3	90.5	94.1	137	2.80E-04	1.94E-04	1.18E-04
	upper	53.5	50.8	51.1	45.5	48.4	43	162.7	139.4	164.5	116	115.6	141.6	4.10E-04	3.10E-04	-
4: KR_Zand siltig, vast	lower	35.1	40.9	62	37.7	31.5	54.4	98.7	119	192.7	81.3	89.7	167.4	1.18E-04	3.04E-05	-
	avg	53.1	54.8	67.3	52.8	50	62.4	150	158.7	217.9	114.1	112	178.4	2.66E-04	2.19E-04	1.47E-04
	upper	71.8	68.7	72.6	67.9	68.7	70.4	202.1	198	243.12	146.8	135	189.3	4.14E-04	4.07E-04	-
5: UR_Zand, siltig, latig	lower	34.8	37.9	36.6	33.3	27.4	27.8	109	122.2	117	87.1	89.45	128	1.56E-04	1.31E-05	-
	avg	56	53.1	43.7	50.13	47	33.7	164.6	159.7	144.3	116.8	111.6	147.7	3.43E-04	2.47E-04	2.06E-04
	upper	77.1	68.4	50.8	66.9	66.6	39.5	219	197	171.7	146.4	134	167.4	5.29E-04	4.80E-04	-
6: ST_Zand, siltig, vast	lower	44.9	26.7	49.4	41.1	21.3	38.6	129.5	82.3	175.6	103.5	71.5	177.1	1.46E-04	0.00E+00	-
	avg	70.8	41.1	54.1	64.6	35.5	43.9	201.7	131	197	139.9	99.7	202.2	3.60E-04	2.67E-04	1.72E-04
	upper	96.7	55.5	58.7	88.1	49.7	49.3	274	179	218.5	176.2	128	227.3	5.75E-04	5.43E-04	-

Table C.2: Comparison of model parameters and soil properties between values from Witteveen+Bos (WB) and Automatic Parameter Determination (APD) for the first and second approach.

author	formula	parameters_in	parameter_c	method_	weight	validity
method_to_alphaE	0.015*10**(0.55*Ic+1.68)	Ic	alphaE	2	1	SBT(34567)
method_to_alphaVs	10**(0.55*Ic+1.68)	Ic	alphaVs	60	1	SBT(34567)
method_to_alphaM_OC_1	0.03*10**(0.55*Ic+1.68)	Ic	alphaM_OC	2	1	SBT(567) Ic_max(2.2)
method_to_alphaM_NC_1	5	Ic	alphaM_NC	2	1	SBT(34567)
method_to_alphaM2_NC	10**(1.09-0.0075*Dr)	Dr	alphaM2_N(	1.38	1	SBT(567)
method_to_alphaM2_OC	10**(1.78-0.0122*Dr)	Dr	alphaM2_O(	1.51	1	SBT(567)
method_to_Dr_1	100*sqrt(Qtn/350)	Qtn	Dr	13	1	SBT(567)
method_to_Dr_2	100*log(Qtn/15.7)/2.41	Qtn	Dr	11	1	SBT(567) consolidation('NC')
method_to_Dr_3	100*log(qc/(61*sigma_eff**0.71))/2.91	qc,sigma_eff	Dr	11	1	SBT(567)
method_to_Dr_4	100*log((qc/pa)/(17.68*(sigma_eff/pa)**0.50))/3.10	qc,pa,sigma_eff	Dr	10	1	SBT(567)
method_to_Dr_5	98*(-1) +66 * log10((qc/9.807)/sqrt(sigma_eff/9.807))	qc,sigma_eff	Dr	6.6	1	SBT(567) consolidation('NC')
method_to_Dr_6	100*(0.268*log(((qt*1000)/pa)/sqrt(sigma_eff/pa))-0.675)	qt,pa,sigma_eff	Dr	7.9	1	SBT(567)
method_to_Eoedref_1	E50ref	E50ref	Eoedref	0	1	SBT(34567)
method_to_Eoedref_2	M_NC * (pa/sigma_eff)**m	M_NC,pa,sigma_eff,m	Eoedref	0	1	SBT(567)
method_to_Es_1	((qt*1000)-sigma_tot) * alphaE	qt,sigma_tot,alphaE	Es	0	1	SBT(34567)
method_to_Es_2	(24.60-6.005*Ic-0.5811*Ic**2)*1000 +qc*(1.084-1.511*Ic+1.090*Ic**2)	Ic,qc	Es	1670	0.4	SBT(34567)
method_to_Es_3	14.429*1000+1.254*qc	qc	Es	2530	0.4	SBT(567)
method_to_Es_4	74*35*sqrt(qc/pa)	qc,pa	Es	4000	0.4	SBT(567)
method_to_Es_5	qc*(-11.9*log10(qc/sqrt(sigma_eff))+45)	qc,sigma_eff	Es	10000	1	SBT(567) consolidation('OC')
method_to_Es_6	qc*(-7.93*log10(qc/sqrt(sigma_eff))+30.17)	qc,sigma_eff	Es	10000	1	SBT(567) consolidation('NC')
method_to_Es_7	qc*(-2.64*log10(qc/sqrt(sigma_eff))+10.71)	qc,sigma_eff	Es	10000	1	SBT(567) consolidation('NC')
method_to_Es_NC_1	(24.60-6.005*Ic-0.5811*Ic**2)*1000 +qc*(1.084-1.511*Ic+1.090*Ic**2)	Ic,qc	Es_NC	1670	0.4	SBT(34567)
method_to_Es_NC_2	14.429*1000+1.254*qc	qc	Es_NC	2530	0.4	SBT(567)
method_to_Es_NC_3	74*35*sqrt(qc/pa)	qc,pa	Es_NC	4000	0.4	SBT(567)
method_to_Es_NC_4	qc*(-2.64*log10(qc/sqrt(sigma_eff))+10.71)	qc,sigma_eff	Es_NC	10000	1	SBT(567)
method_to_Es_NC_5	(1+nu)*(1-2*nu)/(1-nu)*M_NC	nu,M_NC	Es_NC	0	1	SBT(123456789)
method_to_Es_OC_1	((qt*1000)-sigma_tot) * alphaE	qt,sigma_tot,alphaE	Es_OC	0	1	SBT(34567)
method_to_Es_OC_2	qc*(-11.9*log10(qc/sqrt(sigma_eff))+45)	qc,sigma_eff	Es_OC	10000	1	SBT(567)
method_to_Es_OC_3	(1+nu)*(1-2*nu)/(1-nu)*M_OC	nu,M_OC	Es_OC	0	1	SBT(123456789)
method_to_Eurref_1	3*E50ref	E50ref	Eurref	0	1	SBT(34567)
method_to_Eurref_2	Es_OC*(pa/(K0*sigma_eff))**m	Es_OC,pa,K0,sigma_eff,m	Eurref	0	1	SBT(34567)
method_to_E50ref_1	(60000*Dr)/100	Dr	Eoedref	13125	1	SBT(567)
method_to_E50ref_2	Es_NC*(pa/(K0*sigma_eff))**m	Es_NC,pa,K0,sigma_eff,m	E50ref	0	1	SBT(34567)
method_to_gamma0.7_1	(1/(9*G0))*sigma_eff *(1+K0)*sin(radians(2*phip))	G0,sigma_eff,K0,phip	gamma07	0	1	SBT(567)
method_to_gamma0.7_2	(2-Dr/100)*0.0001	Dr	gamma07	0	1	SBT(567)
method_to_G0ref_1	(60000+68000*Dr/100)	Dr	G0ref	13125	1	SBT(567)
method_to_G0ref_2	G0*(pa/(K0*sigma_eff))**m	G0,pa,K0,sigma_eff,m	G0ref	0	1	SBT(567)
method_to_G0_1	(gamma_s / 9.807) *Vs**2	gamma_s,Vs	G0	0	1	SBT(34567)
method_to_G0_2	50 *pa *(((qt*1000)-sigma_tot)/pa)**0.6	qt,sigma_tot,pa	G0	5000	1	SBT(34567)
method_to_Kc_1	(5.581*(Ic*Ic*Ic))-(0.403*(Ic*Ic*Ic*Ic))-21.63*(Ic*Ic)+(33.75*Ic)-17.88	Ic	Kc	0	1	SBT(34567)

Figure C.1: External database of the methods for the HSsmall model (chapter (6). Part 1/2

method_to_Kc_2	1	Ic	Kc	0	1 SBT(9)
method_to_K0	(1-sin(radians(phi_CV)))*OCR**(sin(radians(phi_CV)))	phi_CV,OCR	K0	0	1 SBT(34567)
method_to_K0	0.192 *(qt*1000/pa)**0.22 *(sigma_eff/pa)**(-0.31)*OCR**0.27	qt,pa,sigma_eff,OCR	K0	0	1 SBT(34567)
method_to_K0nc	(1-sin(radians(phi_CV)))	phi_CV	K0nc	0.05	1 SBT(34567)
method_to_m	0.7-(Dr/320)	Dr	m	0	1 SBT(567)
method_to_M_NC_1	alphaM_NC*((qt*1000)-sigma_tot)	qt,sigma_tot,alphaM_NC	M_NC	5	1 SBT(34567)
method_to_M_NC_2	qc*2.17+16.6*1000	qc	M_NC	4970	1 SBT(567)
method_to_M_NC_3	qc * alphaM2_NC	qc,alphaM2_NC	M_NC	0	1 SBT(567)
method_to_M_OC_1	alphaM_OC*((qt*1000)-sigma_tot)	qt,sigma_tot,alphaM_OC	M_OC	5	1 SBT(34567)
method_to_M_OC_2	qc * alphaM2_OC	qc,alphaM2_OC	M_OC	0	1 SBT(567)
method_to_n	(0.381*(Ic))+(0.05*(sigma_eff/pa))-0.15	Ic,sigma_eff,pa	n	0	1
method_to_OCR_1	(0.33*((qt*1000)-sigma_tot)) / sigma_eff	qt,sigma_tot,sigma_eff	OCR	0	1 SBT(34)
method_to_OCR_2	((0.192*(qt*1000/pa)**0.22)/(K0nc * (sigma_eff/pa)**(0.31)))**(1/(sin(radians(phip))-0.27))	qt,pa,K0nc,sigma_eff,phip	OCR	0	1 SBT(567)
method_to_phip_1	phi_CV - 48*PSI	phi_CV,PSI	phip	2.42	1 SBT(34567)
method_to_phip_2	17.6 +11*log10(Qtn)	Qtn	phip	3.35	1 SBT(567)
method_to_phip_3	degrees(arctan((log10(qc/sigma_eff)+0.29)/2.68))	qc,sigma_eff	phip	2.46	1 SBT(567)
method_to_phip_4	phi_CV + psi	phi_CV,psi	phip	1	1 SBT(3456)
method_to_phip_5	28 +12.5 * Dr /100	Dr	phip	3.4	1 SBT(567)
method_to_psi_1	-2 +12.5*Dr/100	Dr	psi	1	1 SBT(567)
method_to_psi_2	3*(0.01*Dr*(14-log(100*qc/pa))-1)	Dr,qc,pa	psi	0.9	1 SBT(567)
method_to_PSI_1	0.56-0.33*log10(Qtncs)	Qtncs	PSI	0.04	1 SBT(34567)
method_to_PSI_2	-log(Qtn/27.6)/11.4	Qtn	PSI	0.03	1 SBT(34567)
method_to_Qtncs	Qtn*Kc	Qtn,Kc	Qtncs	0	1 SBT(34567)
method_to_Rf_fail	1-(Dr/800)	Dr	Rf_fail	0	1 SBT(567)
method_to_Vs_1	sqrt(alphaVs *(qt*1000-sigma_tot)/pa)	alphaVs,qt,sigma_tot,pa	Vs	0	1 SBT(34567)
method_to_Vs_2	51.6*log(fs)+18.5	fs	Vs	35	1 SBT(34567)
method_to_Vs_3	277*(qc/1000)**0.13*(sigma_eff/1000)**0.27	qc,sigma_eff	Vs	21	1 SBT(567)
method_to_Vs_4	13.18*(qc)**0.192*(sigma_eff)**0.179	qc,sigma_eff	Vs	30	1 SBT(567)
method_to_Vs_5	12.02*(qc)**0.319*(fs)**(-0.0466)	qc,fs	Vs	40	1 SBT(567)
method_to_Vs_6	((10.1*log10(qc)-11.4)**1.67)*(100*fs/(qc))	qc,fs	Vs	30	1 SBT(34567)

Figure C.2: External database of the methods for the HSsmall model (chapter 6). Part 2/2

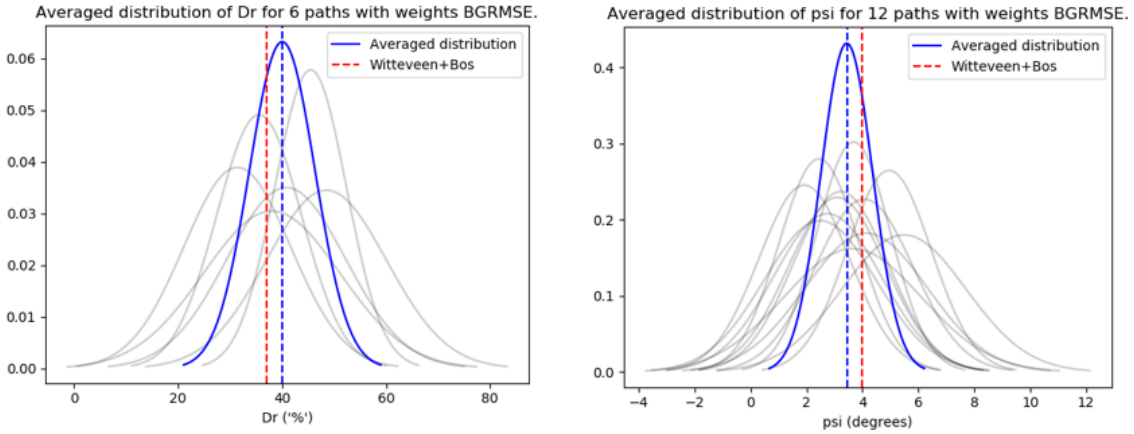

Figure C.3: Averaged distributions for the relative density D_r and the dilatancy angle ψ for the first approach from chapter 6. The vertical red dotted line is the average value from W+B.

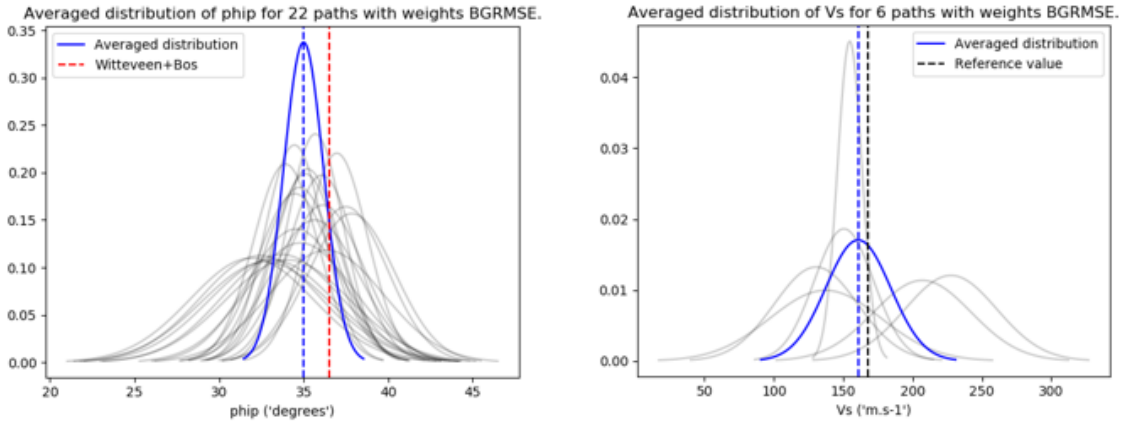

Figure C.4: Averaged distributions for the shear wave velocity V_s and the peak friction angle ϕ_p for the first approach from chapter 6. The vertical red dotted line is the average value from W+B.

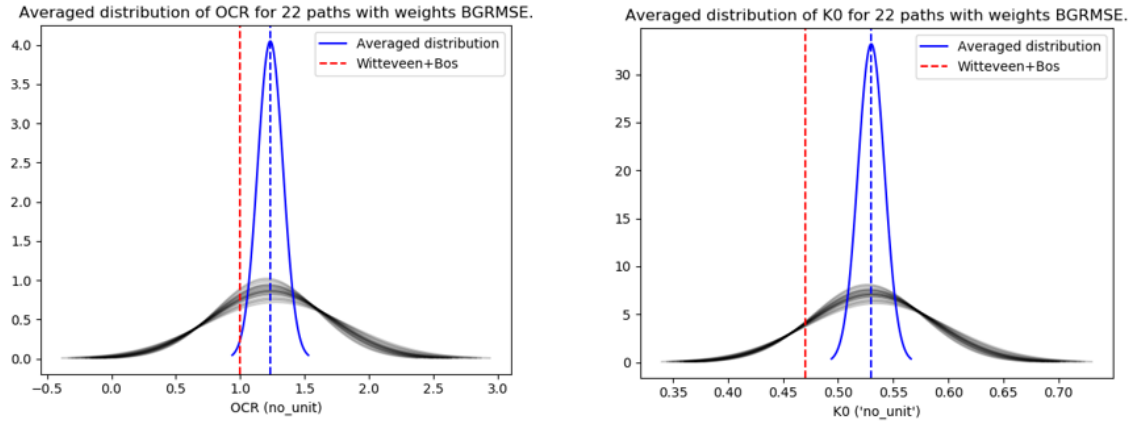

Figure C.5: Averaged distributions for the OCR and K_0 ratio for the first approach from chapter 6. The vertical red dotted line is the average value from W+B.

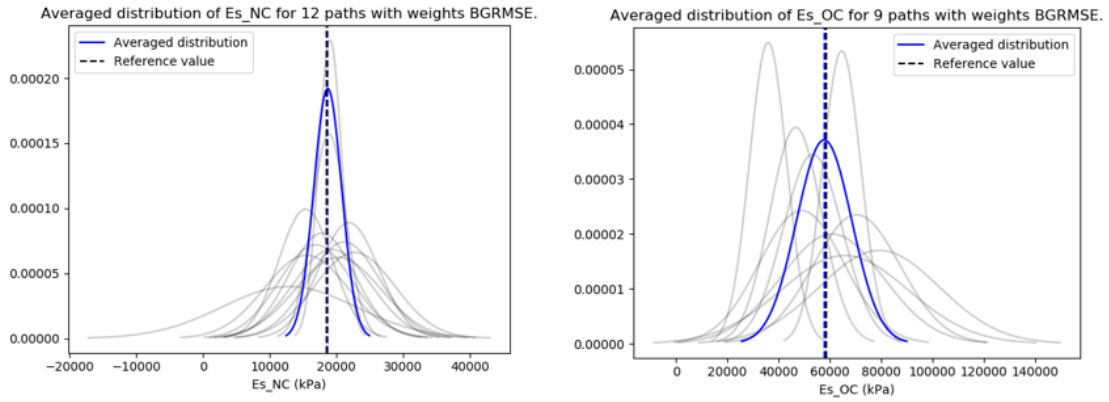

Figure C.6: Averaged distributions for the elastic Young modulus E_s in both normally and over-consolidated states for the first approach from chapter 6. The vertical red dotted line is the average value from W+B.

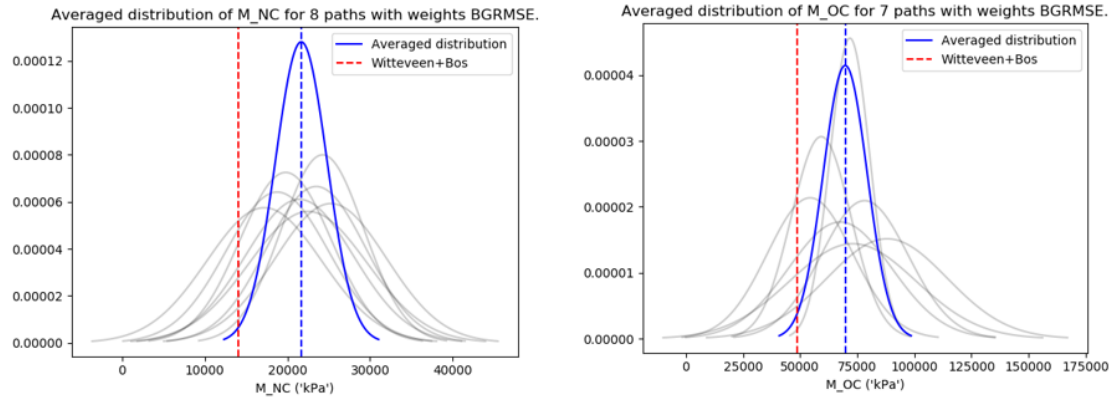

Figure C.7: Averaged distributions for the 1-D constrained modulus M_{CPT} in both normally and over-consolidated states for the first approach from chapter 6. The vertical red dotted line is the average value from W+B.

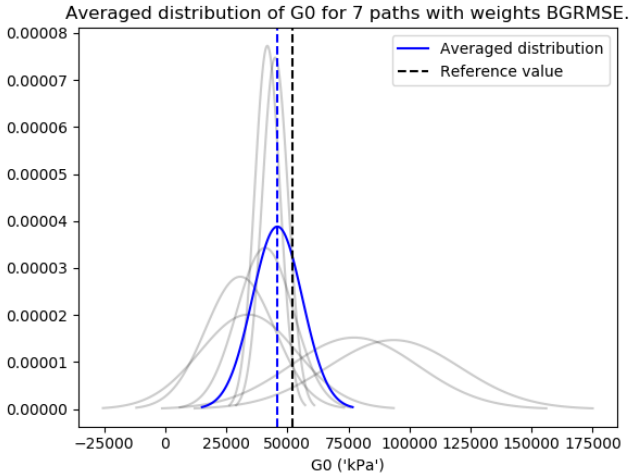

Figure C.8: Averaged distributions for the shear stress modulus G_0 for the first approach from chapter 6. Cluster from the right originates from the equations **??** and A.33, cluster from the left originates from the equation A.32.

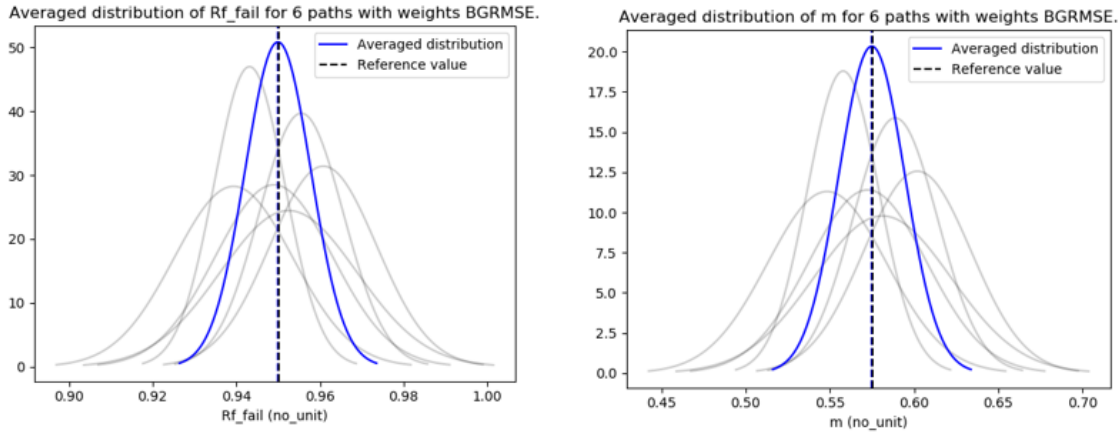

Figure C.9: Averaged distributions for the failure ratio R_{fail} and the stiffness stress exponent m for the first approach from chapter 6. The vertical red dotted line is the average value from W+B.

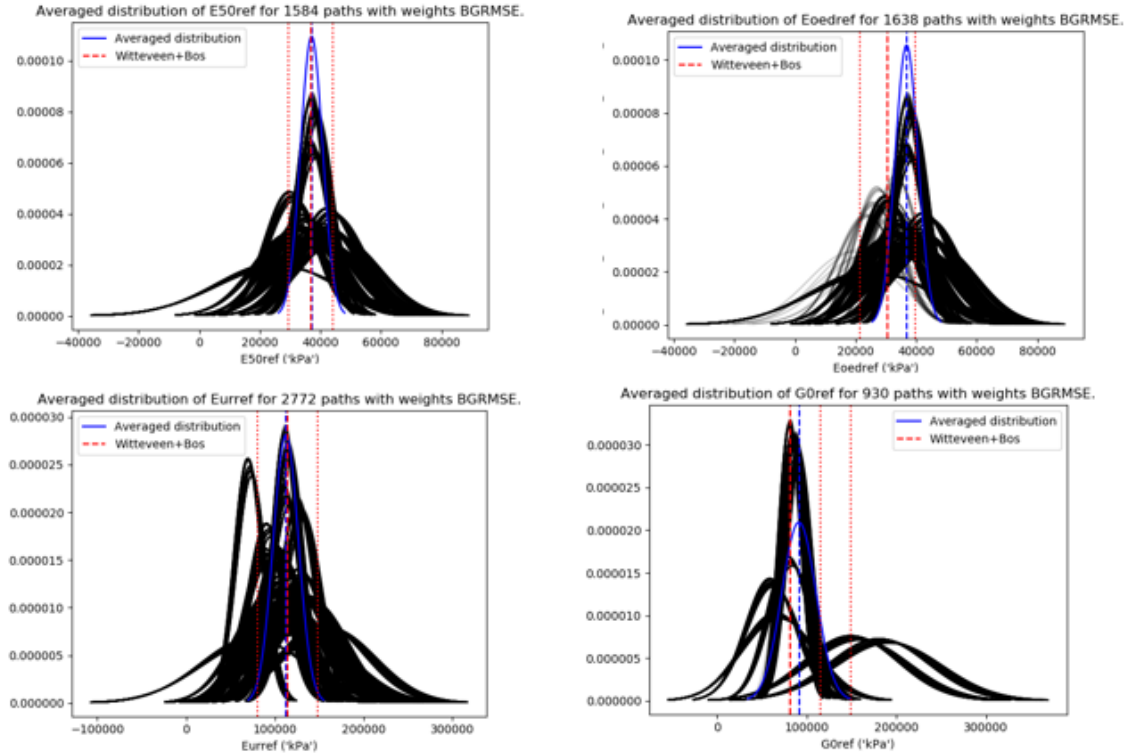

Figure C.10: Averaged distributions for the reference stiffness parameters E_{50}^{ref}, E_{oed}^{ref}, E_{ur}^{ref}, G_0^{ref} for the first approach from chapter 6. The vertical red dotted lines represent the lowe, the upper and the average value from W+B.

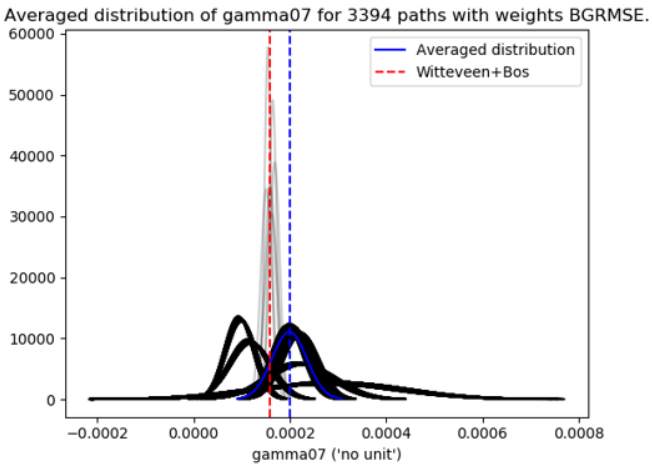

Figure C.11: Averaged distributions for the threshold $\gamma_{0.7}$ for the first approach from chapter 6. The vertical red dotted line is the average value from W+B.

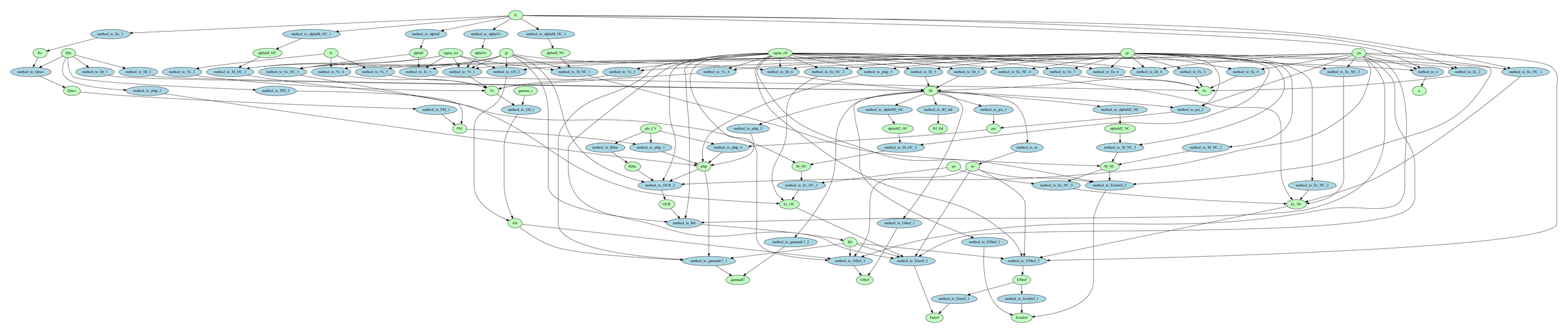
Ic
method_to_Kc_1
method_to_alphaM_OC_1
method_to_alphaE
method_to_alphaVs
method_to_alphaM_NC_1
Kc
Qm
alphaM_OC
fi
alphaE
sigma_tot
alphaVs
qI
alphaM_NC
sigma_eff
qc
ps
method_to_Qmcs
method_to_Dr_1
method_to_Dr_2
method_to_Vs_2
method_to_M_OC_1
method_to_Es_OC_1
method_to_Vs_6
method_to_Vs_5
method_to_Es_1
method_to_Vs_1
method_to_G0_2
method_to_M_NC_1
method_to_Vs_3
method_to_Vs_4
method_to_Dr_6
method_to_Es_OC_2
method_to_phip_3
method_to_Dr_5
method_to_Dr_3
method_to_Es_NC_4
method_to_Es_5
method_to_Es_6
method_to_Dr_4
method_to_Es_3
method_to_Es_4
method_to_Es_NC_3
method_to_n
method_to_Es_2
method_to_Es_NC_1
n
Qmcs
method_to_phip_2
method_to_PSI_2
Vs
gamma_s
Dr
Es
method_to_PSI_1
method_to_G0_1
method_to_alphaM2_OC
method_to_Rf_fail
method_to_psi_1
method_to_alphaM2_NC
method_to_psi_2
PSI
method_to_phip_5
alphaM2_OC
R(_fail
psi
alphaM2_NC
phi_CV
method_to_KOsc
method_to_phip_1
method_to_phip_4
method_to_M_OC_2
method_to_m
method_to_M_NC_3
method_to_M_NC_2
KOsc
phip
M_OC
m0
m
M_NC
method_to_OCR_2
method_to_Es_OC_3
method_to_Es_NC_5
method_to_Eoedref_2
method_to_Es_NC_2
OCR
Es_OC
Es_NC
G0
method_to_K0
method_to_GRef_1
method_to_ESOref_1
K0
method_to_gammaS7_2
method_to_gammaS7_1
method_to_GRef_2
method_to_Eurref_2
method_to_ESOref_2
gammaS7
GRef
ESOref
method_to_Eurref_1
method_to_Eoedref_1
Eurref
Eoedref

Bibliography

[1] Berkom I.E van. An automated system to determine constitutive model parameters from in-situ tests. Master's thesis, Delft University of Technology, 2020.

[2] RafbB F. Obrzud. On the use of the hardening soil small strain model in geotechnical practice. *Numerics in geotechnics and structures*, 2011.

[3] Duncan J.M, Bursey A. Soil modulus correlations. *Geotechnical Special Publication*, 2013.

[4] Phoon K.K., Kulhawy F.H. Characterization of geotechnical variability. *Canadian Geotechnical Journal*, 36(4):612–624, 1999.

[5] Been K. , Jefferies M.G. A state parameter for sands. *Géotechnique*, 35(2):99–112, 1985.

[6] Robertson P.K. , Campanella R.G. Interpretation of cone penetrations test. part i: Sand. *Can. Geotech*, 20:718–733, 1983.

[7] Baldi G. , Bellotti R. , Ghionna V. , Jamiolkowski M., Lo Presti D. Modulus of sands from cpt's and dmt's. *Proc. 12th international conference on soil mechanics and foundation engineering, Rio de Janeiro, 1989. Vol. 1*, pages 165–170, 01 1990.

[8] Lunne T. , Christoffersen H.P. Interpretation of cone penetration data for offshore sands. *15th Annual Offshore Technology Conference, Houston*, pages OTC–4464–MS, 1983.

[9] Mayne P.W. In-situ test calibrations for evaluating soil parameters. *Characterization and Engineering Properties of Natural Soil*, Vol 3:1601–1652, 2007.

[10] Mayne P.W. Nchrp project 20-05, cone penetration testing state-of-practice. 2007.

[11] Robertson P.K. , Wride C.E. Evaluating cyclic liquefaction potential using the cone penetration test. *Canadian Geotechnical Journal*, 35:442–459, 1998.

[12] Kulhawy F., Mayne P. Manual on estimating soil properties for foundation design. *(Tech Rep) Electric Power Research Institute*, 1990.

[13] Brinkgreve R.B.J. Automated model and parameter selection. *Geostrata*, pages 39–45, January 2019.

[14] Robertson P.K., Cabal K.L. Guide to cone penetration testing for geotechnical engineering. *Gregg Drilling Testing*, (6th edition), 2015.

[15] Sayed M.A. Assessment of clay stiffness and strength parameter using index properties. *Journal of Rock Mechanics and Geotechnical Engineering , volume =*.

[16] Brinkgreve R.B.J , Engin E. , Engin H.K. Validation of empirical formulas to derive model parameters for sands. *Numerical Methods in Geotechnical Engineering*, 1st edition edited by Benz and Nordal:137–142, 2010.

[17] Phoon K.K., Kulhawy F.H. Evaluation of geotechnical property variability. *Canadian Geotechnical Journal*, 36(4):625–639, 1999.

[18] Uzielli M., Lacasse S. , Nadim F., Phoon K.K. Soil variability analysis for geotechnical practice. *Characterisation and Engineering Properties of Natural Soils*, 3, 12 2006.

[19] Mackay M.D , Beckham R.J , Conover W.J. A comparison of three methods for selecting values of input variables in the analysis of output from a computer code. *Technometrics 21*, 56:239–245, 01 1979.

[20] Motra H.B., Stutz H., Wuttke F. Quality assessment of soil bearing capacity factor models of shallow foundations. *The Japanese Geotechnical Society*, 56(2):265–276, 2016.

[21] Driels M.R. , Shin Y.S. Technical report: Determining the number of iterations for monte carlo simulations of weapon effectiveness. *Nalval Postgraduate School, Monterey, CA*, 2004.

[22] Lengkeek H.J. Application of geo-statistics and pairwise established cpt-based correlations for line infrastructure. *6th International Conference on Geotechnical and Geophysical Site Characterization*, 202X (Not published yet).

[23] Weglarczyk S. Kernel density estimation and its application. *ITM Web of Conferences*, 23:00037, 01 2018.

[24] Claeskens G. ,Magnus J. , Vasnev A. , Wang W. The forecast combination puzzle: A simple theoretical explanation. *International Journal of Forecasting*, 32:754–762, 2016.

[25] Dormann C.F, Calabrese J.M, Guillera-Arroita G., Matechou E., Bahn V., Barton K., Beale C.M., Ciuti S., Elith J., Gerstner K., Guelat J., Keil P., Lahoz-Monfort J.J., Pollock L.J., Reineking B., Roberts D.R., Schroder B., Thuiller W., Warton D.I, Wintle B.A., Wood S.N., Wuest R.O., Harting F. Model averaging in ecology: a review of bayesian, information-theoretic and tactical approaches. *Ecological Monographs*, 88:756–762, 02 2018.

[26] Buckland S.T ,Burnham K.P. ,Augustin N.H. Model selection: An integral part of inference. *Biometrics*, 53:603–618, June 1997.

[27] Bates J. M. ,Granger C.W.J ,Augustin N.H. The combination of forecasts. *Journal of the Operational Research Society*, 20:451–468, 1969.

[28] Most T. Assessment of structural simulation models by estimating uncertainties due to model selection and model simplification. *Computer and structures*, (89):1664–1672, 2011.

[29] *PLAXIS 2D Connect Edition V20 - Material Models Manual.* Bentley Systems - PLAXIS, 2020.

[30] Lengkeek H.J. Estimation of sand stiffness parameters from cone resistance. *PLAXIS bulletin 13*, pages 15–19, 01 2003.

[31] Jamiolkowski M. , Lo Presti D.C.F , Manassero M. Evaluation of relative density and shear strength of sands from cpt and dmt. *ASCE Geotechnical Special Publication*, (119):201, 2001.

[32] Jamiolkowski M., Ladd C.C., Germaine J.T., Lancellotta R. New developments in field and laboratory testing of soils. *Conference On Soil Mechanics And Foundation Engineering*, August 1985.

[33] Been K. , Jefferies M. , Crooks J. , Becker D. The cone penetration test in sands: Part i, state parameter interpretation. 36:239–249, 01 1986.

[34] Jefferies M. , Been K. *Soil liquefaction - a critical state approach.* Taylor Francis, 2006.

[35] Bolton M.D. Strength and dilatancy of sands. *Géotechnique*, 36(1):65–78, 1986.

[36] Lee J., Eun J. , Lee K. , Park Y. , Kim M. In-situ evaluation of strength and dilatancy of sands based on cpt results. *Japanese Geotechnical Society*, 48(2):255–265, 2008.

[37] Robertson P.K. Estimating in-situ state parameter and friction angle in sandy soils from cpt. *2nd International Symposium on Cone Penetration Testing*, CPT10, Huntington Beach, CA, USA:Paper NO. 43, 2010.

[38] Sadrekarimi A. Estimating relative density of sand with cone penetration test. *Ground improvement*, 169(GI4):253–263, 2016.

[39] Robertson P.K. Interpretation of cone penetration tests - a unified approach. *Canadian Geotechnical Journal*, 46:1337–1355, 11 2009.

[40] Melnikov A.V. , Boldyrev G.G. Correlations between cpt resistance and young modulus of soils. *Soil Mechanics and Foundation Engineering*, 52(3):115–121, 2015.

[41] Massarsch K.R. Determination of shear modulus of soil from static and seismic penetration testing. *Proceedings in honour of Prof A. Anagnostopoulose*, Publisher: Tsotras:335–352, 2015.

[42] Hegazy Y.A. , Mayne P.W. Statistical correlations between vs and cpt data for different soil types. *Proc. Cone Penetration Testing (CPT'95)*, 2:173–178, 01 1995.

[43] Dagger R. , Saftner D. , Mayne P.W. Technical report. cone penetration test design guide for state geotechnical engineers. Publisher: Minnesota Department of Transportation, 2018.